OAK RIDGE NATIONAL LABORATORY LIBRARIES
3 4456 0549996 6

CENTRAL RESEARCH LIBRARY
DOCUMENT COLLECTION

ONAL LABORATORY
operated by
UNION CARBIDE CORPORATION
for the
U.S. ATOMIC ENERGY COMMISSION

UNION CARBIDE

ORNL-TM-1409

2

ELECTRON CAPTURE CROSS SECTIONS AND NEGATIVE ION LIFETIMES

(Thesis)

R.N. Compton, G.S. Hurst, L.G. Christophorou, and P.W. Reinhardt

CENTRAL RESEARCH LIBRARY
DOCUMENT COLLECTION
LIBRARY LOAN COPY
DO NOT TRANSFER TO ANOTHER PERSON
If you wish someone else to see this document, send in name with document and the library will arrange a loan.

Submitted by R.N. Compton as a dissertation to the Graduate School of The University of Tennessee in partial fulfillment of the requirements for the degree of Doctor of Philosophy.

LEGAL NOTICE

This report was prepared as an account of Government sponsored work. Neither the United States, nor the Commission, nor any person acting on behalf of the Commission:

A. Makes any warranty or representation, expressed or implied, with respect to the accuracy, completeness, or usefulness of the information contained in this report, or that the use of any information, apparatus, method, or process disclosed in this report may not infringe privately owned rights; or

B. Assumes any liabilities with respect to the use of, or for damages resulting from the use of any information, apparatus, method, or process disclosed in this report.

As used in the above, "person acting on behalf of the Commission" includes any employee or contractor of the Commission, or employee of such contractor, to the extent that such employee or contractor of the Commission, or employee of such contractor prepares, disseminates, or provides access to, any information pursuant to his employment or contract with the Commission, or his employment with such contractor.

ORNL TM-1409

Contract No. W-7405-eng-26

HEALTH PHYSICS DIVISION

ELECTRON CAPTURE CROSS SECTIONS AND NEGATIVE ION LIFETIMES

R. N. Compton, G. S. Hurst, L. G. Christophorou, and P. W. Reinhardt

Submitted by R. N. Compton as a dissertation to the
Graduate School of The University of Tennessee
in partial fulfillment of the requirements
for the degree of
Doctor of Philosophy

MARCH 1966

OAK RIDGE NATIONAL LABORATORY
Oak Ridge, Tennessee
operated by
UNION CARBIDE CORPORATION
for the
U.S. ATOMIC ENERGY COMMISSION

OAK RIDGE NATIONAL LABORATORY LIBRARIES

3 4456 0549996 6

ACKNOWLEDGMENTS

The authors are indebted to Dr. C. E. Klots for contributions to the theoretical work presented in Chapter V. Appreciation is also extended to Drs. J. E. Turner, J. F. Burns, C. E. Melton, R. H. Ritchie, and H. C. Schweinler for helpful discussions of certain parts of this study.

The authors are also grateful to R. E. Boughner and A. M. Craig, Jr. for the computer programming required to determine the electron capture cross sections.

TABLE OF CONTENTS

CHAPTER	PAGE
I. INTRODUCTION	1
Significance of Negative Ion Studies	1
Classification of Electron Attachment	3
Dissociative Attachment	4
Ion Pair Processes	7
Temporary Non-Dissociative Attachment	8
Radiative Non-Dissociative Attachment	10
Dielectronic Attachment	11
Survey of Methods Used to Study Electron Capture	12
Electron Swarm Method	13
Electron Beam Method	13
Microwave Method	14
Electron Avalanche Method	14
Summary of Electron Beam Studies	15
Lozier Tube	19
Total Ionization Experiments	19
Mass Spectrometric Techniques	21
Electron Path Length	21
Space-Charge Effects	23
Energy Spread of Electrons	23

CHAPTER PAGE

Ion Collection Efficiency 23

Errors in Current and Pressure Measurements 23

Scattered Electrons 24

Object of Negative Ion Studies 25

II. THEORY OF ELECTRON CAPTURE 41

III. DETERMINATION OF ELECTRON CAPTURE CROSS SECTIONS AS A FUNCTION OF ENERGY BY SWARM-BEAM COMBINATION 63

Experimental Apparatus 63

Time-of-Flight Mass Spectroscopy 63

Quasi-Monoenergetic Electron Source 70

The Electron Swarm Method 78

Determination of Electron Capture Cross Sections 85

IV. ELECTRON CAPTURE CROSS SECTIONS AS A FUNCTION OF ENERGY 106

Investigation of H_2O 106

Investigation of C_6H_5Cl, o-$C_6H_4Cl_2$, m-$C_6H_4Cl_2$, p-$C_6H_4Cl_2$, o-$C_6H_4CH_3Cl$; C_6H_5Br, C_6D_5Br, and o-$C_6H_4CH_3Br$; C_6H_5I. 116

Investigation of $C_6H_5NO_2$, o- and m-$C_6H_4CH_3NO_2$ 132

Investigation of C_2H_5Cl 141

Discussion of Results for Halogenated Compounds 144

CHAPTER PAGE

V. LIFETIMES OF NEGATIVE IONS 148

Introduction 148

Measurement of Negative Ion Lifetimes 152

Theory of Long-Lived Negative Ions 160

VI. SUMMARY 173

BIBLIOGRAPHY 175

LIST OF TABLES

TABLE		PAGE
I.	Summary of Retarding Potential Difference Negative Ion Studies	26
II.	Transition Probability Behavior Between Pairs of Electronic States for Homonuclear Diatomic Molecules	60
III.	Transition Probability Behavior Between Pairs of Electronic States for Heteronuclear Diatomic Molecules	61
IV.	Attachment Coefficients and Rates of Capture for Benzene Derivatives in Nitrogen	87
V.	Electron Drift Velocities w(E/P) and Attachment Coefficients $\alpha_o(E/P)$ for O_2 and H_2O in Argon	90
VI.	Evaluation of the Ratio $[\alpha_o(E/P) \times w(E/P)]/f(\epsilon_1, E/P)$ for Various ϵ_1	92
VII.	Data for the Production of O^- from O_2	103
VIII.	Data for the Production of H^- and O^- from H_2O	110
IX.	Electron Capture Data Obtained by the Swarm-Beam Method	120
X.	Electron Capture Data Obtained by the Beam Method	139
XI.	Attachment Coefficients and Rates of Capture for Chloroethane in Nitrogen	142
XII.	Lifetimes of Temporary Negative Ions for Various Ion Energies	158

LIST OF FIGURES

FIGURE PAGE

1. Potential Curves Illustrating Various Types of Electron Capture 5
2. Illustration of the Retarding Potential Difference Method . . . 17
3. Schematic Diagram of Lozier Tube and Schulz's Total Ionization Apparatus 20
4. Plot of the Overlap Integral $\langle \chi_f | \chi_o \rangle$ and the Gradient Matrix Elements, $\langle \chi_f | \nabla_R | \chi_o \rangle$, for the Continuous and Ground Nuclear Wave Functions of H_2^- and H_2 49
5. Comparison of the Experimental and Theoretical Cross Section Curves for the Reaction $e + H_2 \rightarrow H + H^-$ with H and H^- in Their Ground States [taken from Chen (1963)] 50
6. Illustration of Resonance Electron Capture 54
7. Diagram of the Bendix Model 14-206 Mass Spectrometer 65
8. Negative Ion Mass Calibration - Impure Sample of Methane . . . 69
9. RPD Quasi-Monoenergetic Electron Source 71
10. SF_6^- and SF_5^- Ion Currents as a Function of the Electron Accelerating Voltage 76
11. Electron Energy Loss Spectrum of Helium Using SF_6 as a Zero Energy Electron Detector 79

FIGURE PAGE

12. Energy Distribution in Electron Swarms for Different Carrier Gases and E/P 81

13. Swarm Apparatus for Measurement of Electron Attachment Coefficient and Drift Velocity 83

14. $\alpha(E/P)$ vs f_1P/f_2P for Ortho-Chlorotoluene in Nitrogen 86

15. Chlorine Negative Ions from Ortho-Chlorotoluene as a Function of Electron Energy 94

16. Experimental and Calculated Rates of Capture vs E/P for Ortho-Chlorotoluene for Trial Functions Based on Beam Experiments 96

17. Experimental and Calculated Rates of Capture vs E/P for Ortho-Chlorotoluene for Various Types of Trial Functions . . 97

18. Experimental and Calculated Rates of Capture vs E/P for Oxygen for Various Types of Trial Functions 98

19. Electron Capture Cross Section as a Function of Energy for Chlorine Negative Ions from Ortho-Chlorotoluene 100

20. Electron Capture Cross Section as a Function of Energy for Oxygen 101

21. Experimental and Calculated Rates of Capture vs E/P for Water for Trial Functions Based on Beam Experiments 108

FIGURE PAGE

22. Electron Capture Cross Section as a Function of Energy for Atomic Hydrogen Negative Ions from Water 109

23. Atomic Oxygen Negative Ions from Water 113

24. Hydroxyl Negative Ions Produced by Ion Molecule Reactions in Water 114

25. $\alpha(E/P)$ vs f_1P/f_2P for Ortho-Bromotoluene in Nitrogen 117

26. Cl^- Ion Current vs Electron Energy (as Calibrated by SF_6^-) for Chlorinated Benzene Derivatives 119

27. Iodine Negative Ions from Iodobenzene as a Function of Electron Energy 123

28. Electron Capture Cross Section as a Function of Energy for Chlorine Negative Ions from Chlorobenzene 125

29. Electron Capture Cross Section as a Function of Energy for Chlorine Negative Ions from Ortho-Dichlorobenzene 126

30. Electron Capture Cross Section as a Function of Energy for Bromine Negative Ions from Bromobenzene 127

31. Electron Capture Cross Section as a Function of Energy for Bromine Negative Ions from Deuterated Bromobenzene 128

32. Electron Capture Cross Section as a Function of Energy for Bromine Negative Ions from Bromotoluene 129

FIGURE PAGE

33. Comparison of $C_6H_5NO_2^-$ Ion Current with SF_6^- Ion Current as a Function of Electron Energy 130

34. Pressure Dependence of $C_6H_5NO_2^-$ Ion Current 133

35. Dissociative Electron Capture in Nitrobenzene 134

36. $C_6H_5NO_2^-$ and NO_2^- Ion Currents from Nitrobenzene as a Function of Electron Energy 135

37. Comparison of o-$C_6H_4CH_3NO_2^-$ and m-$C_6H_4CH_3NO_2^-$ Ion Currents with SF_6^- Ion Currents as a Function of Electron Energy 137

38. Dissociative Electron Capture in Ortho-Nitrotoluene 138

39. Dissociative Electron Capture in Meta-Nitrotoluene 140

40. Chlorine Negative Ions from Chloroethane 143

41. Schematic Diagram of Negative Ion Lifetime Apparatus 154

42. Separation of Neutral and Negative Currents of Sulphur-Hexafluoride 157

43. Determination of SF_6^{-*} Autodetachment Lifetime 159

44. Lifetime of SF_6^{-*} as a Function of E [$E_A(SF_6) = 1.29$ eV] 167

45. Lifetime of SF_6^{-*} as a Function of E [$E_A(SF_6) = 1.49$ eV] 168

46. Lifetime of SF_6^{-*} as a Function of E [$E_A(SF_6) = 1.69$ eV] 169

CHAPTER I

INTRODUCTION

I. SIGNIFICANCE OF NEGATIVE ION STUDIES

Negative ion studies are of fundamental importance in various fields of physics, chemistry, engineering, and biology. The attention that negative ion research has attracted is illustrated by the many books and review articles which have been written on the subject [e.g., Massey (1950), Branscomb (1957), Bates (1962), Melton (1963), McDaniel (1964), Hasted (1964), and Fiquet-Fayard (1965)].

Investigations of negative ion formation by electron impact has provided a great deal of information about atoms and molecules such as electron affinities, bond dissociation energies, and heats of vaporization. There is promise also that the negative ion mass spectra of complex polyatomic molecules will be less difficult to interpret than positive ion spectra and may afford a superior technique for determining the molecular weight and structure of many molecules. This technique has been illustrated by von Ardenne, Steinfelder, and Tümmer (1961) in a study of the negative ion mass spectra of some condensible aromatic hydrocarbons.

Nuclear physicists have used negative ions of H, N, and He to great advantage in tandem van de Graaff accelerators to double the effective

energy of the bombarding particles. There is good evidence, also, that negative ions which are induced to detach an electron and become neutral can be an efficient source of neutral particles to be used in collision studies.

The high dielectric strength of many gases can be explained by the ability of molecules to remove slow electrons before they attain enough energy to start an avalanche initiating electrical breakdown. A great deal of effort has been directed toward the understanding of this phenomena. Negative ions are also of practical importance in radiation dosimetry in that they can produce spurious counts in radiation counters, and the formation of negative ions makes the absolute determination of electron yields in such devices difficult.

One of the more important consequences of negative ions in nature is to be found in the field of astrophysics. It has long been known that the radiative formation and photodetachment of H^- ions greatly influences the spectral distribution of visible light from the photosphere of the sun. In fact, the first photodetachment absorption spectra was observed from H^- by Widlt (1930) in the solar spectra. McDowell (1961) has also suggested that associative detachment reactions such as $H^- + H \rightleftarrows H_2^-\,(^2\Sigma_u) \rightleftarrows H_2 + e$ might be responsible for the formation of H_2 in stars. A similar reaction, $O^- + H^+ \rightarrow OH^\circ$, has been proposed by Symonds (1965) to account for the abundance of OH radicals in the upper atmosphere. Of course, negative ions

are known to be an important intermediate in determining the number of free electrons in the upper atmosphere which in turn play a significant role in radio and television communication.

Finally, the effect of negative ions on biological structures and their relation to the field of biology in general promises to be the most fruitful application of negative ion research. Attempts have been made to correlate electron accepting or donating power of organic molecules with biological effects such as carcinogenicity; however, the conclusions are not definite due in part to the unavailability of electron capture data on organic molecules.

II. CLASSIFICATION OF ELECTRON ATTACHMENT

Negative ions are formed by collisions of electrons with neutral molecules through basically two different processes: dissociative and non-dissociative electron capture. Different modes of negative ion formation occur within these two broad categories and can be further classified as

(a) $e + AB \rightarrow A + B^-$	Dissociative Attachment
(b) $e + AB \rightarrow A^+ + B^- + e$	Ion Pair Production
(c) $e + AB \rightleftarrows (AB^-)^*$	Temporary Non-Dissociative Attachment
(d) $e + AB \rightarrow AB^- + h\nu$	Simple Radiative Attachment
(e) $e + AB \rightleftarrows (AB^-)^{**} \rightarrow AB^- + h\nu$	Dielectronic Attachment

The classification is completely general in that A and/or B may be an atom or a radical in which case AB would be a diatomic or polyatomic molecule, respectively. The distinction between (c) or (d) and (e) is not obvious from the reactions appearing above, however the reason for separating the dielectronic attachment from radiative or non-dissociative attachment will be made clear. A detailed description of each of the various electron capture mechanisms will now be presented.

Dissociative Attachment

Figure 1a illustrates the most general type of electron capture by a diatomic molecule. The asymptote of the dissociative AB^- curve lies below the asymptote of the AB curve by an amount equal to EA(B), the electron affinity of B. For sake of generality, dissociative transitions are considered through both the attractive and repulsive states of AB^-. Since the speed of the incident electron will be large compared to that of the vibrating nuclei of the molecule, the nuclei may be considered at rest during the time in which attachment takes place. The Franck-Condon principle then states that dissociative attachment transitions can occur only for electron energies between E_1 and E_2 for the attractive states and between E_3 and E_4 for the repulsive states. If the dissociating products are in their ground states, the negative ions resulting from capture into the attractive curve will possess a distribution of kinetic energies from

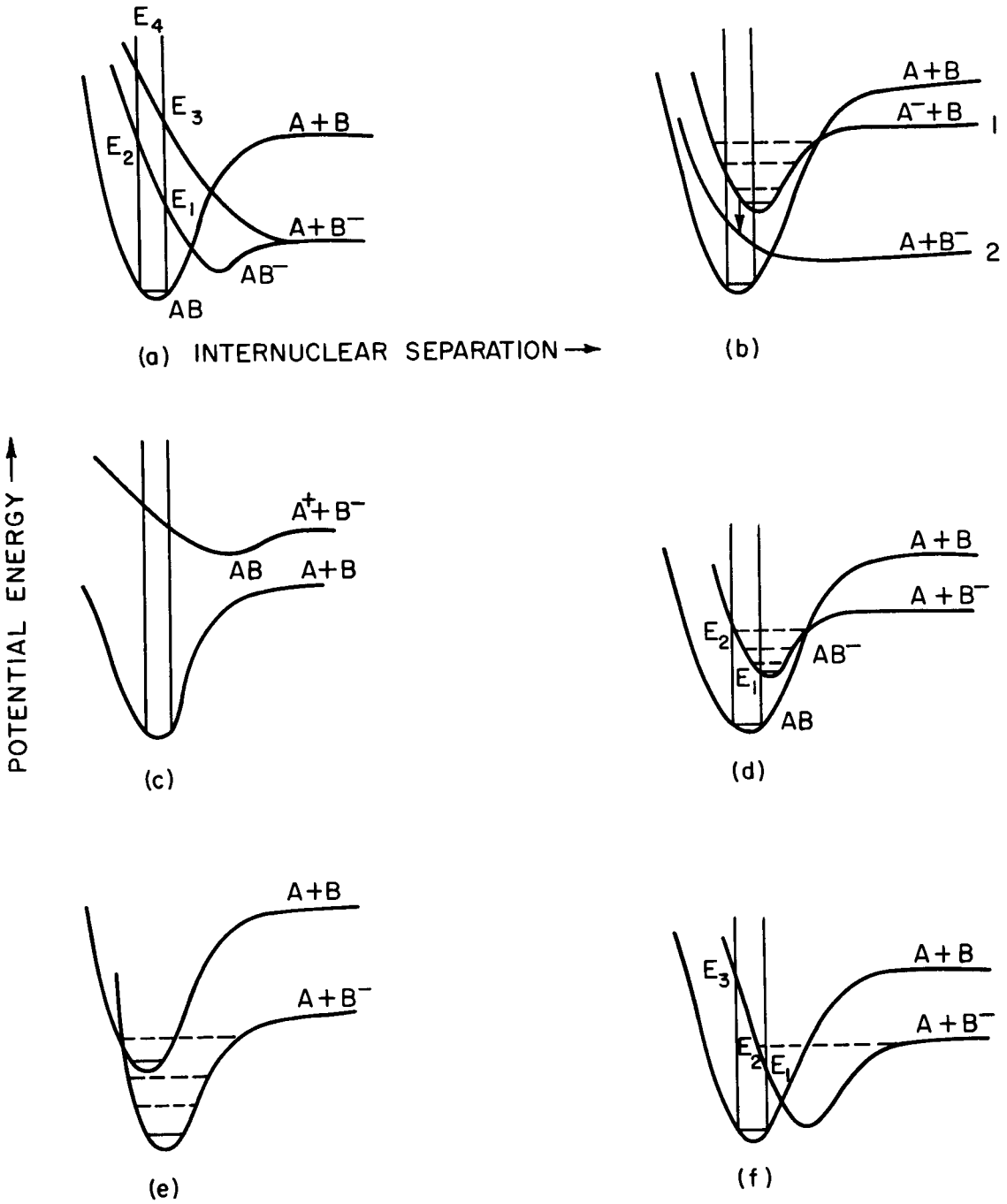

Figure 1. Potential curves illustrating various types of electron capture.

$$KE_{min} = \frac{M_A}{M_A + M_B} \left[EA(B) - D(AB) + E_1 \right] \tag{1}$$

to

$$KE_{max} = \frac{M_A}{M_A + M_B} \left[EA(B) - D(AB) + E_2 \right], \tag{2}$$

and the ions resulting from dissociative attachment through the repulsive curve of AB^- will possess a distribution of kinetic energies from

$$KE_{min} = \frac{M_A}{M_A + M_B} \left[EA(B) - D(AB) + E_3 \right] \tag{3}$$

to

$$KE_{max} = \frac{M_A}{M_A + M_B} \left[EA(B) - D(AB) + E_4 \right] \tag{4}$$

where EA(B) is the electron affinity of the fragment B, M_A is the mass of the neutral fragment A, M_B is the mass of the negative ion B^-, and D(AB) is the dissociation energy of AB. The above expressions for the kinetic energy of the negative ion assume that the momentum of the incident electron is small compared to the momentum of either of the dissociating fragments which is generally but not always true.

It has been suggested also by Chen (1963) that capture may take place through bound states of the negative ion which undergo radiationless intramolecular transitions to repulsive states of the negative ion resulting in dissociative electron capture. These radiationless intramolecular

transitions (Auger transitions) are a result of overlap of the discrete states with a continuum of states of AB^-. Radiationless processes of this type have long been known in light absorption spectroscopy and are called predissociation. These types of processes can be illustrated for diatomic molecules in Figure 1b. Electrons are first captured into the bound state represented by curve 2, and before autodetachment can take place an intramolecular radiationless transition occurs to curve 1 resulting in dissociation into $A + B^-$. The mechanism could be extremely important for polyatomic molecules due to overlap of vibrational states which will lead to predissociation by vibration.

Ion Pair Processes

Electron impact reactions leading to ion pair production are not to be designated as attachment processes since the incident electron is not captured but merely serves to excite the molecule to an electronic level which leads to $A^+ + B^-$. Figure 1c shows the potential energy curves which characterize ion pair production. Ion pair processes are known to occur under photon impact (Dibeler and Walker, 1965) as well. In fact, Figure 1c would apply to electron or photon impact.

The kinetic energy shared by the fragment ions A^+ and B^- will range from

$$KE_{min} = EA(B) - D(AB) - I(A) + E_1 \tag{5}$$

to

$$KE_{max} = EA(B) - D(AB) - I(A) + E_2 \qquad (6)$$

where I(A) is the ionization potential of the atom or radical A.

The behavior of the ion current yield as a function of electron energy is distinctly different from dissociative attachment processes. Experimentally, the ion current is observed to increase approximately linearly with the electron energy beginning at E_1 up to an electron energy of roughly three times E_1 and then steadily decreases with increasing energy.

Temporary Non-Dissociative Attachment

The simplest type of non-dissociative electron capture process is illustrated for diatomic molecules in Figure 1d. Electron capture into discrete states of AB^- will occur between energies E_1 and E_2 resulting in a vibrationally excited AB^- molecular ion.

If the capture process remains an isolated event, the electron will be ejected by autodetachment (Auger process) within a time comparable with a vibration time. Diatomic molecular negative ions formed in this manner have never been detected directly because of their short lifetimes, however the existence of these negative ion states are presumed to play a very important role in the interaction of low-energy electrons with molecules. Stabilized negative ions resulting when energy is transferred, e.g., by collisions, have been observed in a number of instances.

A similar, but less understood, mechanism leading to temporary negative ion formation is presented in Figure 1e. The capture process in this case must be distinctly different from that presented in Figure 1d since the potential curve of AB^- does not cross the Franck-Condon region. The mechanism for this process has been described previously as one of vibrational excitation of the neutral molecule and subsequent capture of the incident electron. An alternate description of this capture process might be presented in terms of a non-verticle transition. That is, if the energy of the incoming electron is sufficiently small the interaction time between the electron and molecule would be long enough to allow the nuclei to relax to a position on the curve of the negative ion curve. Such a transition could be called appropriately a "horizontal" transition.

The negative ion curve shown in Figure 1f crosses the Franck-Condon region in a manner which will allow both dissociative and non-dissociative electron attachment. For the particular case represented, the negative ion current will exhibit a sharp rise with energy beginning at E_2, maximize above E_2 and vanish again at E_3. The kinetic energy of the negative ions will range from zero up to

$$KE_{max} = \frac{M_A}{M_A + M_B} \left[EA(B) - D(AB) + E_2 \right]. \qquad (7)$$

Electrons with energies between E_1 and E_2 will be captured into a bound

state of AB^-. In the absence of collision stabilization or radiation the captured electrons will be autodetached within approximately a vibration time of the molecule.

A number of molecules are known to attach electrons by unimolecular electron capture for times greater than a microsecond. These molecules are large and generally symmetric so that the excess energy of the captured electron is shared with the many degrees of freedom of the molecule for a time long enough to be detected in a conventional mass spectrometer. A part of this dissertation will be devoted to a study of these electron capture processes.

Radiative Non-Dissociative Attachment

Electron can be permanently attached to an atom or molecule through radiation of the excess energy of formation (i.e., kinetic energy of the electron and the electron affinity of the atom or molecules). The radiative capture of electrons will exhibit a continuous emission spectrum beginning at an energy equal to the electron affinity of the atom (or verticle detachment energy of the molecule) and extending to indefinitely higher energies.

It has been stated previously that the probability of radiative attachment is extremely small. The argument for this conclusion is as follows: A 10-eV electron is in the field of an atom for approximately 10^{-15} seconds. If one assumes that during this time the electron-atom system has the same

probability of radiating as a bound electron ($\sim 10^8$ per second), then the probability of radiative stabilization is about 10^{-7} per collision. If one considers a very low-energy electron, however, it is conceivable that the electron can remain in the field of the atom for times which are long compared to 10^{-8} seconds and the attachment cross section could be quite large.

Dielectronic Attachment

Dielectronic attachment can best be described as a process in which an incoming electron excites an atom or molecule and is simultaneously captured into a doubly excited state of the negative ion. The negative ion may then (1) eject the attached electron by auto-detachment or (2) become stabilized by the emission of radiation. The probability that the excited ion will be stabilized by radiation would be the lifetime against autodetachment, τ_a, divided by $\tau_a + \tau_r$, where τ_r is the lifetime against radiation. For atoms and molecules autoionization lifetimes are generally much shorter than radiative lifetimes so that in most cases $\tau_a/(\tau_a + \tau_r)$ will be expected to be small. Bates and Massey (1943) have investigated the probability of a doubly excited ion of atomic oxygen becoming stabilized by this process and have found it to be much smaller than the probability for direct radiative capture. It should be emphasized, nevertheless, that under certain conditions autodetachment lifetimes can be quite long. Holøien and Midtdal (1955)

have shown, for example, that the $^4P_{5/2}$ state of He^- is stable toward autoionization and that He^- would be expected to have an autodetachment lifetime approximately equal to that of the ^3S state of He ($\sim 10^{-3}$ seconds). Of course, radiative stabilization of He^- ($^4P_{5/2}$) cannot occur since He (^2S) does not have an electron affinity. However, this does illustrate the possibility of long lifetimes against autoionization when the Pauli principle forbids certain transitions. There is no reason why dielectronic attachment cannot be an important electron capture mechanism for atoms or molecules whose ground state possesses an electron affinity and whose excited state has a long lifetime against autoionization.

It is interesting to consider the range of lifetimes against autodetachment which is predicted by this mechanism. If we approximate the lifetime of the negative ion as the lifetime against radiation of the excited state of the atom or molecule, then quite a large range of lifetimes is predicted. For example, the lifetime can range from approximately 10^{-15} seconds for O^- (^2S) to approximately 10^{-3} seconds for He^- ($^4P_{5/2}$) to a few milliseconds for long lifetime triplet states.

III. SURVEY OF METHODS USED TO STUDY ELECTRON CAPTURE

Numerous experiments have been designed to study electron capture processes and each of the methods have distinct advantages and disadvantages. An excellent review of these various techniques along with a complete list

of specific references has been compiled recently by Fayard (1965). These methods will be only briefly mentioned in the following.

Electron Swarm Method

Basically, swarm experiments measure the rate of removal of electrons from an electron swarm which has an energy distribution characteristic of the carrier (non-attaching) gas and the pressure reduced electric field E/P. The various swarm techniques differ among themselves only in the mode of production of the electrons or the manner in which the number of electrons captured from the swarm are measured. Swarm experiments measure quantities which are averaged over the electron energy distribution. Therefore, the dependence of the attachment process upon electron energy is unknown. Furthermore, swarm experiments do not, generally, lead to identification of particular kinds of processes involved; e.g., the various types of ions formed are not distinguishable in a swarm experiment. Swarm experiments, however, do provide quite accurate determinations of the absolute rate of electron capture.

Electron Beam Method

A detailed survey of electron beam techniques is given in the next section.

Microwave Method

The change in the resonance frequency of a microwave cavity has been shown by Biondi and Brown (1949) to be proportional to the number density of electrons present in the cavity. Thus, from a measurement of the resonance frequency with and without attaching gas in the microwave cavity the attachment coefficient can be calculated. This method is particularly useful in studying thermal electron capture processes.

Electron Avalanche Method

When electron attachment does not take place in an electron avalanche, the current passing between two electrodes separated by a distance d follows the relationship

$$i = i_o e^{\alpha' d} \tag{8}$$

where i is the current reaching the anode, i_o is the original current emitted from the cathode, and α' is Townsend's first ionization coefficient. Harrison and Geballe have shown that when attachment takes place the relationship above is dependent upon the attachment coefficient. Knowing α' and d, it is possible to determine the attachment coefficient under gas discharge conditions. This method is understandably not very sensitive.

IV. SUMMARY OF ELECTRON BEAM STUDIES

Electron beam experiments are designed to study electron capture processes under single collision conditions. A narrow energy beam of electrons of known mean energy is directed into a gas at low pressure ($\sim 10^{-5}$ mm Hg) and the negative ion yield is studied as a function of the electron energy. Oftentimes mass analysis is employed and the dependence of mass identified negative ions on the electron energy is studied. The investigation of negative ion formation by electron beam techniques is attended with many experimental difficulties. Some of the most formidable problems which have arisen include:

1. Difficulties in obtaining monoenergetic electron beams at low energy.
2. Inaccurate calibration of the electron energy scale.
3. The fragment products often possess a large amount of kinetic energy so that the collection efficiency becomes an extremely important factor.
4. Electronegative gases poison the filament and decrease the electron emission.

Negative ion resonances are typically of the order of a volt or two in width so that the use of an electron beam with a very narrow energy spread is essential in obtaining the true energy dependence of the electron capture

processes. The first real advance in high-resolution electron beam techniques was the retarding potential difference (RPD) apparatus developed by Fox, Hickam, Grove, and Kjeldaas (1955).

The RPD method can best be illustrated with the help of Figure 2. The filament (1), the electron beam defining slits (2, 3, 4, 5), ionization chamber (6), and the electron collector (7) are shown with their appropriate potentials connected through the dashed lines. The ionization chamber is at ground potential and the various other electrodes are maintained at a negative potential with respect to ground. The electrode potentials will be indicated "up" from ground so that the electrons which are emitted from the filament may be envisioned as rolling through a valley created by the potentials applied to the various slit electrodes.

Electrons are emitted from the filament and have an electron energy distribution which is a superposition of the thermal energy distribution characteristic of the temperature of the filament upon the energy distribution due to the voltage drop across the filament produced by the heating current. The width of the electron-energy distribution due to the ambient temperature of the filament is generally small compared to the energy spread due to the voltage drop across the filament. The electrons are drawn from the region surrounding the filament by a positive potential applied to the anode (2) and next pass through a slit which is at the potential of the center of the filament. This electrode provides a uniform potential at the

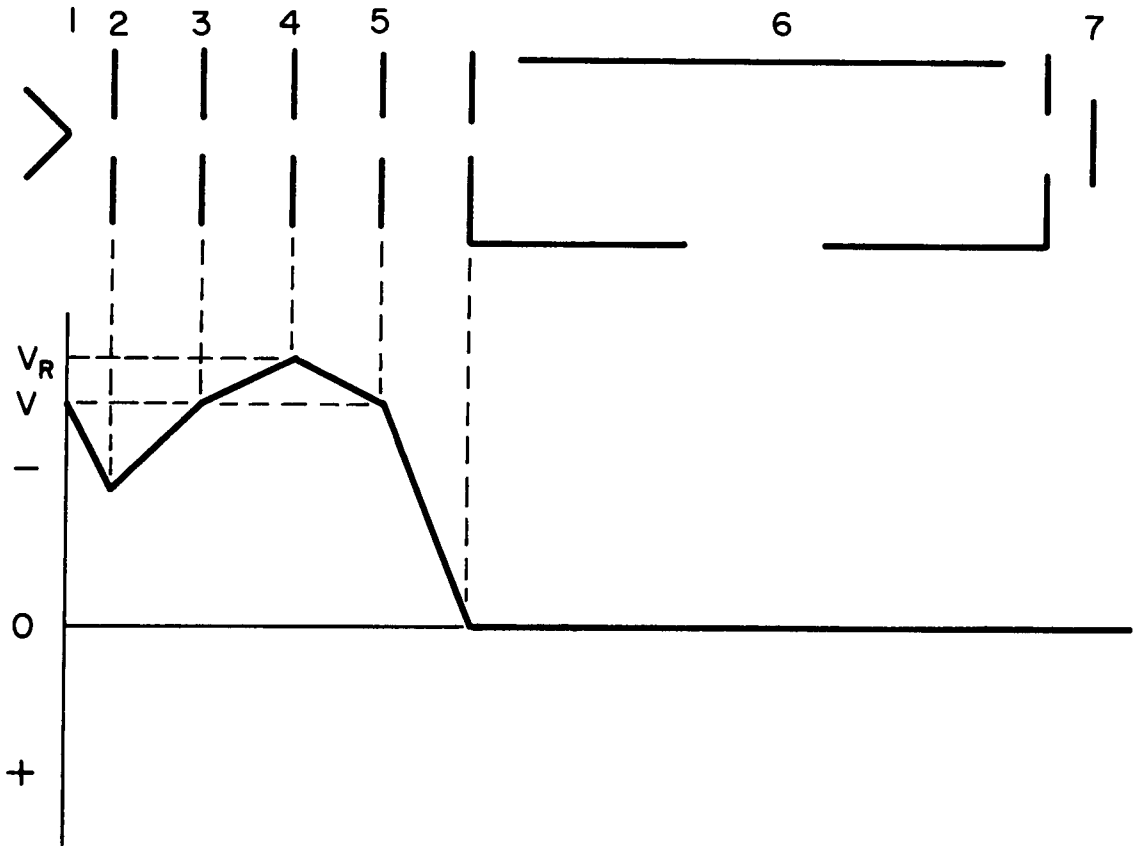

Figure 2. Illustration of the retarding potential difference method.

entrance to the retarding slit (4). The potential of the retarding slit is maintained slightly negative with respect to the center of the filament so that only those electrons which have energies greater than V_R will surmount the potential barrier and enter the ionization chamber. The electron energy distribution will then exhibit a sharp cutoff corresponding to the stopping potential V_R and the energy of the slowest electrons entering the ionization chamber will be the difference in potential between V_4 and ground. If V_4 is decreased by a small amount ΔV_R with respect to the filament, the cutoff energy will be decreased allowing electrons within the energy range $e\Delta V_R$ into the ionization chamber. If the electron filament is held at a constant potential V during the time in which a difference retarding voltage is applied to the retarding electrode, then the difference in the ionization measured will be the ionization produced by a narrow band of electrons of width $e\Delta V_R$ centered around an energy $e(V + \Delta V_R/2)$.

In electron beam experiments an ion drawout field is applied in the ionization chamber to collect the ions which have been formed by electron collision. When this field is applied during the time the electron beam traverses the ion chamber, the electron energy and the electron energy distribution will be seriously affected. This difficulty is easily overcome by pulsing the electron beam gate pulse and the ion drawout pulse out of phase with each other. In this manner the electron beam crosses the ionization chamber under field free conditions and the ions formed by electron collision

are collected a few microseconds later.

The RPD method has been applied to study electron capture processes in three basically different types of apparatus. For future reference these different experiments will be outlined briefly.

Lozier Tube

A schematic diagram of the Lozier type apparatus is shown in Figure 3. Electrons from an RPD source enter the ionization region through the defining slit C. The vanes I and the slits C and L are at ground potential. An ion drawout potential applied to the vanes O serve to aide the collection of negative ions by the cylindrical electrode H. It is important to point out that only those negative ions whose initial direction is within approximately 12° of the perpendicular to the electron beam are collected.

Total Ionization Experiments

Many experimenters have employed a total ionization apparatus to determine absolute electron capture cross sections. The apparatus is similar to that of the Lozier type, however there are no vanes perpendicular to the electron beam which might seriously affect negative ion collection. One such apparatus which was employed by Schulz is reproduced in Figure 3. The ion collector C is held at a slightly positive potential with respect to ground so that a slight field penetration occurs through the grid into the ionization chamber. This insures complete collection of all the ions which

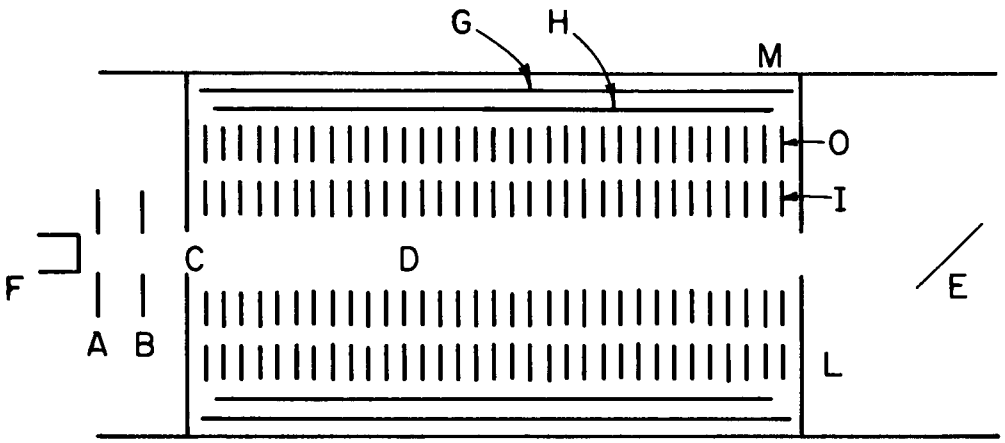

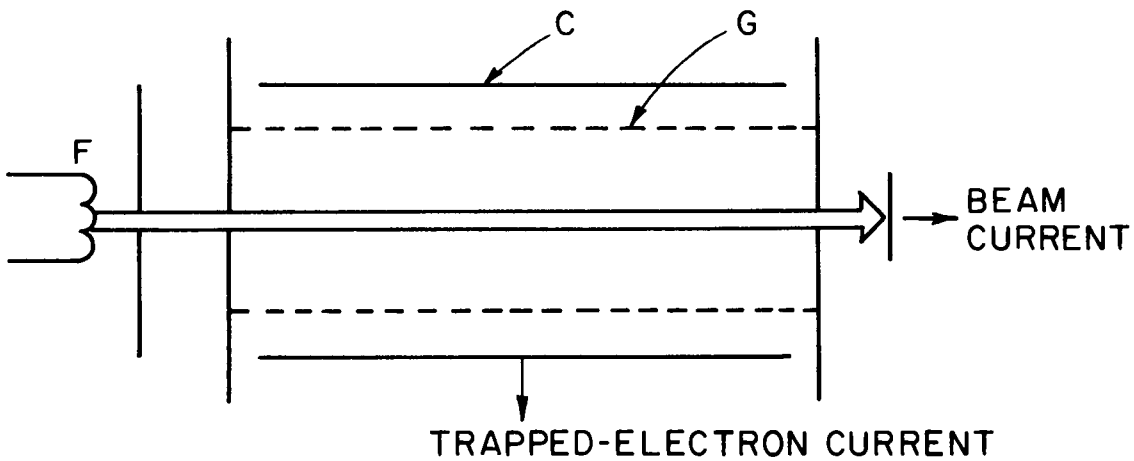

Figure 3. Schematic diagram of Lozier tube and Schulz's total ionization apparatus.

are produced by electron attachment. Unfortunately, electrons which have suffered energy loss through electronic excitation are also collected.

Mass Spectrometric Techniques

Various types of mass spectrometers have employed RPD electron sources to investigate electron capture by electronegative gases. It is virtually impossible to determine electron capture cross sections or ion kinetic energies by this technique, however the appearance potential of ions of specific mass and the dependence of the cross section on electron energy can be determined with a high degree of precision.

It is extremely difficult to determine electron capture cross sections using electron beam techniques. A few of the difficulties encountered have been discussed by Tozer (1958) and will be outlined below.

Electron Path Length

The determination of electron capture cross sections will naturally require a knowledge of the length of the path along which the electron beam is producing ionization. In many experiments the end points of the path length are somewhat difficult to define thereby introducing an error in the measurement of the path length.

Magnetic fields are always used to confine the electron beam in single collision experiments; therefore, any electrons which are non-axial will increase their path length due to the so called "spiralling". The exact

expression for the maximum increase in path length, $(\Delta \ell)_{max}$, for a non-axial electron of energy E emerging from a defining slit of width d along a magnetic field of strength H can be shown to be

$$(\Delta \ell)_{max} = \ell \left[\frac{1 - \sqrt{1 - 2.2 \times 10^{-4} \left(\frac{d^2 H^2}{E} \right)}}{\sqrt{1 - 2.2 \times 10^{-4} \left(\frac{d^2 H^2}{E} \right)}} \right] \tag{9}$$

where H is expressed in gauss, d in mm, and E in electron volts. It is also implicit in the derivation that E is always greater than $2.2 \times 10^{-4}\, d^2 H^2$. When $d^2 H^2/E$ is sufficiently small, Equation (9) reduces to the expression developed by Massey and Burhop (1952), i.e.,

$$\Delta \ell = \ell \left[1.1 \times 10^{-4} \frac{d^2 H^2}{E} \right]. \tag{10}$$

Equations (9) and (10) differ considerably when the electron energy is low. Furthermore, the maximum possible increase is seen to be quite large for low-energy electrons and leads to cross sections which are greater than the true value.

Craggs, Thorburn, and Tozer (1957) were able to eliminate this problem by plotting the difference ion current vs H^2 and extrapolating to $H^2 = 0$.

Space-Charge Effects

Many times it is found that the apparent cross section is a function of the electron current density. The reason for this dependence is not completely understood; however, this difficulty has been eliminated by extrapolating the cross section to zero electron current (zero space-charge) conditions.

Energy Spread of Electrons

The width of the electron beam must be small compared to the width of the electron capture resonance or a gross underestimate of the cross section will be made. This is true particularly for very narrow resonances such as O^- from CO and SF_6^- from SF_6.

Ion Collection Efficiency

The geometry of the apparatus may hinder the complete collection of negative ions (see, for example, the Lozier apparatus in Figure 3, page 20). Also, the existence of anisotropies in the angular distribution of dissociation products may seriously affect the magnitude and shape of the experimentally determined negative ion resonances (see Chapter II, pages 58-62).

Errors in Current and Pressure Measurements

The determination of cross sections always involves uncertainties due to current and pressure measurements, however this proves to be a

particularly important problem in investigation of negative ion formation. This is due to (1) the extremely small currents observed resulting from the small cross sections which are typical of negative ion formation, and (2) space charge difficulties which require low pressures in the reaction region.

Scattered Electrons

In most total ionization experiments, e.g., in the Lozier type apparatus, elastically and inelastically scattered electrons can contribute to the negative ion current which will result in an overestimate of the electron capture cross section.

There has been one investigation reported in the literature which has determined the microscopic attachment cross section $\sigma_c(\epsilon)$ from the macroscopic or mean cross section $\overline{\sigma}_c(\epsilon)$ which is averaged over known energy distributions. This procedure was presented in a series of three papers by Biondi (1958), Fox (1958), and Biondi and Fox (1958) where the electron capture cross section for the case of I^- from I_2 was calculated from a combination of $\overline{\sigma}_c(\epsilon)$ determined from microwave measurements and the energy dependence of $\sigma_c(\epsilon)$ deduced from electron beam experiments.

Table I is a summary of most of the existing data in the literature concerning electron capture by electron beam experiments which have employed the RPD technique. The table gives the ion observed (or in the case

of total ionization experiments, the most probable ion), the appearance potential, the position of the negative ion peak, and the magnitude of the attachment cross section. It should be emphasized that only in the case of total ionization experiments or Lozier type experiments can one place any degree of accuracy on the measured value of the attachment cross section and the cross section measurements reported by mass spectrometer experiments are order of magnitude values only. The last column gives the type of beam experiment which was performed: Lozier Tube (L. T.), Total Ionization (T. I.), or Mass Spectrometer (M. S.).

V. OBJECT OF NEGATIVE ION STUDIES

The objects of the present investigation are:

1. To develop a method which combines the better qualities of the electron swarm and electron beam techniques to obtain electron capture cross sections as a function of the electron energy.
2. To use this method to obtain the electron attachment cross sections for oxygen, water, and a series of halogenated hydrocarbons.
3. To establish the existence of long-lived ($\tau > 10^{-6}$ seconds) temporary negative ions and to determine their half lives.
4. To set up a theoretical model which will describe non-dissociative electron capture by complex molecules and to compare the theory with experiments on cross sections and lifetimes.

TABLE I

SUMMARY OF RETARDING POTENTIAL DIFFERENCE NEGATIVE ION STUDIES

Molecule	Reference	Products	Appearance Potential (eV)	Position of Maximum (eV)	Cross Section (cm^2)	Apparatus
H_2	a	$H^- + H$ $H^- + H^*$	13.8 ± 0.2	10.0 14.2	1.2×10^{-20} 3.5×10^{-20}	T.I.
	b	$H^- + H^*$		13.9	2.22×10^{-20}	
HD	b	$(H^-+D)+(D^-+H)$		13.95	1.56×10^{-20}	T.I.
D_2	b	$D^- + D$		14	1.07×10^{-20}	T.I.
O_2	c	$O^- + O$ $O^- + O^+ + e$ $O^- + O^{+*} + e$	4.53 ± 0.03 17.4 21.3	5.98		M.S.
	d	$O^- + O$	4.4	6.7	1.3×10^{-18}	T.I.
	e	$O^- + O$	3.75	6.2		?
	f	$O^- + O$	4.7	6.7	2.25×10^{-18}	L.T.
	g	$O^- + O$	4.63	6.2	1.3×10^{-18}	T.I.

TABLE I (continued)

Molecule	Reference	Products	Appearance Potential (eV)	Position of Maximum (eV)	Cross Section (cm^2)	Apparatus
O_2	h	$O^- + O$	4.3	6.7		M.S.
	i	$O^- + O$		6.5	1.5×10^{-18}	T.I.
	j	$O^- + O$ $O^- + O^+ + e$ $O^- + O^{+*} + e$	4.9 17.1 20.2			M.S.
HCl	k	$Cl^- + H$ $Cl^- + H^+ + e$	0.66 ± 0.02 14.5 ± 0.1	0.66		M.S.
	l	$Cl^- + H$	0.62 ± 0.05	0.77		M.S.
	g	$Cl^- + H$	0.46 ± 0.02	0.60	3.9×10^{-18}	T.I.
HBr	g	$Br^- + H$	0.43 ± 0.01	0.50	5.8×10^{-17}	T.I.
	l	$Br^- + H$	0.10 ± 0.05	0.21 ± 0.05		M.S.
HI	l	$I^- + H$	0.03 ± 0.03	0.05 ± 0.05		M.S.
HF	l	$F^- + H$	1.88 ± 0.06	4.0 ± 0.2		M.S.

TABLE I (continued)

Molecule	Reference	Products	Appearance Potential (eV)	Position of Maximum (eV)	Cross Section (cm^2)	Apparatus
Cl_2	m	$Cl^- + Cl$ $Cl^- + Cl^+ + e$	1.6 ± 0.05 11.93 ± 0.06	2.4 ± 0.1		M. S.
Br_2	m	$Br^- + Br$ $Br^- + Br^+ + e$ $Br^- + Br^+ + e$	0.03 ± 0.03 10.34 ± 0.04 12.27 ± 0.05	0.03 ± 0.03		M. S.
I_2	m, n	$I^- + I$ $I^- + I^+ + e$	0.03 ± 0.03 8.67 ± 0.07	0.34 ± 0.07		M. S.
	o, p	$I^- + I$	0.03 ± 0.03	0.03 ± 0.03	3×10^{-15}	T. I., M.S.
F_2	q	$F^- + F$	~ 0	0.45		M. S.
CO	d	$O^- + C$	9.4	10.1	1.6×10^{-19}	T. I.
	r	$O^- + C$	9.35	10.1	2.7×10^{-19}	L. T.
	i	$O^- + C$		9.9	2.3×10^{-19}	T. I.
	s	$O^- + C$ $O^- + C^+$ $O^- + C^+$	9.5 20.95 23.65	10.94		L. T.

TABLE I (continued)

Molecule	Reference	Products	Appearance Potential (eV)	Position of Maximum (eV)	Cross Section (cm^2)	Apparatus
CO	t	$O^- + C$	9.39 ± 0.05 20.92 ± 0.05 22.47 ± 0.05	10.07		M.S.
NO	u	$O^- + N$	6.99 ± 0.05			M.S.
	v	$O^- + N$ $O^- + N^+ + e$	7.18 ± 0.06 19.5 ± 0.2			T.I.
	i	$O^- + N$		8.15	1.27×10^{-18}	T.I.
LiF	w	$Li^- + F$ $Li^- + \cancel{F}\ Li_2F$ $Li_2F + \cancel{Li} + F^-$ $LiF + Li + F^-$	5.71 7.66 3.55 6.5			M.S.
LiCl	w	$Li^- + Cl$ $Li^- + Cl$ $Li + Cl^-$ $Li + Cl^-$	4.63 6.10 3.36 5.60			M.S.
LiBr	w	$Li^- + Br$ $Li^- + Br$ $Li + Br^-$	4.09 5.35 4.85			M.S.

TABLE I (continued)

Molecule	Reference	Products	Appearance Potential (eV)	Position of Maximum (eV)	Cross Section (cm^2)	Apparatus
LiI	w	$Li^- + I$	3.27			M. S.
		$Li^- + I$	4.55			
		$Li + I^-$	3.95			
NaF	w	$Na^- + F$	4.66			M. S.
		$Na^- + F$	6.30			
		$Na + F^-$	2.55			
		$Na + F^-$	5.25			
NaCl	w	$Na^- + Cl$	4.04			M. S.
		$Na + Cl^-$	2.90			
NaBr	w	$Na^- + Br$	3.36			M. S.
		$Na + Br^-$	3.75			
NaI	w	$Na^- + I$	2.84			M. S.
		$Na + Br^-$	3.25			
KF	w	$K^- + F$	4.78			M. S.
		$K + F^-$	2.40			
		$K^* + F^-$	5.60			
KCl	w	$K^- + Cl$	3.93			M. S.
		$K + Cl^-$	2.60			
		$K^* + Cl^-$	4.50			

TABLE I (continued)

Molecule	Reference	Products	Appearance Potential (eV)	Position of Maximum (eV)	Cross Section (cm^2)	Apparatus
KBr	w	$K^- + Br$ $K + Br^-$	3.36 3.80			M.S.
KI	w	$K^- + I$ $K + I^-$	2.85 3.20			M.S.
RbCl	w	$Rb^- + Cl$	4.00			M.S.
RbBr	w	$Rb^- + Br$ $Rb + Br^-$	3.44 3.85			M.S.
RbI	w	$Rb^- + I$ $Rb + I^-$	2.90 3.30			M.S.
CsF	w	$Cs^- + F$	5.10			M.S.
CsCl	w	$Cs^- + Cl$	4.20			M.S.
CsBr	w	$Cs^- + Br$	3.55			M.S.
CsI	w	$Cs^- + I$	3.01			M.S.

TABLE I (continued)

Molecule	Reference	Products	Appearance Potential (eV)	Position of Maximum (eV)	Cross Section (cm^2)	Apparatus
CO_2	d	$O^- + CO$ $O^- + CO$	3.85 6.6	4.4 8.2	1.5×10^{-19} 4.5×10^{-19}	T.I.
	h	$O^- + CO$ $O^- + CO$	3.8 6.6	4.4 8.4		M.S.
	x	$O^- + CO$	6.7	7.8	$5.07 \pm 0.5 \times 10^{-19}$	L.T.
	y	$O^- + CO$ $O^- + CO$	3.96 ± 0.1 7.0 ± 0.2			M.S.
	i	$O^- + CO$ $O^- + CO$		4.3 8.1	1.7×10^{-19} 4.9×10^{-19}	T.I.
H_2O	g	$H^- + OH$ $H^- + \ldots$		6.4 8.6	4.8×10^{-18} 1.3×10^{-18}	T.I.
	v	$H^- + OH$ $H^- + \ldots$ $O^- + \ldots$		6.5 ± 0.1 8.8 ± 0.1 12.0		T.I.

TABLE I (continued)

Molecule	Reference	Products	Appearance Potential (eV)	Position of Maximum (eV)	Cross Section (cm^2)	Apparatus
H_2S	y	$S^- + H_2$	2.15 ± 0.15			M. S.
		$S^- + \ldots$	5.35 ± 0.15			
		$S^- + \ldots$	8.1 ± 0.2			
		$HS^- + \ldots$	2.19			
CS_2	y	$S^- + CS$	3.04 ± 0.1			M. S.
		$S^- + \ldots$	5.6 ± 0.15			
		$S^- + \ldots$	7.2 ± 0.2			
		$CS^- + S$	5.5 ± 0.1			
		$C^- + \ldots$	6.2 ± 0.2			
		$C^- + \ldots$	7.5 ± 0.3			
SO_2	y	$O^- + SO$	4.21 ± 0.1			M. S.
		$O^- + \ldots$	6.6			
		$SO^- + O$	4.58 ± 0.1			
		$SO^- + \ldots$	7.1			
		$S^- + \ldots$	3.75 ± 0.15			
NH_3	y	$NH_2^- + H$	5.19 ± 0.1			M. S.
NO_2	z	$O^- + NO$	1.35 ± 0.05	1.90	$\sim 10^{-18}$	M. S.
		$O^- + \ldots$	~ 2.5	3.0		
		$O^- + \ldots$	7.5 ± 0.3	8.75		

TABLE I (continued)

Molecule	Reference	Products	Appearance Potential (eV)	Position of Maximum (eV)	Cross Section (cm^2)	Apparatus
N_2O	aa	$O^- + N_2$ $N_2O^{-*} \rightarrow O^- + N_2^*$	0	0.7		T. I.
	bb	$O^- + N_2$	0			M. S.
	i	$O^- + N_2$		2.2	9.78×10^{-18}	T. I.
PH_3	cc	$H^- + \ldots$ $H^- + \ldots$	5.4 ± 0.1 7.5 ± 0.2			M. S.
		$P^- + \ldots$ $P^- + \ldots$	5.7 ± 0.2 8.3 ± 0.3		3×10^{-19}	
		$PH^- + \ldots$ $PH^- + \ldots$ $PH^- + \ldots$	(2.1 ± 0.2) 6.3 ± 0.3 8.1 ± 0.3		2×10^{-18}	
		$PH_2^- + H$	2.3 ± 0.1 5.2 ± 0.2		4×10^{-18}	
AsH_3	cc	$AsH_2^- + H$	2.0 ± 0.1 5.2 ± 0.2		6×10^{-18}	M. S.

TABLE I (continued)

Molecule	Reference	Products	Appearance Potential (eV)	Position of Maximum (eV)	Cross Section (cm^2)	Apparatus
AsH_3	cc	$AsH^- + H_2$	2.0 ± 0.1		3×10^{-18}	M. S.
		$AsH^- + \ldots$	6.2 ± 0.3			
		$As^- + H_3$	5.3 ± 0.2		9×10^{-19}	
		$As^- + \ldots$	7.8 ± 0.3			
		$H^- + AsH_2$	5.3 ± 0.1			
		$H^- + \ldots$	7.4 ± 0.3			
SiH_4	cc	$SiH_3^- + H$	7.0 ± 0.2		2×10^{-18}	M. S.
		$SiH_2 + \ldots$	8.0 ± 0.2		1×10^{-18}	
		$SiH^- + \ldots$	7.9 ± 0.2		7×10^{-19}	
		$Si^- + \ldots$	8.2 ± 0.2		2×10^{-19}	
		$H^- + \ldots$	7.9 ± 0.2			
O_3	dd	$O^- + O_2$	0		10^{-17} to 10^{-18}	M. S.
		$O_2^- + O$	0.42 ± 0.03			
SF_6	ee	SF_6^-	0.0	< 0.05	$\sim 10^{-15}$	M. S.
		$SF_5^- + F$	0.0	< 0.10	$\sim 10^{-17}$	

TABLE I (continued)

Molecule	Reference	Products	Appearance Potential (eV)	Position of Maximum (eV)	Cross Section (cm^2)	Apparatus
SF_6	ff	SF_6^- SF_5^- F^-	{0.0	{0.03 ± 0.03	$\sim 1.3 \times 10^{-15}$	T.I.
	g	SF_6^- SF_5^- F^-	{~0	{~0	5.7×10^{-16}	T.I.
	gg	SF_6^- SF_5^- SF_4^- SF_3^- F^-	~0 ~0 ? ? ?	~0 ~0 ~5 ~10 ?		M.S.
	i	SF_6^- SF_5^- F^-	{0	0.1	2.4×10^{-16}	T.I.

TABLE I (continued)

Molecule	Reference	Products	Appearance Potential (eV)	Position of Maximum (eV)	Cross Section (cm^2)	Apparatus
CF_3I	g	I^- (?)		0.05 0.9	7.8×10^{-17} 3.2×10^{-17}	T. I.
CCl_2F_2	g	Cl^- (?)		0.15	5.4×10^{-17}	T. I.
BCl_3	g	Cl^- (?)		0.4	2.8×10^{-17}	T. I.
CCl_4	g	Cl^- (?)		0.02 0.60	1.3×10^{-16} 1.0×10^{-16}	T. I.
CCl_4	hh	Cl^- Cl^-	0.0 0.40	0.0 0.75		M. S.
C_7F_{14}	ff	$C_7F_{14}^-$ $C_7F_{13}^-$ $C_6F_{11}^-$	$\{\sim 0$	0.15	7.5×10^{-15}	T. I.
$SbCl_3$	ii	$Cl^- + SbCl_3$(?)	~0.01		1.8×10^{-16}	T. I.

TABLE I (continued)

Molecule	Reference	Products	Appearance Potential (eV)	Position of Maximum (eV)	Cross Section (cm^2)	Apparatus
CCl_3F	jj	$Cl^- + CCl_2F$	0			M. S.
		$F^- + CCl_3$	1.80 ± 0.10			
		$CCl_3^- + F$	2.75 ± 0.10			

[a] G. J. Schulz, Phys. Rev. 113, 816 (1959).

[b] D. Rapp, T. E. Sharp, and D. D. Briglia, Phys. Rev. Letters 14, 533 (1965).

[c] D. C. Frost and C. A. McDowell, J. Am. Chem. Soc. 80, 6183 (1958).

[d] G. J. Schulz, Phys. Rev. 128, 178 (1962).

[e] P. L. Randolph and R. Geballe, thesis, University of Washington, 1958.

[f] J. D. Craggs, C. Thorburn, and B. A. Tozer, Proc. Roy. Soc. (London) A240, 473 (1957).

[g] I. S. Buchel'nikova, Soviet Phys.—JETP 35 (8), 783 (1959).

[h] R. K. Curran as reported by G. J. Schulz, Phys. Rev. 128, 178 (1962).

References to Table I (continued)

[i]D. Rapp and D. D. Briglia, J. Chem. Phys. 43, 1480 (1965).

[j]R. Thorburn, Applied Mass Spectroscopy (The Institute of Petroleum, London, 1954), p. 185.

[k]R. E. Fox, J. Chem. Phys. 26, 1281 (1957).

[l]D. C. Frost and C. A. McDowell, J. Chem. Phys. 29, 5-3 (1958).

[m]D. C. Frost and C. A. McDowell, Can. J. Chem. 38, 406 (1960).

[n]D. C. Frost and C. A. McDowell, J. Chem. Phys. 29, 964 (1958).

[o]R. E. Fox, Phys. Rev. 109, 2008 (1958).

[p]M. A. Biondi and R. E. Fox, Phys. Rev. 109, 2012 (1958).

[q]J. F. Burns, Carbide and Carbon Chemical Company Report K-1147 (1954).

[r]J. D. Craggs and B. A. Tozer, Proc. Roy. Soc. (London) A247, 337 (1958).

[s]M. A. Fineman and A. W. Petrocelli, J. Chem. Phys. 36, 25 (1962).

[t]C. R. Lagergren, thesis, University of Minnesota, 1955 (unpublished).

[u]D. C. Frost and C. A. McDowell, J. Chem. Phys. 29, 1424 (1958).

[v]G. J. Schulz, J. Chem. Phys. 33, 1661 (1960).

References to Table I (continued)

[w]H. Ebinghaus, Z. Naturforschung 19a, 727 (1964).

[x]J. D. Craggs and B. A. Tozer, Proc. Roy. Soc. (London) A254, 229 (1960).

[y]K. Kraus, Z. Naturforschung 16a, 1378 (1961).

[z]R. E. Fox, J. Chem. Phys. 32, 285 (1960).

[aa]G. J. Schulz, J. Chem. Phys. 34, 1778 (1961).

[bb]R. K. Curran and R. E. Fox, J. Chem. Phys. 34, 1590 (1961).

[cc]H. Ebinghaus, K. Kraus, W. Müller-Duysing, and H. Neuert, Z. Naturforschung 19a, 732 (1964).

[dd]R. K. Curran, J. Chem. Phys. 35, 1849 (1965).

[ee]W. M. Hickam and R. E. Fox, J. Chem. Phys. 25, 642 (1956).

[ff]R. K. Asundi and J. D. Craggs, Proc. Phys. Soc. (London) 83, 611 (1964).

[gg]D. Edelson, J. E. Griffiths, and K. B. McAfee, Jr., J. Chem. Phys. 37, 917 (1962).

[hh]R. E. Fox and R. K. Curran, J. Chem. Phys. 34, 1595 (1961).

[ii]V. E. Grob, J. Chem. Phys. 39, 972 (1963).

[jj]R. K. Curran, J. Chem. Phys. 34, 2007 (1961).

CHAPTER II

THEORY OF ELECTRON CAPTURE

Theoretical descriptions of electron capture have been formulated in two manners: (1) coupling of electronic and nuclear motion and (2) resonance capture. There are at present no review articles to refer to on this subject. In fact, the resonance capture formalism has arisen only in the past two years. For this reason it will be of interest to present a detailed survey of these existing theories of electron attachment.

Bloch and Bradbury (1935) and Massey (1950) discussed the physical grounds for the process of electron capture by arguing that the influence of the kinetic energy of the nuclei on the electron wave functions gives rise to transitions resulting in electron capture. Stanton (1960) verified this statement by showing that capture is possible due to the breakdown of the separation of nuclear and electronic motion in the Schrödinger equation, i.e., the nuclear kinetic energy operator is the perturbation operator. Chen (1963) has presented a distorted wave method for calculating dissociative attachment cross sections using the kinetic energy operator as the perturbing term in the Hamiltonian. Using this procedure, Chen determined the dissociative attachment cross section for the reaction $e + H_2 \rightarrow H + H^-$. Unfortunately, Chen's results were ambiguous because of uncertainties in the potential curves of H_2^- ($^2\Sigma_u^+$) [see footnote 31 of Chen (1963)]. However, when the

effective nuclear potential of $H_2^-(^2\Sigma_u^+)$ was approximated by a Morse curve, good agreement was found between the calculated and experimental attachment cross sections for the reaction $e + H_2 \rightarrow H + H^-$. This agreement between theory and experiment gives added support to the notion that coupling terms between the electronic and nuclear motion are responsible for dissociative electron capture. The inclusion of these coupling terms has provided explanations for other diverse phenomena such as predissociation [Kronig (1928)] and Λ-type doubling [Van Vleck (1929)].

Recently efforts have been made to formulate the theory of electron capture in terms of resonance electron scattering [see, for example: Bardsley et al. (1964), Bardsley et al. (1965), Herzenberg (1965), and O'Malley (1965)]. The mathematical framework of these treatments was borrowed from existing theories in nuclear physics which treat resonance neutron scattering. In particular, the calculations of Bardsley et al. (1964, 1965) and Herzenberg (1965) were carried out through a modification of the Kapur-Peierls (1938) formalism originally developed for resonance scattering in nuclear physics and the treatment of O'Malley (1965) used the Feshbach (1962) definition of a resonance to calculate electron capture cross sections. These methods do not take into account the non-adiabatic terms in the Hamiltonian involving the nuclear kinetic energy and the connection between the two different theories is not understood at the present time. Along this line O'Malley (1965) has pointed out that when one explicitly allows for a

resonance state between the electron-molecule system, the electrostatic interaction is responsible for the attachment transition and not the kinetic energy operator.

In the following discussion the underlying principles of each of the above theories will be outlined and the results will be discussed with respect to existing experimental data.

Referring to the treatment of Stanton (1960), it can be shown in the following manner that it is impossible to account for electron capture in terms of the electrostatic interaction between the electron and the molecule and that capture is possible only through the breakdown of the separation of the nuclear and electronic wave functions.

The Schrödinger equation for the initial or final (electron plus neutral molecule or negative ion) state would be

$$\mathcal{H}\Psi = i\hbar\left(\frac{\partial\Psi}{\partial t}\right) \tag{11}$$

where $\mathcal{H}$, the total Hamiltonian, is equal to the Hamiltonian for the electronic energy, $\mathcal{H}^e$, and the Hamiltonian for the nuclear energy, $\mathcal{H}^n$, i.e.,

$$\mathcal{H} = \mathcal{H}^e + \mathcal{H}^n \tag{12}$$

$$\mathcal{H}^e = -\sum_i \left(\frac{\hbar^2}{2m_e}\right)\nabla_i^2 + V_{ne} + V_{ee} \tag{13}$$

$$\mathcal{H}^n = -\sum_\alpha \left(\frac{\hbar^2}{2m_\alpha}\right)\nabla_\alpha^2 + V_{nn}\,. \tag{14}$$

Using MO notation, the total wave function can be written as a product,

$$\Psi = \sum_i x_i \vec{\xi}_i \sum_j y_{ij} \vec{\eta}_{ij} e^{-iw_{ij}t} \tag{15}$$

where the x_i and y_{ij} are probability amplitudes for the electronic eigenfunction $\vec{\xi}_i$ and the nuclear motion eigenfunctions, $\vec{\eta}_{ij}$, respectively.

Since the $\vec{\xi}_i$'s are defined to be eigenfunctions of $\mathcal{H}^e$ and the $\vec{\eta}_{ij}$'s are eigenfunctions of $\mathcal{H}^n$ plus the electronic energy for the ith configuration, we have

$$\mathcal{H}^e \vec{\xi}_i = E_i^e \vec{\xi}_i \tag{16}$$

and

$$\left(\mathcal{H}^n + E_i^e\right)\vec{\eta}_{ij} = E_{ij} \vec{\eta}_{ij}. \tag{17}$$

Substitution of (15) into (11) and utilizing (16) and (17) results in

$$\sum \dot{x}_i \vec{\xi}_i \sum y_{ij} \vec{\eta}_{ij} e^{-iw_{ij}t} + \sum x_i \vec{\xi}_i \sum \dot{y}_{ij} \vec{\eta}_{ij} e^{-iw_{ij}t} = 0 \tag{18}$$

where all derivatives of the electronic eigenfunctions with respect to the nuclear coordinates have been ignored, i.e.,

$$\frac{\partial \vec{\xi}_i}{\partial R} \cong 0 . \tag{19}$$

This is equivalent to saying that the motion of the electrons is the same as it would be if the nuclei were not allowed to move. Stanton refers to this as the adiabatic approximation as opposed to the slightly different

Born-Oppenheimer separation approximation [Born and Oppenheimer (1927)].

Because of the linear independence of the function in Equation (18), the only solution is

$$\dot{x}_i = \dot{y}_{ij} = 0 \tag{20}$$

and since x_i and y_{ij} are time independent, there can be no transitions occurring between the eigenfunctions of $\mathcal{H}^e$. This result has the importance that within the adiabatic approximation capture of a free electron is impossible. Briefly, the argument for this conclusion is as follows:

Consider the problem of attachment of a free electron to a molecule. The total wave function can be written as the sum of all possible bound states and free states, i.e.,

$$\Psi = \sum x_i \vec{\xi}_i \sum y_{ij} \vec{\eta}_{ij} e^{-iw_{ij}t} . \tag{21}$$

If we begin at $t = 0$ with the electron being very far away from a molecule, the wavefunction will be vanishingly small if the coordinates of the bound and unbound electrons are assigned values in the neighborhood of the nuclei. Consequently, the overlap integral between $\Psi_{(t=0)}$ and $\vec{\xi}_B$ will be zero. The original wavefunction, therefore, contains no contribution from a negative ion state at $t = 0$ and since $\dot{x}_i = 0$, a negative ion state can never occur. Notice also that in cases where $\vec{\xi}_B$ might extend to infinity it does so at the expense of being infinitesimal over all space and since $\Psi_{(t=0)}$

is localized, the overlap between $\vec{\xi}_B$ and $\Psi_{(t=0)}$ again vanishes.

This demonstrates that within the adiabatic approximation $\left(\text{i.e., } \frac{\partial \xi_i}{\partial R} \approx 0\right)$ capture of a free electron by a neutral molecule is impossible. When the adiabatic approximation is removed, however, the neglected terms can be treated as a perturbation and will produce interactions between electronic and nuclear motion leading to electron capture. In order to develop an expression for the electron capture cross section, it is convenient to turn to the distorted wave treatment of Chen (1963).

The Schrödinger equation for N-electrons, whose coordinates are referred to the center of mass of the nuclei, and two nuclei of mass m_1 and m_2, is

$$\left(-\frac{1}{2\mu}\nabla_R^2 + \mathcal{H}\right)\Psi = i\frac{\partial \Psi}{\partial t} \tag{22}$$

where

$$\mathcal{H} = \frac{1 + m_1 + m_2}{2(m_1 + m_2)} \sum_{i=1}^{N} \nabla_i^2 + V_{total}, \tag{23}$$

V_{total} is the total potential energy of the system, and ∇_R^2 is the Laplacian with respect to the internuclear separation.

If the nuclei are held fixed, the Schrödinger equation for the electronic energy is

$$\mathcal{H}\psi_n(\vec{r}, \vec{R}) = \mathcal{E}_n(\vec{R})\,\psi_n(\vec{r}, \vec{R}) \tag{24}$$

and the wavefunction for the total system can be written as a sum of

products,

$$\Psi = \sum_n \int \chi_n(\vec{R})\, \psi_n(\vec{r}, \vec{R}) \tag{25}$$

where $\chi_n(\vec{R})$ is the wavefunction for the relative nuclear motion.

Substituting Equation (25) into Equation (24) and including terms involving the derivative of the electronic wavefunction with respect to the nuclear separation, we obtain a set of equations for the nuclear wavefunctions:

$$\left\{\nabla_R^2 + 2\mu \left[E_n - V_{n(\vec{R})}\right]\right\} \chi_{n(R)} = -\sum \left[2 \langle \psi_n | \nabla_R | \psi_{n'} \rangle \nabla_R + \langle \psi_n | \nabla_R^2 | \psi_{n'} \rangle\right] \chi_{n'(\vec{R})} \tag{26}$$

where E_n is the total energy and $V_{n(\vec{R})}$ is the effective nuclear potential energy obtained by including the diagonal coupling terms into the electronic energy $\mathcal{E}_{n(\vec{R})}$.

Neglecting all non-diagonal matrix elements in (26) except the initial state $n' =$ "0" and the final state $n =$ "f", we have

$$\left\{\nabla_R^2 + 2\mu \left[E_f - V_{f(\vec{R})}\right]\right\} \chi_{f(R)} = -\left[2 \langle \psi_f | \nabla_R | \psi_o \rangle \nabla_R + \langle \psi_f | \nabla_R^2 | \psi_o \rangle\right] \chi_{o(\vec{R})} \tag{27}$$

where χ_f and χ_o are solutions to the original and final distorted wave equations,

$$\left[\nabla_R^2 + 2\mu\, \mathcal{E}_{o(\vec{R})}\right] \chi_{o(\vec{R})} = 0 \tag{28}$$

$$\left[\nabla_R^2 + 2\mu\, \varepsilon_{f(\vec{R})}\right] \chi_{f(\vec{R})} = 0 \,. \tag{29}$$

The differential cross section $d\sigma_{fo}(\theta_o, \varphi_o)$ is, therefore,

$$d\sigma_{fo}(\theta_o, \varphi_o) = \left(\frac{g}{16\,\Pi^2\, k_o}\right) \left| \langle \chi_f | 2 \langle \psi_f | \nabla_R | \psi_o \rangle \nabla_R + \langle \psi_f | \nabla_R^2 | \psi_o \rangle | \chi_o \rangle \right|^2 d\Omega_f \tag{30}$$

where g = 1 or 2 for heteronuclear or homonuclear diatomic molecules, respectively, k_o is the magnitude of the incoming electron's propagation vector and $d\Omega_f$ is the differential solid angle for the final state.

Chen applied this method to calculate the electron capture cross section for the reaction $e + H_2 \rightarrow H + H^-$. Figure 4 shows the matrix elements $\langle \chi_f | \chi_o \rangle$ and $\langle \chi_f | \nabla_R | \chi_o \rangle$ needed for the calculation. Figure 5 shows the cross section obtained when the potential curve for H_2^- $(^2\Sigma_u^+)$ was approximated by a Morse curve compared with the experimental results of Schulz (1959a). As was pointed out earlier, the magnitude of the theoretical attachment cross section is of the same order as the experimental measurements. Of equal significance is the prediction of two maxima of almost equal magnitude in the calculated cross section. The two maxima are a consequence of the matrix elements $\langle \chi_f | \nabla_R | \chi_o \rangle$ (see Figure 4). The result that two peaks can occur from a single negative ion state is highly significant. For instance, structure in negative ion cross sections can be explained

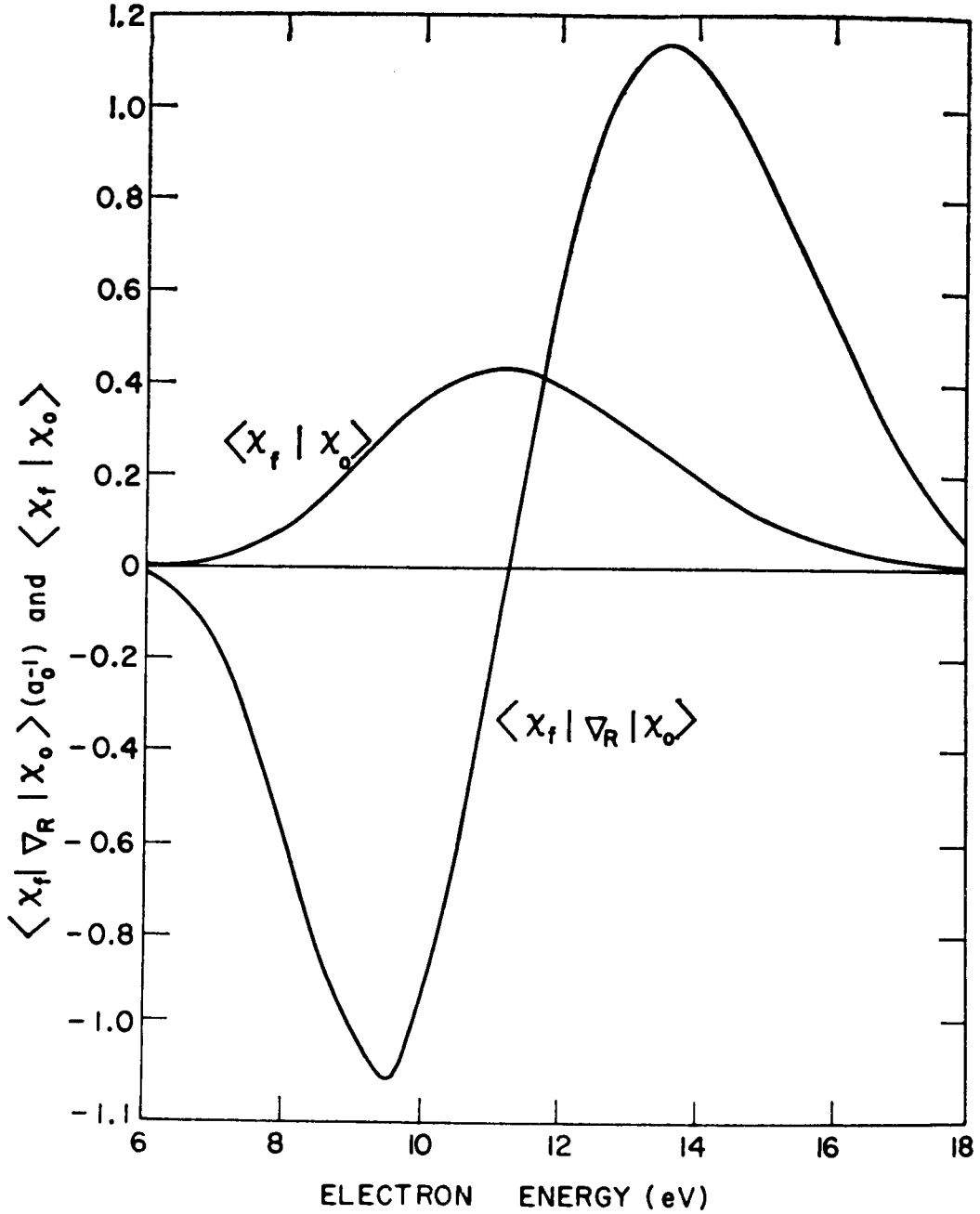

Figure 4. Plot of the overlap integral $\langle \chi_f | \chi_o \rangle$ and the gradient matrix elements, $\langle \chi_f | \nabla_R | \chi_o \rangle$, for the continuous and ground nuclear wave functions of H_2^- and H_2. The potential curve for H_2^- was approximated by a Morse curve [taken from Chen (1963)].

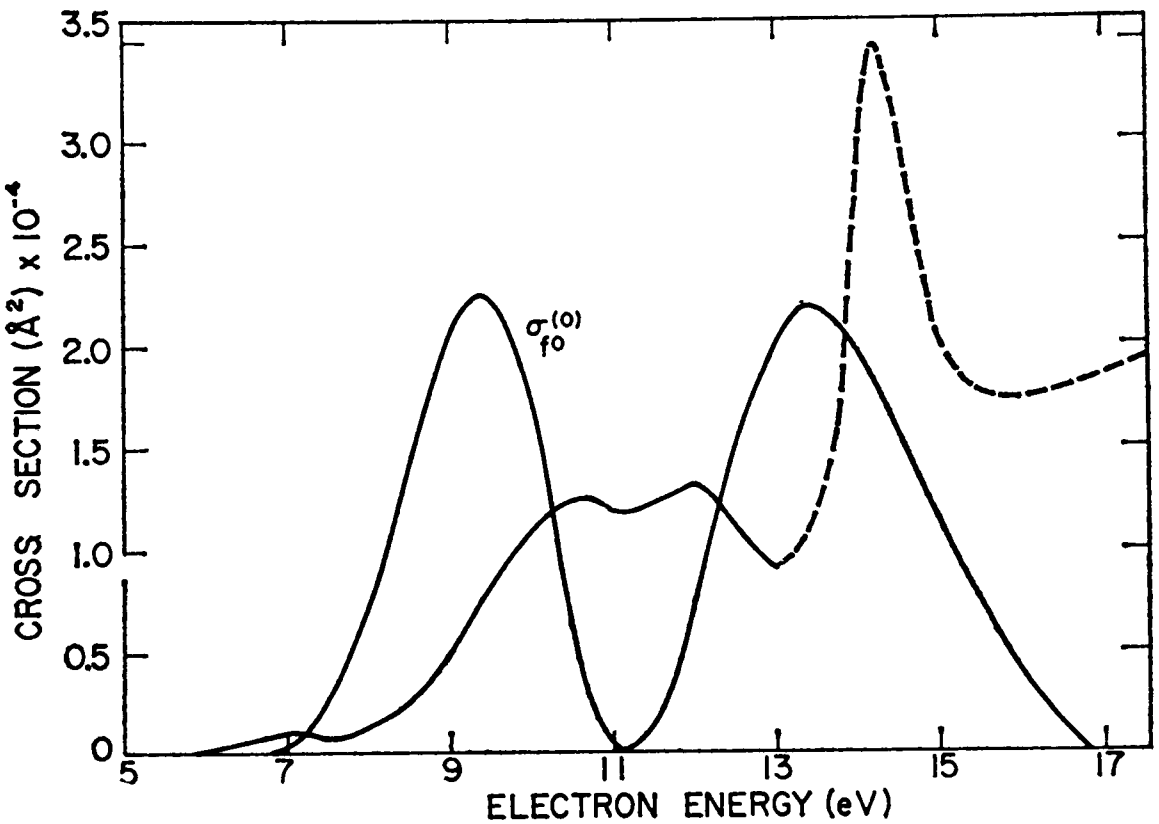

Figure 5. Comparison of the experimental and theoretical cross section curves for the reaction $e + H_2 \rightarrow H + H^-$ with H and H^- in their ground states [taken from Chen (1963)].

without reference to excited states. In particular, the structure in the experimental cross section at ~ 11 eV for H^- from H_2 can be explained by the gradient matrix elements $\langle \chi_f | \nabla_R | \chi_o \rangle$ of $|\mathcal{H}_{fo}|$ and no violence is done to the selection rules developed by Stanton (1960) which predicts that electron capture into the gerade state of H_2^- $(^2\Sigma_g^+)$ is forbidden.

The contribution of the non-scalar matrix elements $\langle \chi_f | \nabla_R | \chi_o \rangle$ has one other consequence which should be mentioned. It has often been stated by investigators in the field of negative ion research that "the yield of negative ions as a function of electron energy should be a reflection of the ground vibrational state of the neutral molecule upon the potential energy curve of the negative ion". In view of Chen's results, this is a gross misstatement and the "reflection" could be greatly distorted.

One further comment concerning the validity of the use of the kinetic energy operator to describe electron capture might be made. Bloch and Bradbury (1935) also found their electron capture data for O_2 to be consistent with the assumption that capture of an electron by a transition from a free state into a bound state is a result of weak coupling between the electronic and nuclear motion.

The application of resonance scattering to the problem of electron capture was first introduced by Bardsley, Herzenberg, and Mandl (1964). BHM employed the WKB approximation to solve the Schrödinger equation and obtain an expression for dissociative electron capture cross sections. The

resonance peaks in the cross section are obtained by assuming that for each peak the wave function is given by a single electron resonance when the electron is in the internal regions of the molecule. It is emphasized that coupling between the nuclear and electronic motion is not needed to produce a resonant ion since the wave function would be of a resonance form in the vicinity of a resonance energy even if the nuclei are not allowed to move.

In the internal region of the molecule resonance electron states, ψ_n, are defined which are functions of the electron space and spin coordinates and the internuclear separation $(\vec{R})$ in the usual sense of the Born-Oppenheimer approximation. Since the resonance formalism is concerned only with the electronic motion, we can write

$$\mathcal{H}\,\psi_{n(\vec{r},\,\vec{R})} \equiv W_n\,\psi_{n(\vec{r},\,\vec{R})} \tag{31}$$

where W_n is defined through

$$W_n \equiv E_n - i\frac{1}{2}\Gamma_n \tag{32}$$

with E_n and Γ_n being real numbers. Γ_n is the partial width of the resonance and, therefore, $\hbar/\Gamma_n$ is the lifetime of the ionic resonance. The total wave function would be represented by a series sum,

$$\Psi = \sum_n \vec{\xi}_n(\vec{R})\,\psi_{n(\vec{r},\,\vec{R})}, \tag{33}$$

$\vec{\xi}_{n(\vec{R})}$ and $\psi_{n(\vec{r},\,\vec{R})}$ being the nuclear and electronic wave functions, respectively. By proper matching of the "internal" and "external"

wavefunctions, the Schrödinger equation reduces to

$$(E_n - \mathcal{H}_n - W_n)\, \xi_{n(\vec{R})} = F_{n(\vec{R})} \tag{34}$$

where E_n is the total energy and $F_{n(\vec{R})}$ is an inhomogeneous term which is proportional to the amplitude of the incident wave and the initial wave function $\vec{\xi}_o$. The final expression as given by BHM is much too lengthy to be presented here, however the main features of the results can be discussed by referring to Figure 6.

The presence of an electron changes the potential such that the dissociating nuclei are described by a wavefunction $\vec{\xi}_{n(\vec{R})}$ whose amplitude decreases exponentially with R due to the imaginary term in W_n. The damping term represents the many possible fates of the negative ion resonance other than dissociative capture, i.e.,

$$e + H_2 \rightleftarrows (H_2^-) \begin{cases} \nearrow H_2^* + e \\ \searrow H + H + e \end{cases} .$$

Beyond the point R_c where the neutral and negative ion curves cross, $\vec{\xi}_n$ is undamped and the amplitude of $\vec{\xi}_{n(R>R_c)}$ determines the cross section. The many unknown parameters involved in the BHM cross section make a direct comparison of experiment and theory very difficult. However, a qualitative explanation for the small capture cross section was given by BHM [and more recently by Herzenberg (1965) and Demkov (1965)] to be due to the small

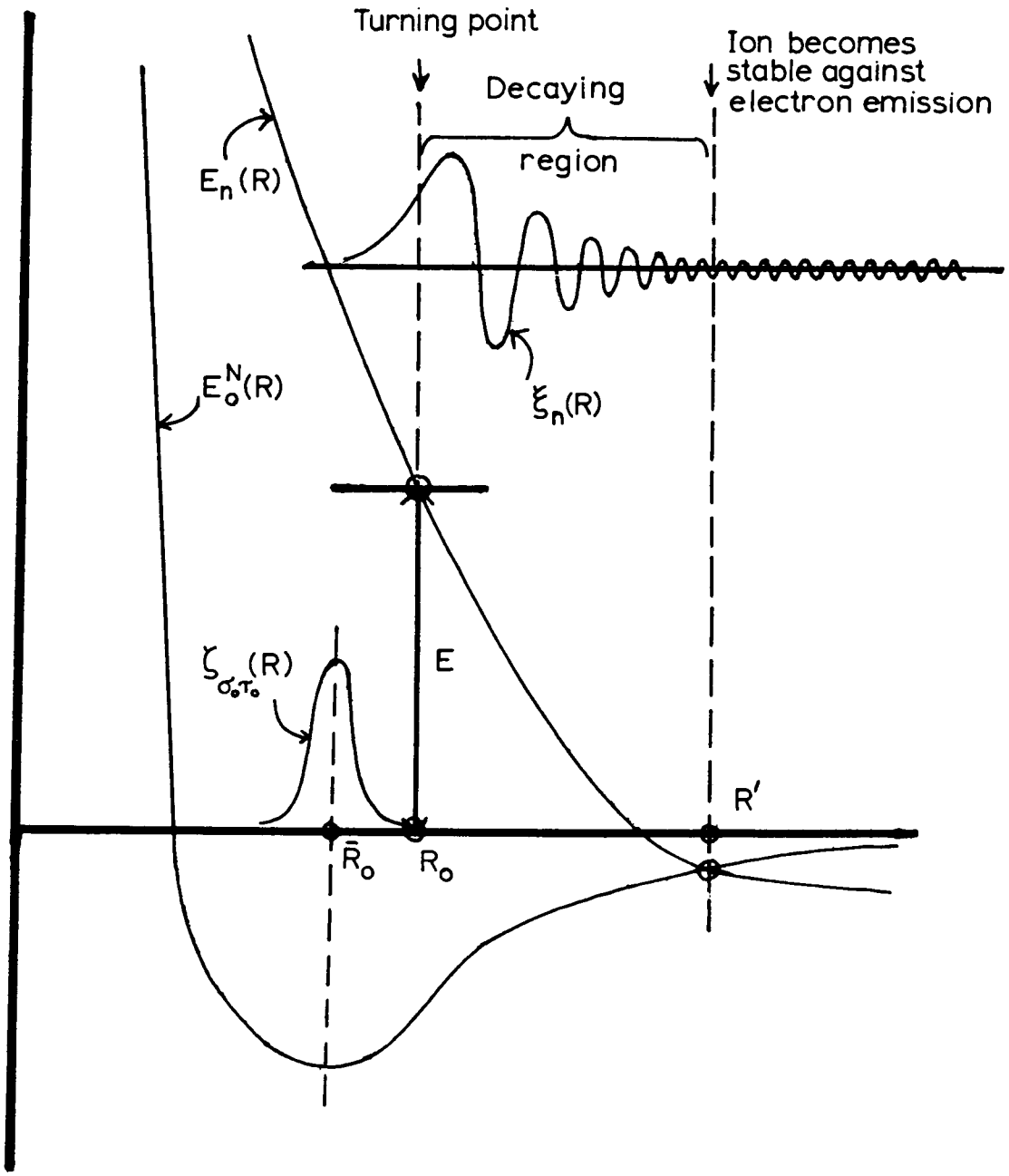

Figure 6. Illustration of resonance electron capture. The exponential damping of the outgoing wave $\vec{\xi}_n$ between R_o and R_c is due to emission of an electron leaving the molecule either dissociated or excited. The cross section is determined from the amplitude of $\vec{\xi}_n$ for $R > R_c$ [taken from Herzenberg and Mandl (1964)].

"survival probability" of the negative ion state once it is formed. That is to say, after capture has occurred, backward transitions can take place before the negative ion state dissociates to give a negative ion. The probability of the negative ion formation per capture will be given by

$$w = e^{-2/h \int_{t(R_o)}^{t(R_c)} \Gamma dt} = e^{-2\overline{\Gamma}\tau/h} \tag{35}$$

where $\overline{\Gamma}$ is the mean width of the AB^- curve in the region R_o (mean internuclear distance) to R_c (crossing point of AB and AB^-) and τ is the lifetime of the negative ion state.* The cross section can be quite easily a few orders of magnitude smaller if $\overline{\Gamma}$ is greater than 0.1 eV. The widths of negative ion resonances are generally greater than 0.1 eV so that this explanation appears quite reasonable. Stockdale and Hurst (1964) found that the

---

*Holstein (1951) first proposed this idea to describe the dissociative attachment of electrons to diatomic molecules. In accord with the Franck-Condon principle, reactions of the type $e + AB \rightarrow A + B^-$ proceed in two stages: the electron is first captured by a neutral molecule AB without alternation of the positrons and velocities of the nuclei and then the molecular ion AB^- dissociates into $A + B^-$. In the region where the potential curve for AB^- lies above that of the AB curve, the molecular ion is unstable toward autoionization (or autodetachment). Therefore, the cross section for the production of B^- will be a product of the cross section for the formation of AB^- times the probability e^{-T_S/τ_A} that AB^- will dissociate without autodetachment. τ_A is interpreted as the autodetachment lifetime and T_S the time required for the ion B^- and neutral A to separate to the crossing point of the AB and AB^- potential curves.

ratio of the attachment cross section for H^- from H_2O to D^- from D_2O could be explained by assuming that dissociation is in competition with auto-detachment. By requiring the probability of electron emission to be much larger than the probability of dissociation, they concluded that the ratio of the cross section for the two processes would be equal to the ratio of the velocity of separation of H^- to the velocity of separation of D^-. The predicted ratio of 1.42 agreed qualitatively with the measured value of 1.66.

Demkov (1965) has suggested that the concept of "survival probability" gives a qualitative explanation of the experimental results of Fite and Brackman (1963) in which a shift of the maximum towards lower energy and an increased cross section occurs when the O_2 molecules are heated ($\sim$2-eV shift for $T \approx 2000°$ K). Demkov (1965) points out that if the first three vibrational levels of O_2 are appreciably populated, then electron capture will take place at larger R and since the time for dissociation would become smaller, the cross section would be correspondingly larger. Hence, the O^- curve would appear to shift to lower energies. It is difficult to understand, however, how the O^- curve can shift continuously from $\sim$6.5 eV to $\sim$5 eV as the temperature increases from 300° K to 1930° K. It would seem that the intermediate curves should exhibit "bumbs" corresponding to capture by molecules in the $\nu = 1$, 2, etc. state as the temperature is increased. The more recent experiments of Fite, Brackman, and Henderson (1965) indicate that rotational excitation is playing a major role in the capture process in

which case a "smooth" translation would be expected. This argument can also provide an explanation for the large isotope effect observed by Rapp, Sharp, and Briglia (1965) in the dissociative attachment of H^- from H_2 and D^- from D_2 since the time of dissociation increases by $\sqrt{2}$ when H_2 is substituted by D_2.

O'Malley (1965) has presented a resonance capture cross section expression similar to that of BHM which is somewhat easier to relate to experiment,

$$\sigma_c = \left(\frac{4\Pi}{k^2}\right)\left(\frac{\Gamma_a}{\Gamma_d}\right)\left(\frac{\Pi}{\alpha}\right)\chi^2_{n(\epsilon)} \tag{36}$$

where

$$\epsilon = \frac{E - E_o - \Delta_d}{\Gamma_d/2}, \quad \frac{\Gamma_d}{2} = \frac{V'}{\alpha}, \quad \Delta_d \approx \frac{1}{2}\hbar w_c \ . \tag{37}$$

Γ_a is the autoionization width averaged over rotational states; Γ_d is the dissociation width; χ_n is the normalized vibrational wave function; V' is the slope of the negative ion potential curve in the Franck-Condon region; Δ_d is related to an approximate asymptotic expansion of the overlap integral; and w_c is the vibrational frequency. O'Malley points out that it is unlikely that this theory could explain either the extremely small cross section ($\sim 10^{-20}$ cm^2) observed for H^- from H_2 or the large isotope effect observed by Rapp, Sharp, and Briglia (1965). In an attempt to reconcile this apparent failure of the resonance theory, O'Malley explains that there is no guarantee

that negative ion resonance curves will exist for H_2^- at internuclear separations corresponding to the Franck-Condon region. That is, if the H_2^- curve merges with the initial $^1\Sigma_g$ curve and disappears, there will be no resonance curve and $\sigma_c \equiv 0$. O'Malley goes further to state that the small cross section observed could then be alternately explained by the following mechanism:

$$e + H_2\,(^1\Sigma_g) \rightarrow H_2\,(^3\Sigma_u) + e \begin{matrix} \nearrow H + H + e \\ \searrow H + H^- \end{matrix} .$$

That is to say, as the two protons in the $^3\Sigma_u$ state dissociate, one of them carries away an electron. The large isotope effect could also be explained since the $H - H^-$ system would dissociate faster than the $D - D^-$ system and $\sigma(H^-/H_2)$ would be correspondingly greater than $\sigma(D^-/D_2)$. A test of this hypothesis would be to look for slow electrons (< 1 eV) at the position of the negative ion resonance. Unfortunately, an experiment of this type has not been reported.

Theoretical attempts have been made to develop selection rules which will apply to dissociative electron capture. G. H. Dunn (1962) has investigated the existence of anisotropies in the angular distribution of molecular dissociation products when an electronic transition to an antibonding state of a molecule occurs via electron impact. A table of selection rules were developed based on group theory which are a consequence of the fact that for a scalar operator the matrix elements are non-zero only for transitions

between states belonging to the same irreducible representation of the group of symmetry operations. Treating the interaction potential between the electron and molecule as a scalar sum of Coulomb terms, and employing the fact that symmetries existing before the collision must be preserved, it was shown that transitions to certain negative ion states are forbidden and that anisotropies are to be expected in a majority of the dissociative attachment processes. In particular, when the molecular axis is parallel to the direction of the incident electron, $\vec{k}$, the transition probability vanishes except for $\Delta\Lambda = 0$, $+ \rightarrow +$, $- \rightarrow -$ (for both homonuclear and heteronuclear diatomic molecules). A different behavior of the transition probability occurs when the internuclear axis is perpendicular to $\vec{k}$. Since rotation times of a molecule are long compared to vibration times, the resulting dissociating products will exhibit an angular dependence. Tables II and III show the selection rules of Dunn in which X|O indicates that transitions occur only when $\vec{k}$ is aligned perpendicular to the internuclear axis, O|X when $\vec{k}$ is parallel, O|O denotes that no transitions occur, and X|X signifies that the cross section will exhibit no angular dependence (isotropic).

The implications of the existence of these anisotropies impose serious consequences on the experimental measurement of electron capture cross sections, ion kinetic energy measurements and the shapes of electron capture cross sections as a function of energy. The use of these selection rules on the other hand may be helpful in interpreting experimental data. For instance,

TABLE II

TRANSITION PROBABILITY BEHAVIOR BETWEEN PAIRS OF ELECTRONIC STATES FOR HOMONUCLEAR DIATOMIC MOLECULES

	Σ_g^+	Σ_g^-	Σ_u^+	Σ_u^-	Π_g	Π_u	Δ_g	Δ_u
Σ_g^+	X|X	O|O	O|X	O|O	O|O	X|O	X|O	O|O
Σ_g^-		X|X	O|O	O|X	O|O	X|O	X|O	O|O
Σ_u^+			X|X	O|O	X|O	O|O	O|O	X|O
Σ_u^-				X|X	X|O	O|O	O|O	X|O
Π_g					X|X	O|X	O|O	X|O
Π_u						X|X	X|O	O|O
Δ_g							X|X	O|X
Δ_u								X|X

TABLE III

TRANSITION PROBABILITY BEHAVIOR BETWEEN PAIRS OF ELECTRONIC STATES FOR HETERONUCLEAR DIATOMIC MOLECULES

	Σ^+	Σ^-	Π	Δ
Σ^+	X|X	O|O	X|O	X|O
Σ^-		X|X	X|O	X|O
Π			X|X	X|O
Δ				X|X

since transitions from $^3\Sigma_g^-$ to $^2\Pi_g$ states are forbidden by Dunn's selection rules, this supports the suggestion of Hurst (1959) that oxygen molecules capture thermal energy electrons through the $^4\Sigma_u^-$ state and not the $^2\Pi_g$ state.

There is one obvious conflict existing in the literature concerning the selection rules for electron attachment. Stanton (1960) has concluded that since ∇_α does not effect the spin part of $\vec{\xi}_R$ and for diatomic molecules ∇_α does not change the symmetry species, then the entire kinetic energy matrix elements will vanish unless the states of the negative ion contain as many molecular spin orbitals of a given spin-symmetry type as the neutral molecule states. Application of Stanton's selection rule to H_2 predicts that transitions from the ground $^1\Sigma_g^+$ state of H_2 to the $^2\Sigma_g^+$ state of H_2^- is strictly forbidden. This result is in direct opposition to Dunn's prediction (see Table I, page 26). However, the recent experimental results of Schulz and Asundi (1965) show that H^- is formed at low electron energies (peaking at ~ 3.73 eV), presumably arising from the $^2\Sigma_u^+$ state of H_2^-. The higher energy peaks previously observed at about 10 eV result, therefore, from the $^2\Sigma_g^+$ state of H_2^- in agreement with Dunn's selection rules.

CHAPTER III

DETERMINATION OF ELECTRON CAPTURE CROSS SECTIONS AS A FUNCTION OF ENERGY BY SWARM-BEAM COMBINATION

I. EXPERIMENTAL APPARATUS

Time-of-Flight Mass Spectroscopy

A Bendix time-of-flight mass spectrometer, model 14-206, was employed for mass analysis in the negative ion studies described in this work. The time-of-flight mass spectrometer has many advantages:

1. The entire mass spectrum can be displayed on an oscilloscope.
2. Two or more mass peaks can be monitored simultaneously.
3. The ion source is completely open and there are no narrow slits to limit the effectiveness of the large cross section of the electron beam.
4. The alignment and focusing is less critical than the conventional sector type mass spectrometer.
5. The size and shape of the spectrometer tube is not restricted by the requirement of a magnetic field.
6. Time-of-flight mass spectrometers are accessible for studying primary and secondary reactions in the flight tube (e.g., spontaneous decay, or ion-molecule reactions).

7. Time-of-flight mass spectrometers are particularly useful for studying ion species of short duration.

The main disadvantage of the time-of-flight instrument is that the mass resolution is not as good as that of the magnetic spectrometer. However, most studies of a basic research nature do not require high mass resolution and the time-of-flight mass spectrometer proves to be an extremely versatile instrument.

A simplified diagram of the model 14-206 time-of-flight mass spectrometer is shown in Figure 7. Negative ions are created by a short duration electron beam pulse and are then pulsed from the ion chamber into an ion acceleration field by a negative pulse of 50 to 150 volts applied to the backing plate. Once the ions have passed through the double grid system separating the ionization chamber from the ion acceleration region they are accelerated to between 2 to 6 keV and then travel down a field free flight tube. The ions will gain a kinetic energy dependent only on their charge; therefore, ions of the same charge but of different mass will have different times of flight. The spectra will be composed of bunches of ions of the same e/m. The ion bunches strike the electron multiplier (EM) cathode and liberate secondary electrons. The secondary electrons experience a field drawing them away from the cathode and into the multiplying section of the EM. A magnetic field is aligned parallel to the surface of the resistance strip electron multiplier so that the electron bunches describe a cyclodial

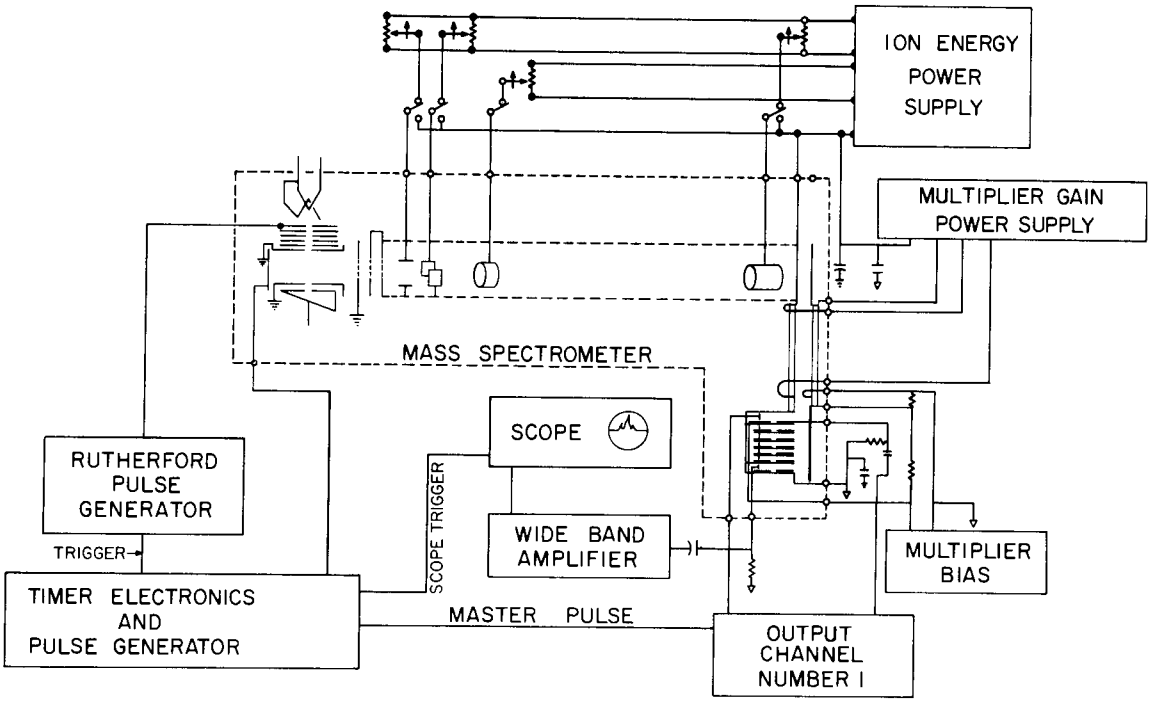

Figure 7. Diagram of the Bendix model 14-206 mass spectrometer.

path down the multiplier dynode strip. The field lines are at an angle to the dynode strip so that upon each collision the newly created secondaries will gain enough energy after one period of the cycloid to produce other secondaries. The ultimate gain of the EM is determined by the impact angle and the number of cycloids which is determined by the potential at the input of the multiplier. For a detailed description of this type of electron multiplier, the reader is referred to Goodrich and Wiley (1961).

The EM in Figure 7 shows six analog anodes which are normally biased negatively and a scope anode which is biased positively to collect electron pulses at all times. A gating pulse generated in the analog allows a particular anode to accept electron bunches at a specified time. This gating pulse is variable in time so that it can be synchronized with the arrival of an electron bunch representing a given mass number. Since the time of transit of an electron through the electron multiplier is short compared to ion transit times, the difference between the starting time of the backing plate pulse and the analog gate pulse will be the time of flight of the ion.

The time of flight for ions of mass M and constant energy eV down a flight tube of length L is

$$\mathrm{TOF} = L\left(\frac{M}{2\ eV}\right)^{1/2} . \tag{38}$$

If the collector is sensitized for a short time Δt at time t, the resolution for ions of the same energy would be

$$\frac{\Delta M}{M} = \frac{2\Delta t}{t} . \tag{39}$$

The band width of the multiplier is sufficient to amplify pulses as narrow as 10 nanoseconds so that theoretically the resolution should approach approximately 1/1000 for time of flights in the range of 10 microseconds. In practice, however, the resolution is not limited by the response time of the EM but rather by the initial velocity (thermal and reaction) and the distribution of starting positions of the ions. The effect of different initial positions of the ions is minimized by employing the fact that ions initially close to the first grid acquire less energy and are eventually overtaken by those initially closer to the backing plate. It can be shown that a particular value of the ratio of the ion pulse voltage to the ion acceleration field gives a maximum resolution. For this reason it is necessary to vary the ion pusher plate pulse voltage to obtain maximum resolution when the ion acceleration voltage is changed. This is called "space focusing" or "bunching".

For positive ions it is possible to obtain additional focusing by delaying the ion pusher pulse with respect to the electron gate pulse. The positive ions are attracted by the potential well created by the electron beam so that proper delay timing will allow the ions to start from approximately the same position. This procedure is termed "time lag focusing". Unfortunately, for negative ions the electron beam is a potential hill and time delay between the two pulses will result in poorer resolution. In fact, it was discovered that upon delay of the pusher pulse the O^- ion peak from H_2O split into two peaks corresponding to ions starting from different sides

of the electron beam. The separation between the two peaks varied linearly with the delay time between the electron beam pulse and the backing plate pulse. Therefore, it is necessary in negative ion studies to keep the two pulses as close together as possible.

In theory the mass of an ion could be calculated from a measurement of the time of flight, path length, and the ion acceleration voltage [Equation (38)]; however, the latter two quantities generally are not known very precisely which in turn makes the mass calibration inaccurate.

The most accurate mass analysis is obtained when a "calibrating gas" is introduced into the ion source which produces ions of known mass. Fixing the position of two known masses allows one to determine the mass of any other ion by either of the following two procedures:

1. By plotting the log of the time of flight versus the log of the mass for the two known masses, the mass of any unknown ion can be determined directly from the graph. Figure 8 shows a plot of TOF vs M on a log-log scale for an impure sample of methane. The slope of the line is, of course, one-half so that only one known mass is actually required for this calibration procedure.
2. Recording a mass spectrum with the mass scanner of the analog and employing the fact that the time interval between the arrival of masses M_1 and M_2 is proportional to $(\sqrt{M_1} - \sqrt{M_2})$, the mass

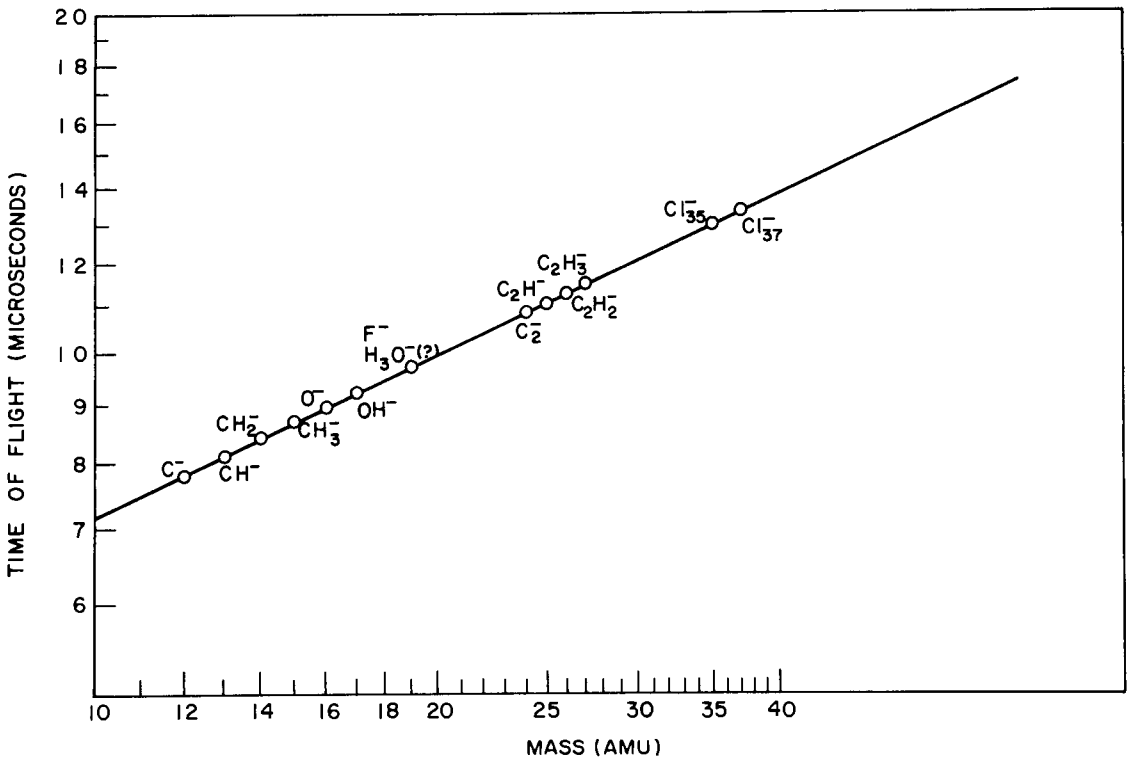

Figure 8. Negative ion mass calibration - impure sample of methane.

scale can be marked off on the spectrum chart, thereby fixing the unknown masses. This proved to be the most accurate and quickest method of mass analysis.

Quasi-Monoenergetic Electron Source

A schematic diagram of the RPD electron gun which was used to produce the quasi-monoenergetic electron beam is presented in Figure 9. The electron beam is normally biased to cut off by a 3-volt negative potential applied to electrode (1). A positive pulse of 1-microsecond duration is used to gate the electron beam approximately 1.5 microseconds before a pulse is applied to backing plate (7) to pulse the negative ions out of the ionization region into the ion acceleration field. Employing a +7-volt electron gate pulse, the energy distribution of the electrons leaving the filament was least affected and the maximum number of electrons was attained with a 0.1-volt retarding region. Defining grids (2) and (4) are connected to the center of the filament and serve to shield the retarding grid (3) from the electron gate pulse and provide a uniform potential at the slit of the retarding grid. The energy of the electron beam was determined from the potential between retarding grid (3) and ground.

Three main contributions to the spread in the electron energy distribution were reflection of electrons from the electron collector and other source electrodes, misalignment of the electron beam, and stray electric fields in the collision chamber.

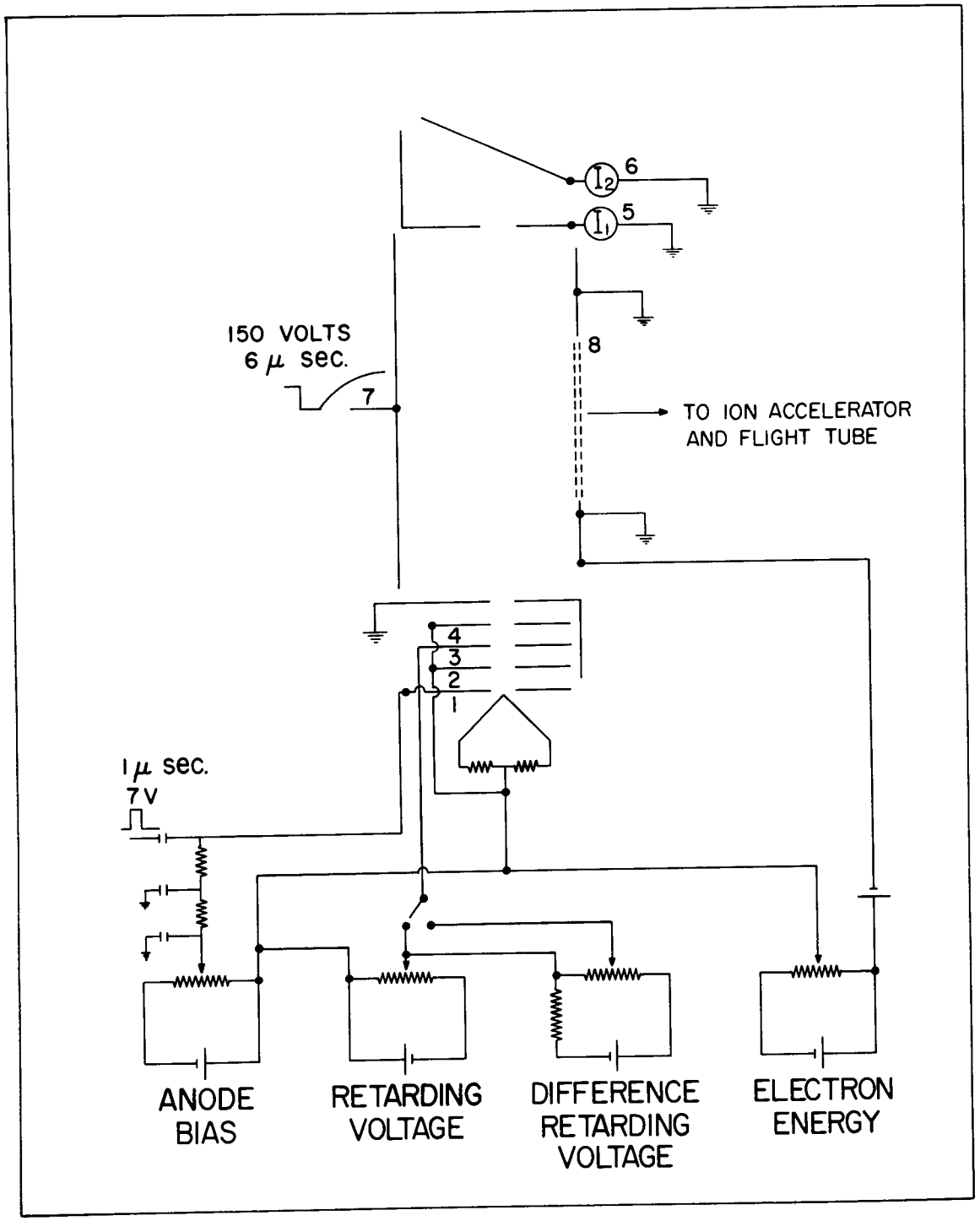

Figure 9. RPD quasi-monoenergetic electron source.

The number of reflected electrons was greatly diminished by electrodepositing platinum black on all of the electrodes in the collision region. Special attention was given to the electron collector (6) and electron collector shield (5). Because of surface reactions with the halogenated benzene derivatives, insulating deposits were believed to be formed which resulted in broadening of the electron energy distribution. This necessitated replating the source electrodes with platinum black many times during the course of this investigation. The electron beam defining grids were also plated with platinum black. This increased the stability of the electron beam in passing through the grid system and yielded a sharper electron energy distribution (i.e., SF_6^- resonance; see later in this section).

Misalignment of the electron beam, resulting from improper positioning of the source magnets, produced an increased spread in the electron energy distribution and often times a second maxima in the SF_6^- resonance [see also Frost and McDowell (1958)]. Proper alignment of the electron beam was achieved by minimizing the ratio of the collector shield current (I_1) to the collector current (I_2). After focusing the electron beam in this procedure, the collector shield was grounded before measurements were taken. It was also found necessary to operate the electron collector at ground potential.

Schulz (1960b) has pointed out the importance of assuring a field free collision region along the path of the electron beam when employing SF_6 to

calibrate the electron energy scale. By observing the small current ($\sim 10^{-11}$ amp) to the collector shield, it was possible to detect stray electric fields in the collision chamber. It was observed that by varying the ion acceleration voltage from 2 to 6 kV the current to the collector shield would increase by a factor of ten. After completely shielding the ion source and electron gun with gold foil, the collector shield current was unaffected by changes in the ion acceleration voltage. This indicated that stray electric fields due to the ion acceleration voltage had been eliminated and that field penetration through the double grid (8) was negligible.

A potential as small as 0.1 eV applied to the pusher plate (7) greatly increased the current to the collector shield. A residual voltage was detected on the ion pusher plate at the instant the electron beam was traversing the collision chamber. This potential was dependent on the voltage of the pusher plate and was a consequence of overshoot of the pusher plate pulse from the previous cycle. By observing the electron gate pulse position and the pusher plate pulse base line simultaneously on an oscilloscope, it was possible to bias the pusher plate so that the potential was zero at the moment the electron beam crossed the collision chamber.

Upon admitting halogenated benzene derivatives into the mass spectrometer, an initial shift in the electron energy scale was observed. The effect was most pronounced for the chlorine-containing compounds and to a lesser extent for the bromine, iodine, and nitro-containing benzene derivatives.

This effect has been ascribed to a change in the surface potentials possibly due to surface reactions with the halogenated compounds [Fox (1957), Fox and Curran (1961)]. Operating the ion source at approximately 150° C to 200° C appeared to minimize this effect and also allowed the source to be operated for a longer period of time before it was necessary to replate the source electrodes with platinum black. At these temperatures the background pressures were of the order of 5×10^{-7} Torr in the ion source and 1×10^{-7} Torr in the flight tube region.

The interpretation of low-energy electron impact data (< 2 eV) previous to the investigation of Hickam and Fox (1956) was uncertain because of uncalibrated electron energy scale and unknown electron energy distribution. The utilization of the resonance capture process in sulphur hexafluoride (SF_6) by Hickam and Fox (1956), however, allowed an improvement in the measurement of the low-energy electron capture resonances.

The very low-energy electron capture resonance in SF_6 which yields a maximum in the difference ion current at ~ 0.03 eV was employed in this work to give a first estimate of the electron energy scale, and to indicate the electron beam energy distribution. Hickam and Fox (1956) showed that the SF_6^- difference ion current as a function of the electron energy was equivalent to the derivative of the retarding analysis curve of the difference electron current with the exception of a 0.02-volt shift toward lower energy. Since they employed a difference retarding voltage of 0.1 volt, it was

concluded that the width of the electron capture resonance in SF_6 was less than 0.1 volt and, therefore, a plot of the difference ion current as a function of the electron energy would be a mirror image of the electron energy distribution. Figure 10 shows the SF_6^- and SF_5^- ion current as a function of the electron accelerating voltage obtained in this work. Much more will be said about non-dissociative electron capture resonances such as this in Chapter V, pages 152-172.

Although the SF_6^- ion current and the halogen negative ion currents were measured concurrently, the energy scale determined by SF_6^- may still be erroneous. Thus Schulz (1960b) pointed out earlier that use of SF_6 to calibrate the electron energy scale under certain conditions may be in serious error. In particular, if a potential V exists along the path of the electron beam and if V is positive with respect to the entrance slit of the collision chamber, the difference between the peaks of SF_6^- current and the halogen negative ion current will be decreased by an energy approximately equal to V. This uncertainty in the electron energy scale, however, can be removed by the energy calibration technique described in Section III of this chapter which combines electron swarm and electron beam data.

The energy scale for positive ion formation is established very precisely by the use of a calibrating gas such as one of the rare gases where the appearance potential is known quite accurately. However, there are no known calibration gases (i.e., gases which exhibit an accurately known

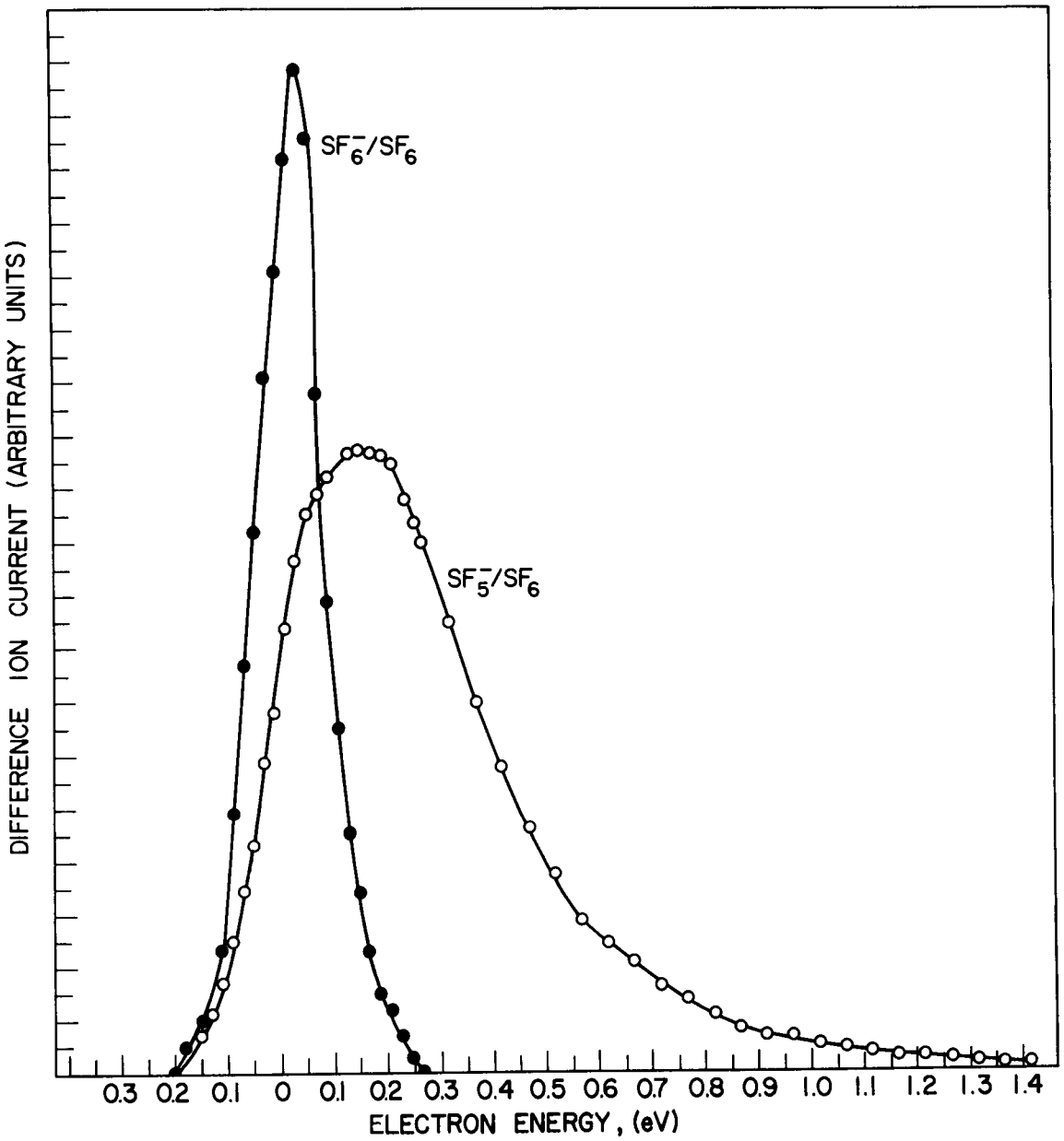

Figure 10. SF_6^- and SF_5^- ion currents as a function of the electron accelerating voltage.

appearance potential or negative ion peak) which can be used to study electron capture at electron energies greater than 5 volts. In fact, the difficulties which are encountered when employing SF_6 as a calibrating gas suggest that there are no unambiguous calibrating gases which can be employed in negative ion studies. Branscomb (1958) has reviewed the various calibrating gases which have been employed previously for negative ion experiments.

During the course of this investigation a technique was developed which will allow one to calibrate the electron energy scale quite accurately at energies around 10 eV. It was shown in Figure 10, page 76, that SF_6 captures electrons at essentially zero energy, and it was further found that at higher energies the ion current was extremely small, probably due to capture of low-energy electrons which are emitted by collisions of high-energy electrons with surfaces in the ion source. When another gas is introduced into the ion source at pressures of $\sim 10^{-4}$ mm Hg, other SF_6^- ion peaks occur at higher energies which correlate extremely well with known energy levels of the gas which is mixed with SF_6. These SF_6^- peaks at higher energies are due to slow electrons produced when electrons lose energy by electronic excitation of the secondary gas. The overall reaction can be written as

$$e\,(\text{fast}) + X \rightarrow X^* + e\,(\text{slow}),$$

$$e\,(\text{slow}) + SF_6 \rightarrow SF_6^- \ .$$

Figure 11 shows a typical electron energy loss spectrum of helium. This technique offers the advantage of being a truly zero-energy electron detector so that the threshold of excitation processes are being obtained directly. Therefore, the electron energy scale could be established for negative ion studies by introducing a three-component mixture into the mass spectrometer consisting of SF_6, He (for example), and the gas to be studied. Many times the gas to be studied will possess known energy levels which could be used to establish the electron energy scale and the procedure would require only a two-component mixture.

Needless to mention, this technique can be employed to study electron impact excitation of atoms and molecules and is particularly useful in studying excitation of triplet states by electron impact. Other gases such as N_2, H_2, and $(CH_3CO)_2$ were studied with very encouraging results.

II. THE ELECTRON SWARM METHOD

The excellent review of the various electron swarm methods has been presented recently by Fiquet-Fayard (1965). The particular swarm method of Bortner and Hurst (1958) employing a modified parallel plate ionization chamber [see Christophorou, Compton, Hurst, and Reinhardt (1965)] was applied in the swarm attachment studies described in this thesis.

In the electron swarm method the electrons collide many times with the gaseous medium through which they travel and, therefore, their energies

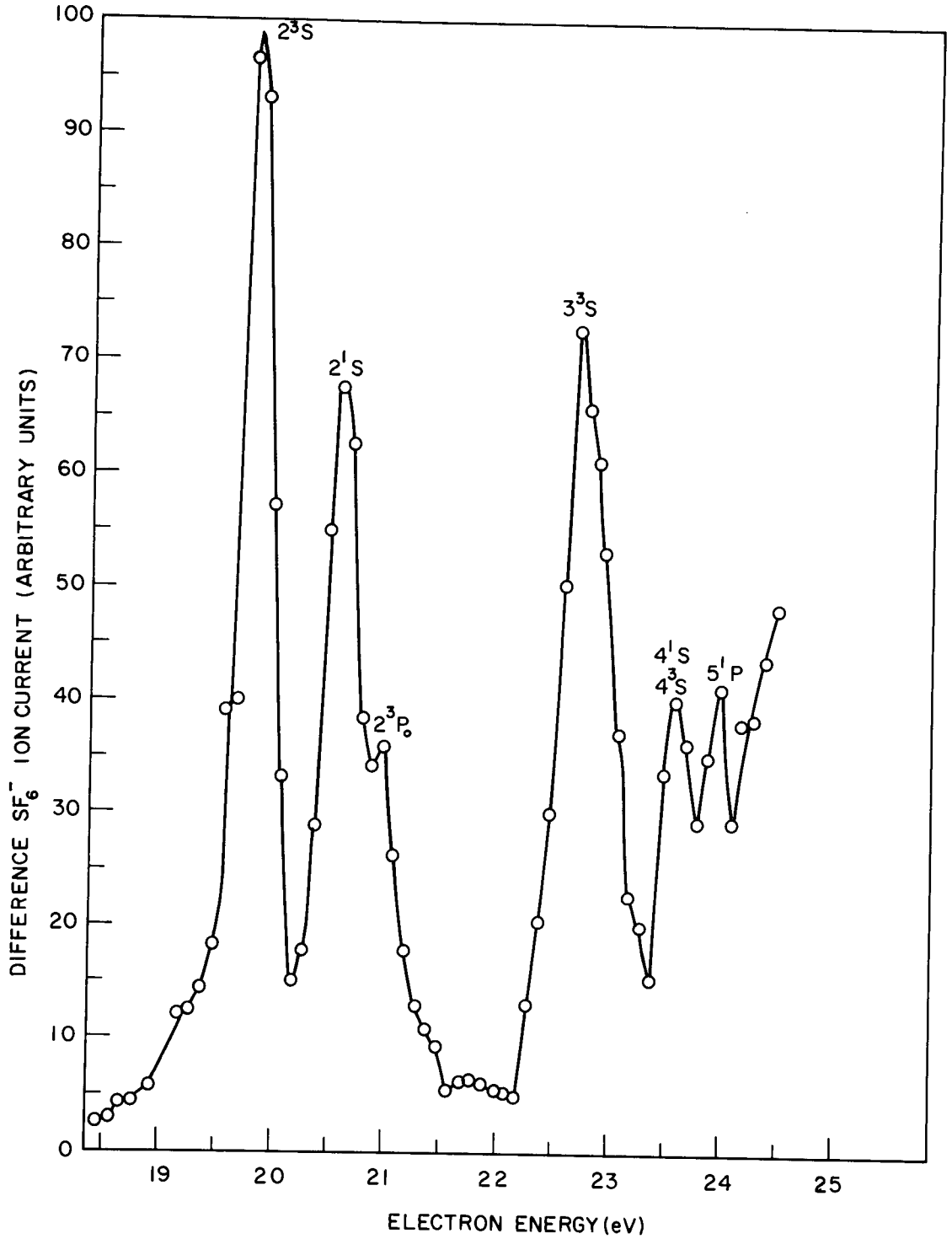

Figure 11. Electron energy loss spectrum of helium using SF_6 as a zero energy electron detector.

extend over a wide range. The distribution of electron energies is characterized by a function $f(\epsilon, E/P)$ which is determined by the gaseous medium and the "pressure reduced electric field". The quantity $f(\epsilon, E/P)$ is defined by the relationship $f(\epsilon, E/P)d\epsilon$ = number of electrons in an energy range $d\epsilon$ about an energy ϵ.

Certain non-attaching or carrier gases are used to determine the electron energy distribution $f(\epsilon, E/P)$. The sample gas, or attaching gas, is added to the carrier gas at a pressure f_1P which is generally much less than the pressure of the carrier gas f_2P so that $f(\epsilon, E/P)$ is characteristic of the carrier gas alone. By a proper choice of the carrier gas and E/P, the mean electron energy of the electron swarm can be made to peak over the range from thermal to ~ 10 eV. Figure 12 shows $f(\epsilon, E/P)$ for the carrier gases ethylene (C_2H_4), nitrogen (N_2), and argon (Ar) for various E/P. Stockdale and Hurst (1964) have shown that $f(\epsilon, E/P)$ remains thermal for $E/P \lesssim 0.15$ V cm^{-1} Torr^{-1} for the carrier gas ethylene. The dependence of $f(\epsilon, E/P)$ on E/P is not known for ethylene, however the dependence of the rate of electron capture on E/P will allow one to determine whether a particular capture process peaks above or below 3/2 kT.

In the swarm method of Bortner and Hurst (1958) electrons are produced by alpha particle ionization (from a ^{239}Pu source) in a plane which is normal to the applied electric field at a distance of 7 cm from the collecting electrode.

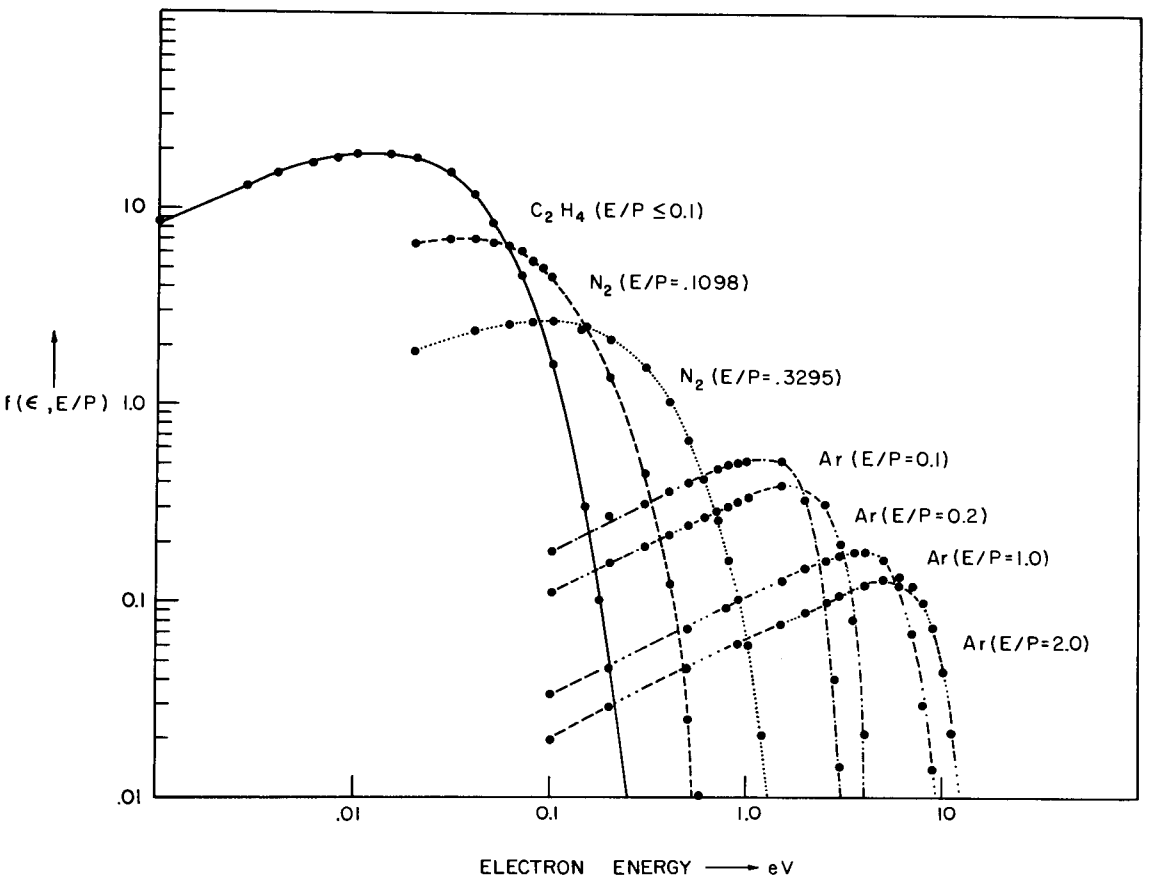

Figure 12. Energy distribution in electron swarms for different carrier gases and E/P.

The attachment coefficient $\alpha(E/P)$ (the probability of capture per cm traveled in the field direction per Torr of sample gas) is calculated from measurements of the "pulse height" produced in the parallel plate chamber (with an amplifier of suitable transient response) and the free electron drift velocity. These two quantities are measured both for the carrier gas and the mixture containing the carrier gas plus the sample gas. The arrangement currently used to measure these quantities is shown in Figure 13. The electron drift velocity is obtained by measuring the delay between pulses arriving from a gas discharge tube (located at the end of the drift space) and a photodiode. The photodiode is triggered by a pulsed light source while the gas discharge tube, which is opened to the chamber gas, is triggered by the arrival of the electrons.

In summary, the electron swarm method measures the absolute values of $\alpha(E/P)$ and $w(E/P)$. Since $\alpha(E/P)$ is the probability of capture per cm traveled in the field direction per Torr of attaching gas and $w(E/P)$ is the electron swarm drift velocity in the field direction, their product $\alpha(E/P)w(E/P)$ gives the experimentally measured rate of electron capture per second per Torr of sample gas.

Theoretically, the attachment coefficient, $\alpha(E/P)$, the capture cross section, $\sigma_c(\epsilon)$, and the electron drift velocity, $w(E/P)$ are related by

$$\alpha(E/P) \times w(E/P) = N_o(2/m)^{1/2} \int_0^\infty \epsilon^{1/2} \sigma_c(\epsilon)\, f(\epsilon, E/P) d\epsilon \qquad (40)$$

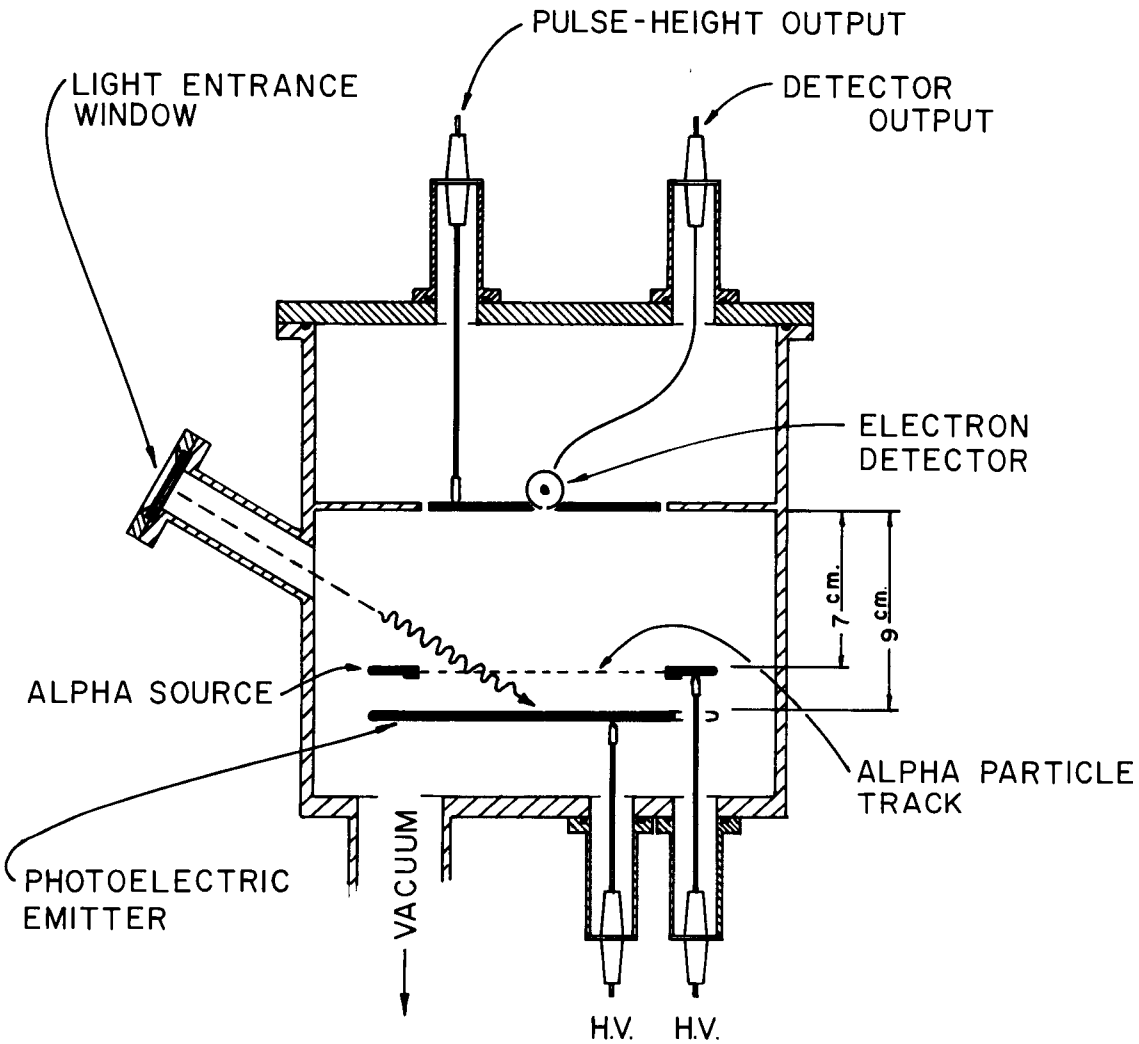

Figure 13. Swarm apparatus for measurement of electron attachment coefficient and drift velocity.

where N_o is the number of sample gas molecules per cm^3 at 1 Torr, m is the electron mass, and $f(\epsilon, E/P)$ is the electron energy distribution function. Therefore, Equation (40) relates the "macroscopic" swarm capture rates, $\alpha(E/P) \times w(E/P)$, to the microscopic electron capture cross section, $\sigma_c(\epsilon)$.

The measured quantity $\alpha(E/P) \times w(E/P)$ can be used in Equation (40) to obtain the capture cross section for the specific case of dissociative electron capture, where the captured electron is removed permanently from the electron swarm. In this case no ambiguity arises in the interpretation of $\alpha(E/P)$. However, for permanent non-dissociative electron capture, $\alpha(E/P) \times w(E/P)$ is a function of the carrier gas employed, due to stabilization by collisions. Therefore, the carrier gas affects $\alpha(E/P) \times w(E/P)$ both through its influence on $f(\epsilon, E/P)$ and through its role in stabilization. In this case, $\sigma_c(\epsilon)$ represents the product of cross section for capture times the fraction of negative ions which are stabilized by collision.

When temporary negative ions are formed by non-dissociative electron attachment, the experimental quantity $\alpha(E/P)$ is difficult to determine in swarm experiments. For cases in which the lifetime of the temporary negative ion is long compared to the response time of the amplifier (used in the Bortner-Hurst method), the measured rate of capture is properly measured. On the other hand, if the lifetime of the ion is of the same order of magnitude or smaller than the response time of the amplifier, then the experimentally determined rates will be smaller than the actual

rates. Electrons which become autodetached from temporary negative ions will return to the electron swarm and contribute to the observed pulse height thereby reducing the actual attachment coefficient.

III. DETERMINATION OF ELECTRON CAPTURE CROSS SECTIONS

In this section a procedure will be described whereby the absolute rates for electron capture, $\alpha(E/P) \times w(E/P)$, obtained from the swarm experiments and the difference negative ion currents, $I(\epsilon)$, obtained from the beam experiments are combined to determine electron capture cross sections as a function of the electron energy, ϵ. As examples of the method, electron capture cross sections will be calculated explicitly for Cl^- from ortho-chlorotoluene and O^- from oxygen. For sake of completeness, the delta-function approximation procedure (i.e., the cross section is represented by a delta function of one particular energy) which has been used by previous investigators will be included.

The calculated attachment coefficients are presented as a function of the ratio f_1P/f_2P in Figure 14. The $\alpha(E/P)$ values fall on a straight line independently of the total pressure. For $f_1P/f_2P \rightarrow 0$, $\alpha(E/P) \rightarrow \alpha_o(E/P)$, where $\alpha_o(E/P)$ is interpreted as the attachment coefficient for the sample gas when the distribution of electron energies is characteristic of the carrier gas alone. Table IV summarizes the swarm data for $w(E/P)$ (in pure N_2), $\alpha_o(E/P)$, and $\alpha_o(E/P) \times w(E/P)$ for o-$C_6H_4CH_3Cl$ in mixtures with N_2.

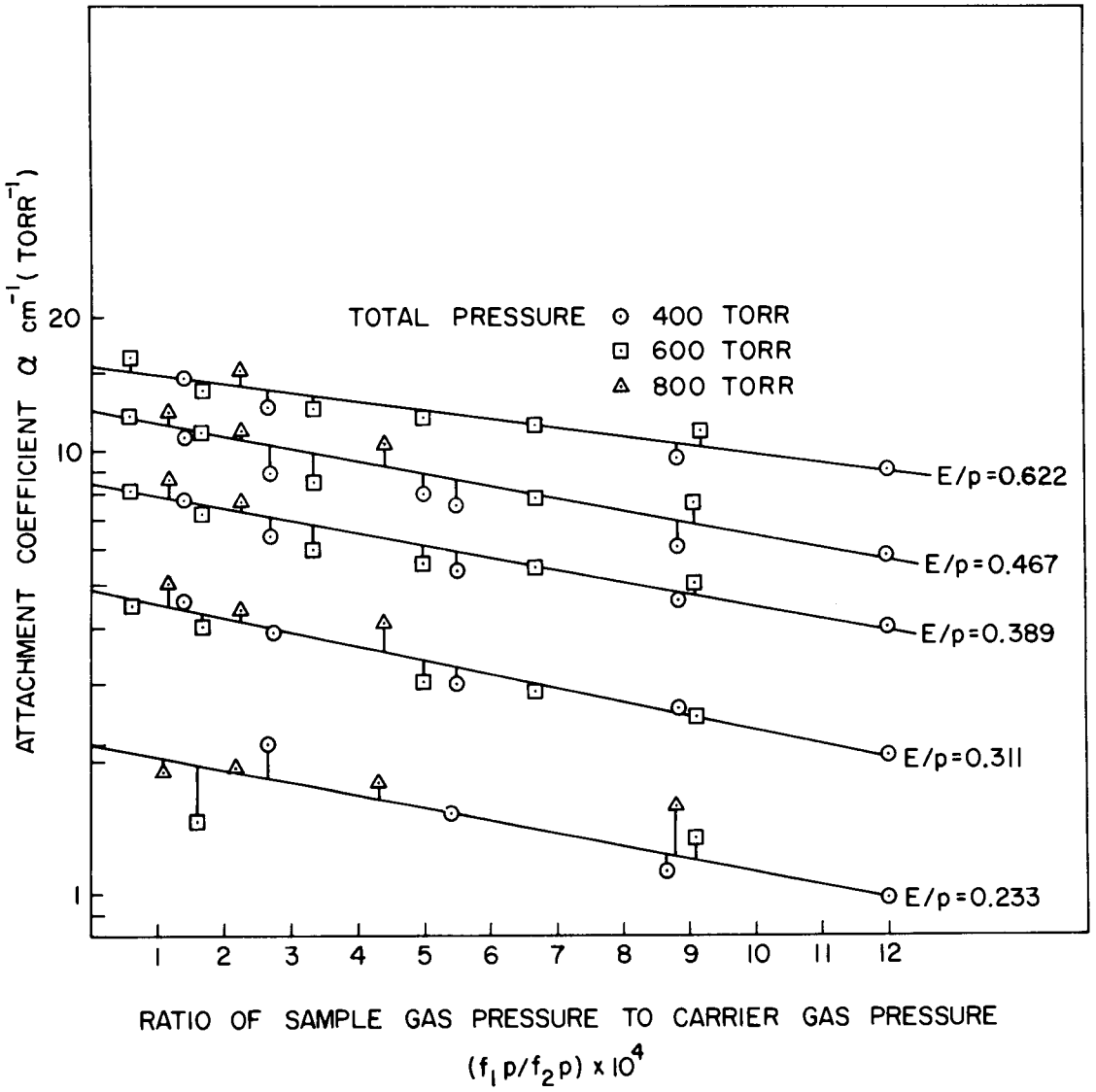

Figure 14. $\alpha(E/P)$ vs f_1P/f_2P for ortho-chlorotoluene in nitrogen.

TABLE IV

ATTACHMENT COEFFICIENTS AND RATES OF CAPTURE FOR BENZENE DERIVATIVES IN NITROGEN

Compound	E/P ($V\ cm^{-1}\ Torr^{-1}$)	$\alpha_o(E/P)$ ($cm^{-1}\ Torr^{-1}$)	$\alpha_o(E/P) \times w(E/P)$ ($sec^{-1}\ Torr^{-1}$)
C_6H_5Cl	0.220	3.43	1.31×10^6
	0.275	5.50	2.28
	0.330	8.55	3.76
	0.384	12.0	3.54
	0.439	15.0	7.28
	0.494	17.5	8.86
	0.549	19.2	10.18
	0.604	20.2	11.21
	0.659	20.7	12.0
$o\text{-}C_6H_4Cl_2$	0.117	64	20.8×10^6
	0.140	100	33.8
	0.156	128	44.5
	0.194	205	75.9
	0.220	235	93.5
	0.330		150.0
$m\text{-}C_6H_4Cl_2$	0.1	75.2	25×10^6
	0.15	204.8	74.3
	0.2	354.2	140
	0.25	463.4	197
	0.3	530.3	237.6
	0.35	546.1	255.6
	0.4	542.4	263.6
	0.5	553	292.5
	0.6	534	300.2
	0.8	449	300
	1.0	354	270.4

TABLE IV (continued)

Compound	E/P ($V\ cm^{-1}\ Torr^{-1}$)	$\alpha_o(E/P)$ ($cm^{-1}\ Torr^{-1}$)	$\alpha_o(E/P) \times w(E/P)$ ($sec^{-1}\ Torr^{-1}$)
$p\text{-}C_6H_4Cl_2$	0.1	12.3	4.08×10^6
	0.15	21.9	7.95
	0.2	32.0	12.94
	0.25	38.0	16.0
	0.3	44.8	20.1
	0.35	45.4	21.25
	0.4	47.4	23.04
	0.5	48.0	25.4
	0.6	44.0	24.3
	0.8	35.4	23.6
	1.0	26.5	20.2
$o\text{-}C_6H_4CH_3Cl$	0.3	4.83	2.05×10^6
	0.35	7.55	3.38
	0.4	9.65	4.55
	0.45	11.3	5.56
	0.5	12.75	6.54
	0.55	13.85	7.34
	0.6	15.0	8.25
C_6H_5Br	0.22	19.1	7.3×10^6
	0.33	48.4	21.3
	0.44	74.4	36.1
	0.55	85.4	45.3
	0.66	90.8	52.5
	0.77	88.3	55.0
	0.88	82.4	54.9
	0.99	79.5	56.4
C_6D_5Br	0.2	18.5	6.9×10^6
	0.25	30	12.1
	0.3	44	18.7
	0.35	60	26.9
	0.4	73	34.4
$o\text{-}C_6H_4CH_3Br$	0.45	44.8	22.1×10^6
	0.5	49.2	25.2
	0.55	53.6	28.4
	0.6	56.4	30.8

In Table V the data are given also for w(E/P) (in pure Ar), $\alpha_o(E/P)$ and $\alpha_o(E/P) \times w(E/P)$ for O_2 in mixtures with Ar. Therefore, from the swarm experiments $\alpha(E/P) \times w(E/P)$ is known for a number of values of E/P.

Let $\alpha_i w_i$ denote the measured rate of attachment for the ith value of E/P and let various trial functions be used for the cross section $\sigma_c(\epsilon)$ and denote $(\alpha w)_{ij}$ as the calculated αw for the ith value of E/P and the jth specification of the trial function. For each trial function j a best fit to the experimental swarm data is obtained from Equation (41):

$$\sum_i \left[(\alpha w)_{ij} - \alpha_i w_i\right]^2 = \text{minimum} = M_j \, . \tag{41}$$

Various trial functions j can be used in an effort to find a j for which $M_j \rightarrow$ minimum.

First make the assumption that $\sigma_c(\epsilon)$ differs from zero only when ϵ is within a small range of the resonance energy ϵ_1 (i.e., assume $\sigma_c(\epsilon_1)$ to be a δ-function). This is a trial cross section whose width is always narrower than the true cross section. The δ-function approximation was used in the past for analysis of electron capture data obtained by the swarm method [see Stockdale and Hurst (1964)] in the absence of electron beam data. The delta function approximation is included here only to show its limitations as compared to the swarm-beam technique. Equation (40) can then be written as

$$\alpha(E/P) \times w(E/P) = N_o(2/m)^{1/2} \, \epsilon_1^{1/2} \, f(\epsilon_1, E/P) \int_o^\infty \sigma_c(\epsilon) d\epsilon \, . \tag{42}$$

TABLE V

ELECTRON DRIFT VELOCITIES w(E/P) AND ATTACHMENT COEFFICIENTS $\alpha_o(E/P)$ FOR O_2 AND H_2O IN ARGON

Compound	E/P ($V\,cm^{-1}\,Torr^{-1}$)	w(E/P) ($cm\,sec^{-1}$)	$\alpha_o(E/P)$ ($cm^{-1}\,Torr^{-1}$)	$\alpha_o(E/P) \times w(E/P)$ ($sec^{-1}\,Torr^{-1}$)
O_2 in Ar	0.30	2.8×10^5	0.0318	0.89×10^4
	0.35	2.9	0.103	2.99
	0.40	3.1	0.22	6.82
	0.45	3.15	0.42	13.23
	0.50	3.2	0.65	20.80
H_2O in Ar	0.40	3.2×10^5	0.18	0.058×10^6
	0.45	3.24	0.57	0.185
	0.50	3.30	1.20	0.396
	0.55	3.35	2.0	0.670
	0.60	3.40	3.0	1.02
	0.65	3.44	4.1	1.41
	0.70	3.51	5.3	1.86
	0.75	3.55	6.6	2.34

Combining Equation (42) into Equation (41) results in

$$\sum \left[N_o (2/m)^{1/2} \epsilon_1^{1/2} f_i(\epsilon_1) \int_o^\infty \sigma_c(\epsilon) d\epsilon - \alpha_i w_i \right]^2 = M_j . \tag{43}$$

Thus, by the least squares procedure, one finds ϵ_1 and $\int_o^\infty \sigma_c(\epsilon) d\epsilon$ which make Equation (43) a minimum. In practice, one may find an approximation to ϵ_1 from the requirement that

$$\frac{\alpha_o(E/P) \times w(E/P)}{f(\epsilon_1, E/P)} = \text{constant (independent of } E/P), \tag{44}$$

where α_o was defined in Section II. This method was used previously to find ϵ_1 and $A \equiv \int_o^\infty \sigma_c(\epsilon) d\epsilon$. An example of this analysis, which in the present discussion is regarded as an initial estimate, is shown in Table VI for o-$C_6H_4CH_3Cl$. For $\epsilon_1 = 0.87$ eV, Equation (44) is satisfied for various E/P and, therefore, $\epsilon_1 = 0.87$ eV is taken to be the initial estimate of the energy at which $\sigma_c(\epsilon)$ peaks. An initial estimate of 1.3×10^{-17} cm^2 eV was found for $\int_o^\infty \sigma_c(\epsilon) d\epsilon$. A computer program was used for the minimization of M_j, i.e., Equation (43), and this gave the values of 0.85 eV and 1.1×10^{-17} cm^2 eV for ϵ_1 and $\int_o^\infty \sigma_c(\epsilon) d\epsilon$, respectively. Initial estimates for ϵ_1 and $\int_o^\infty \sigma(\epsilon) d\epsilon$ in the case of O_2 are 5.5 eV and 8.10×10^{-19} cm^2 eV, respectively. Final values of ϵ_1 and $\int_o^\infty \sigma_c(\epsilon) d\epsilon$ obtained by using Equation (43) are 5.53 eV and 8.24×10^{-19} cm^2 eV.

The assumption will now be made that the shape of the electron capture cross section can be taken to be the difference ion current as a function of

TABLE VI

EVALUATION OF THE RATIO $\frac{\alpha_o(E/P) \times w(E/P)}{f(\epsilon_1, E/P)}$ FOR VARIOUS ϵ_1

Compound	E/P ($V\ cm^{-1}\ Torr^{-1}$)	α_o ($cm^{-1}\ Torr^{-1}$)	Electron Energy ϵ_1 (eV) $\frac{\alpha_o(E/P) \times w(E/P)}{f(\epsilon_1, E/P)} \times 10^{-6}$									
			0.4	0.5	0.6	0.7	0.8	0.85	0.87	0.88	0.9	1.0
$o\text{-}C_6H_4CH_3Cl$ in N_2	0.3	4.83	1.86	3.54	6.14	9.71	15.57	21.51	23.98	25.14	27.82	49.7
	0.35	7.55	2.94						23.55			
	0.4	9.65	3.86	5.84	8.49	11.83	18.98	21.92	23.83	24.84	27.15	39.92
	0.45	11.3	4.84						23			
	0.5	12.75	5.86	7.77	10	13.32	19.14	22.43	23.67	24.44	25.84	33.98
	0.55	13.85	6.62						23.10			
	0.6	15.0	7.5	9.92	11.58	15.0	20.07	22.32	23.42	24.1	25.3	33.15

the electron energy as determined from the electron beam experiments. However, it will not be assumed that the electron energy scale as obtained by the electron beam experiments is entirely accurate. The difference ion current as a function of the electron energy is assumed to be related with the electron capture cross section through the following relationship:

$$\sigma_{bj}(\epsilon) = K_j T_j I(\epsilon) \tag{45}$$

where T_j is a simple translation of $I(\epsilon)$ along the energy axis and K_j is a constant associated with the energy transformation T_j. The operator T_j then serves to calibrate the electron energy scale and K_j is a measure of the electron capture cross section. [If $I(\epsilon)$ is normalized to unity, then K_j is the capture cross section at the maximum.]

The experimentally determined $I(\epsilon)$ curve for Cl^- from ortho-chlorotoluene is shown in Figure 15.

If the cross section defined by Equation (45) is introduced into Equation (41) by making use of Equation (40), the least squares procedure leads to

$$\sum \left[N_o (2/m)^{1/2} K_j \int_o^\infty \epsilon^{1/2} T_j I(\epsilon) f_i(\epsilon) d\epsilon - \alpha_i w_i \right]^2 = M_j . \tag{46}$$

Formally, then, each transformation T_j of $I(\epsilon)$ results in values of M_j and K_j which are found from Equation (46) and the solution of

$$\frac{dM_j}{dT_j} = 0 . \tag{47}$$

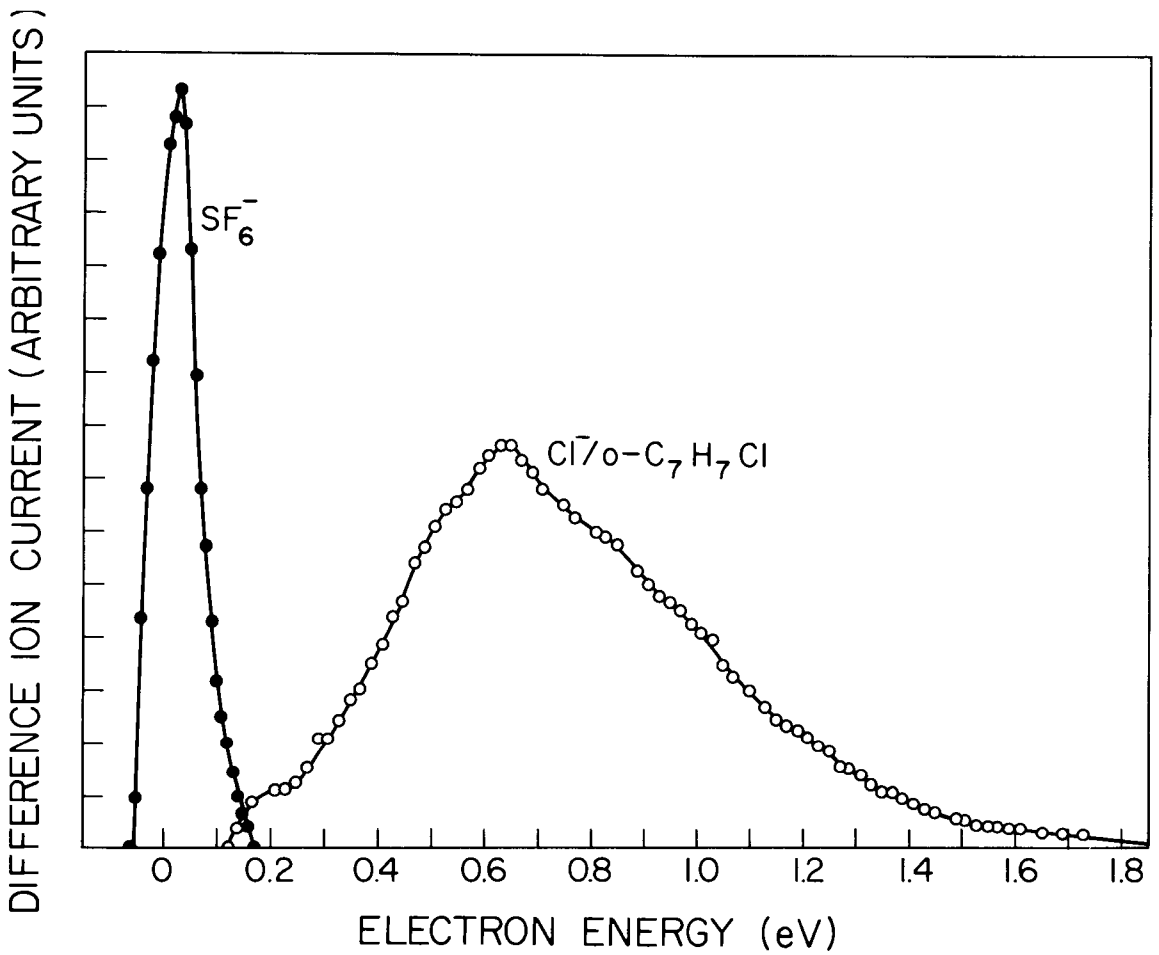

Figure 15. Chlorine negative ions from ortho-chlorotoluene as a function of electron energy.

For each energy transformation T_j, K_j will be a constant. Various energy transformations T_j were tried between the two extremes ($T_j = 0 \rightarrow 0$ and $T_j = 0 \rightarrow j_{max}$) shifting in this manner the $I(\epsilon)$ curve along the positive energy axis by j eV. Only a few values of $T_j I(\epsilon)$ were used and these amounted to a simple transformation of the whole function $I(\epsilon)$ along the energy axis. For the transformation T_j which gave the smallest M_j, K_j was calculated and was introduced into Equation (45). Equation (45) is then the cross section for electron capture as a function of electron energy.

In Figure 16 the swarm experimental rates and the calculated capture rates (based on the electron beam data for various energy translations T_j) are plotted as a function of E/P for the case of o-$C_6H_4CH_3Cl$. For $T_j = 0 \rightarrow 0.42$ eV the swarm experimental rates are in complete agreement with those obtained from the beam data. Figures 17 and 18 compare the observed and calculated rates of capture using both types of trial functions $[\sigma(\epsilon_1), T_j I(\epsilon)]$ for o-$C_6H_4CH_3Cl$ and O_2, respectively. In the case of O_2, $T_j(\text{opt}) = 0 \rightarrow 0$ eV, and a positive or negative shift of the $I(\epsilon)$ curve along the energy axis by 0.5 eV results in a considerable disagreement between the beam calculated rates and the swarm experimental rates (the disagreement being more pronounced the larger the energy shift). This indicates the sensitivity of this method in determining the energy at which $\sigma_c(\epsilon)$ peaks. Using the method which has just been described, the $I(\epsilon)$ curves can be normalized and absolute values of the capture cross section as a function

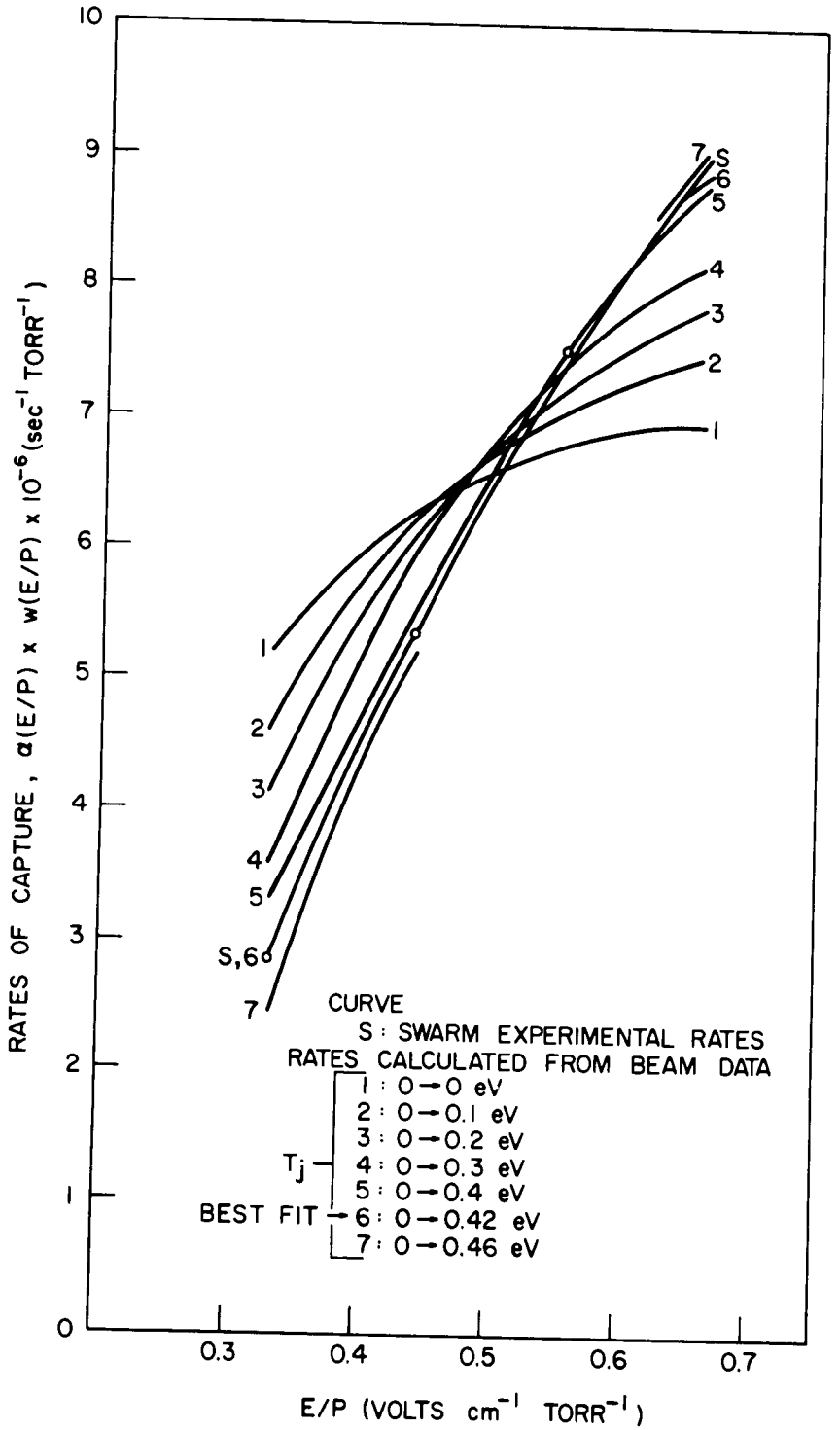

Figure 16. Experimental and calculated rates of capture vs E/P for ortho-chlorotoluene for trial functions based on beam experiments.

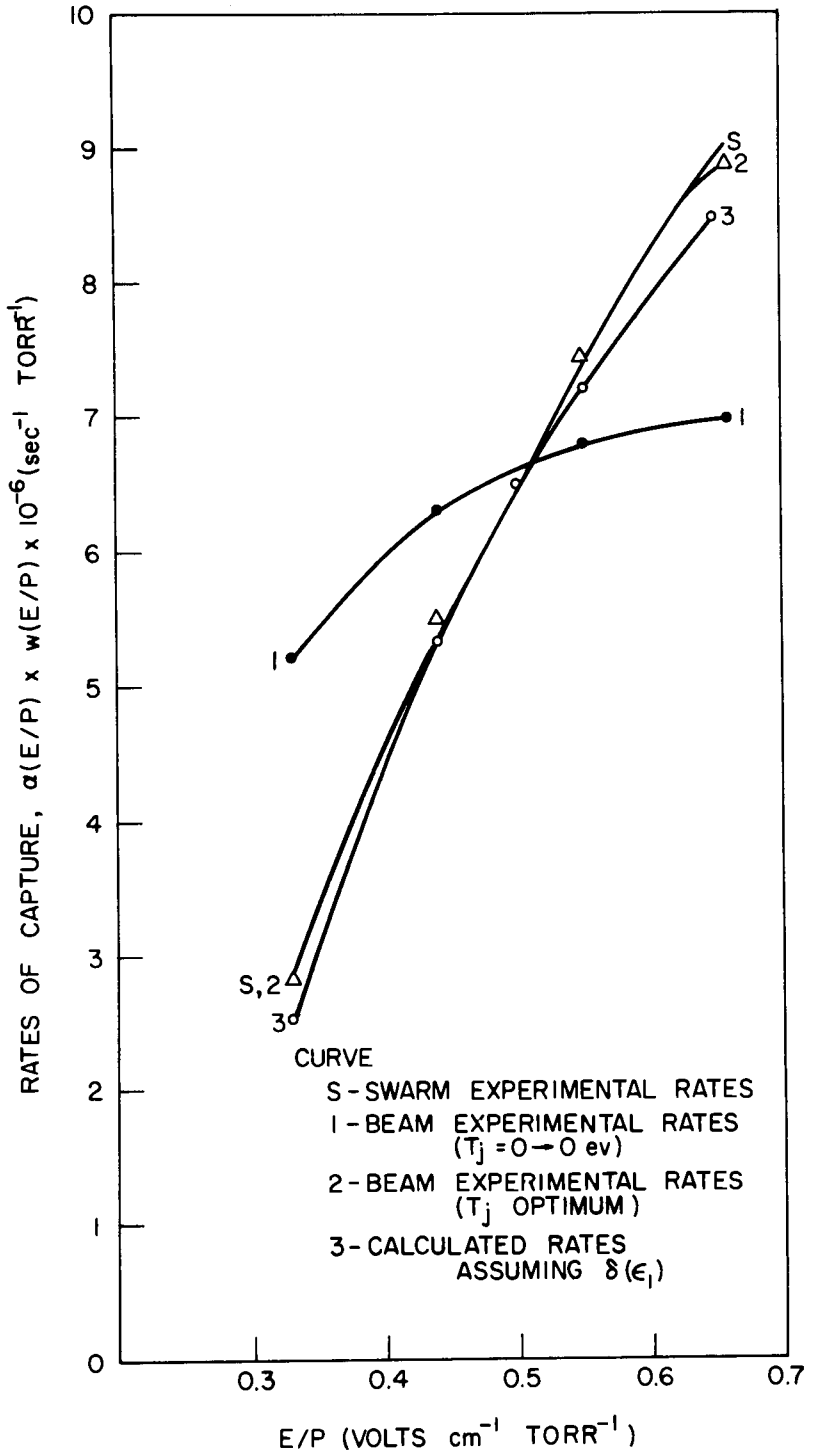

Figure 17. Experimental and calculated rates of capture vs E/P for orthochlorotoluene for various types of trial functions.

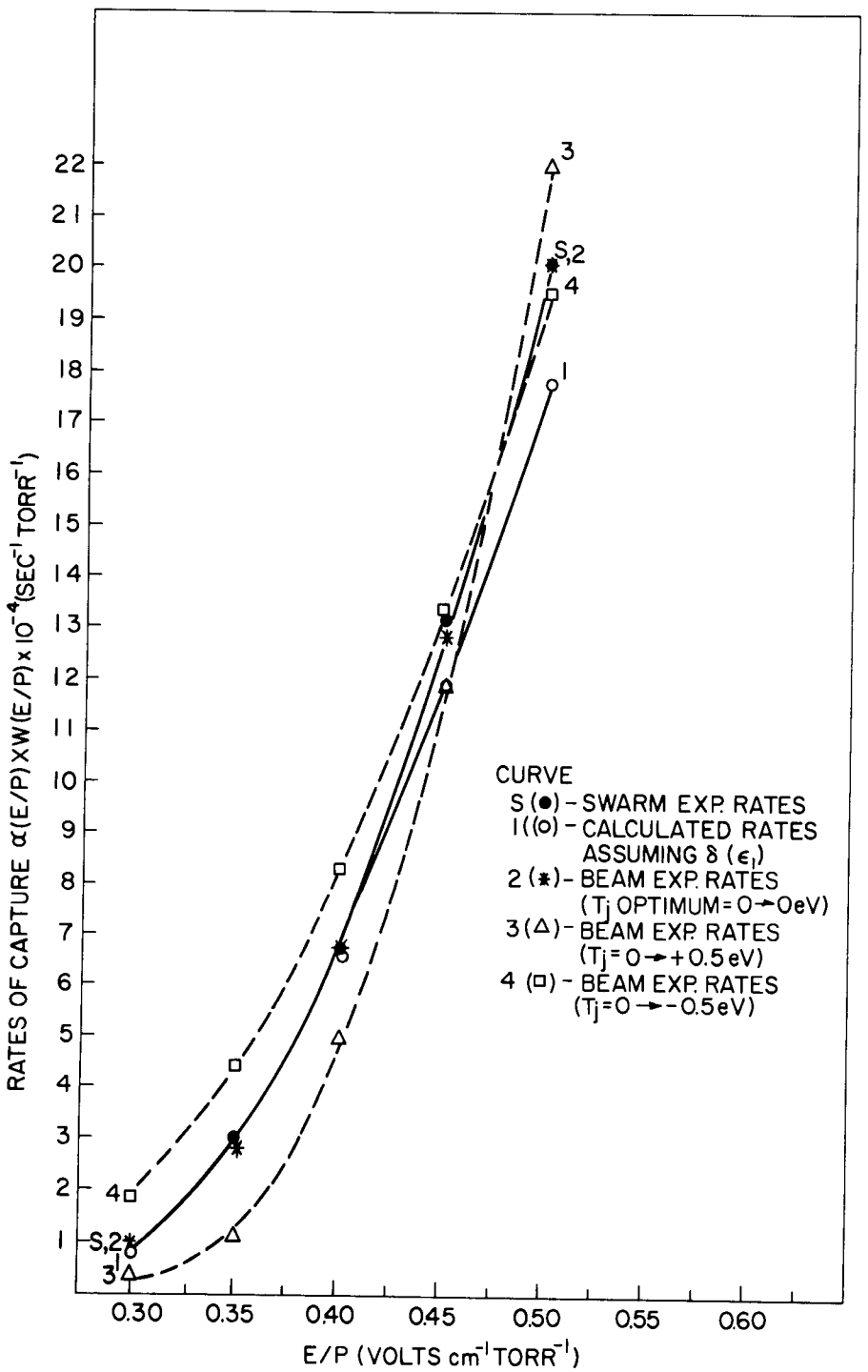

Figure 18. Experimental and calculated rates of capture vs E/P for oxygen for various types of trial functions.

of electron energy ϵ, $\sigma_c(\epsilon)$, can be calculated. Figures 19 and 20 show $\sigma_c(\epsilon)$ for o-$C_6H_4CH_3Cl$ and O_2. The cross sections are plotted against electron energy in eV and are given in units of cm^2. Since these cross sections are based on electron beam data which are just translated in energy and are then normalized in magnitude, both operations being determined by fitting the swarm data, they may be appropriately described as "swarm normalized beam cross sections".

In summary, the following two points should be emphasized:

1. The actual energy at which $\sigma_c(\epsilon)$ peaks is neither ϵ_1, calculated from the swarm data $[\sigma_c(\epsilon) \simeq \delta(\epsilon_1)]$, nor $\epsilon_b(max)$, found in the beam experiments $[\sigma_c(\epsilon) \simeq \sigma_b(\epsilon)]$, but $\epsilon_b(max) + T_j(opt)$. This energy, $\epsilon_b(max) + T_j(opt)$, is obtained when the capture rates $\alpha \times w$ vs E/P computed from the beam data best fit the swarm experimental rates. It has to be stressed at this point that the swarm-beam combination establishes a new energy calibration method which is entirely independent of the electron beam calibration technique. The sign (positive) of $T_j(opt)$ observed in these experiments is in accord with the direction in which errors in the energy scale (when SF_6 is employed for calibration) can be made as pointed out by Schulz (1960b). The magnitude of $T_j(opt)$ (0.15 eV to 0.42 eV for various halogenated benzene derivatives to be reported) is probably well within the potential uncertainties

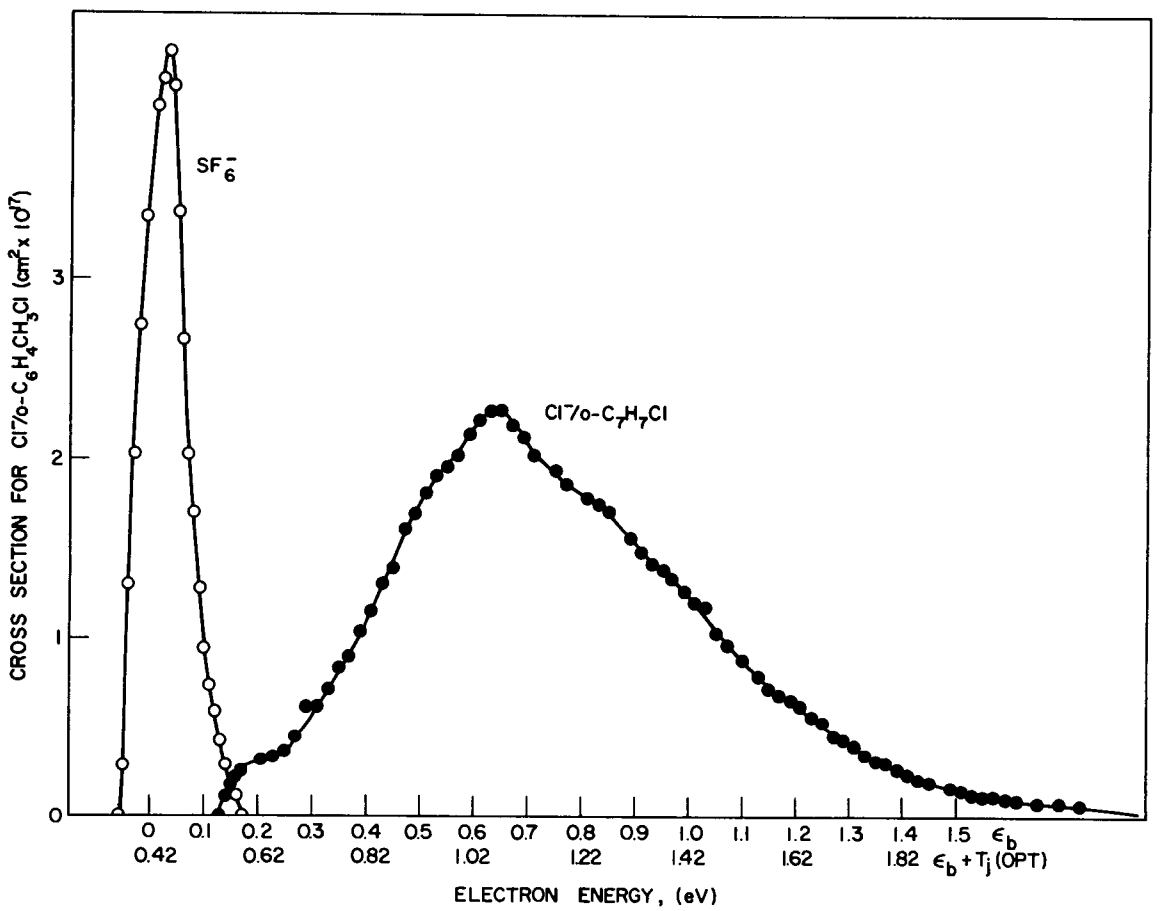

Figure 19. Electron capture cross section as a function of energy for chlorine negative ions from ortho-chlorotoluene.

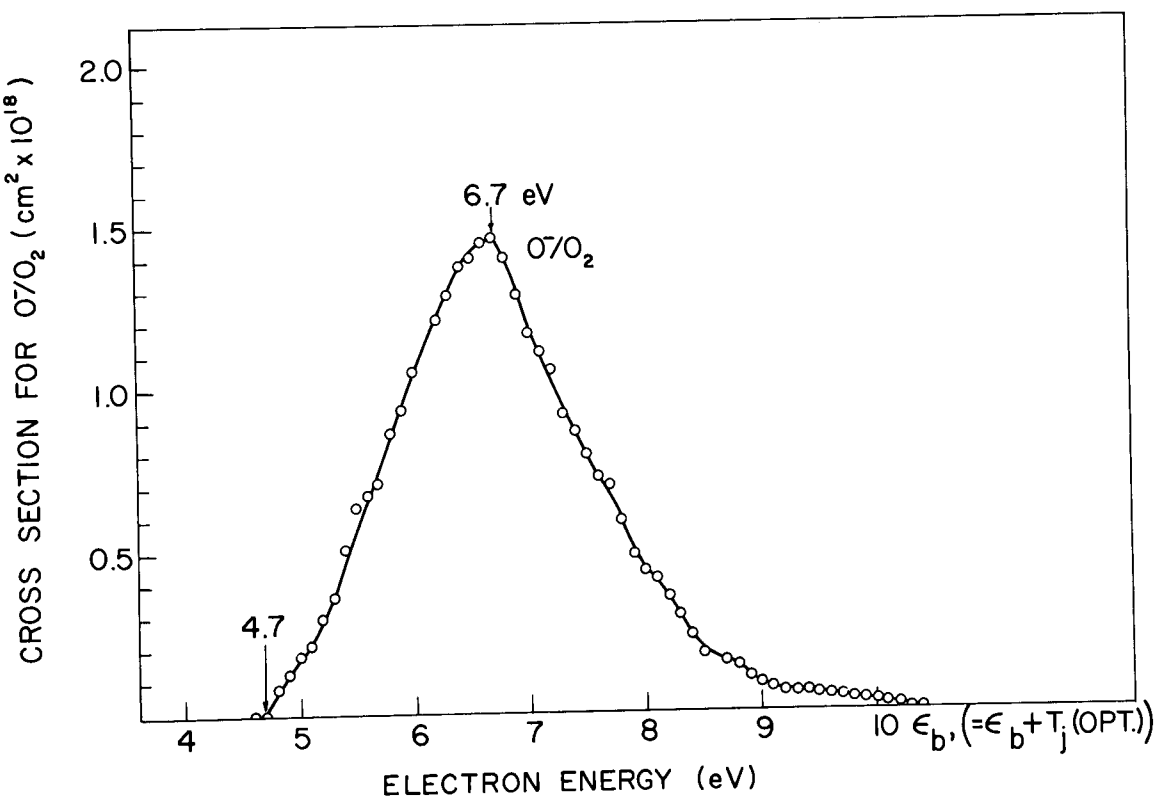

Figure 20. Electron capture cross section as a function of energy for oxygen.

expected in these studies. These potentials have been shown to be quite large [Pauly, Petmecky, and Schmidt (1965)] and could easily account for the required positive energy shifts.

2. Absolute capture cross sections as a function of electron energy can be determined through the combination of swarm-beam data.

The significance of point 1 may be seen by referring to Table I, page 26, where data obtained by various investigators on the low-energy electron capture by a number of halogenated compounds are tabulated (only data obtained from RPD techniques are included). A considerable disagreement is found to exist on the energy at which the electron capture processes peak, although in some cases SF_6 was used for energy calibration (e.g., I^- from I_2, Br^- from HBr, or Cl^- from CCl_4). Such a discrepancy is unlikely to occur in the combined swarm-beam method. Even at higher energies there is still a considerable disagreement as can be seen from Table VII where the available data on O^- from O_2 are presented. In the combined swarm-beam technique the capture rates $\alpha \times w$ vs E/P computed from the beam data on O_2 best fit the swarm rates for $T_j = 0 \rightarrow 0$ eV, i.e., for $\epsilon_b(\max) + T_j(\text{opt}) = 6.7$ eV. This value is in good agreement with most of the recent experiments reported in Table VII.

With respect to point 2, the significance of the swarm-beam combination in determining absolute electron capture cross sections must be emphasized. As a rule, mass spectroscopy and beam experiments report

TABLE VII

DATA FOR THE PRODUCTION OF O^- FROM O_2

	Onset (eV)	ϵ_b(max) (eV)	σ_b(max) (cm^2)
Present work	4.9	6.7	1.5×10^{-18}
Schulz[a]	4.4	6.7	1.3×10^{-18}
Craggs *et al.*[b]	4.7	6.7	2.25×10^{-18}
Randolph and Geballe[c]	3.75	6.2	
Lozier[d]	4.5	7.2	
Buchel'nikova[e]	4.63	6.2	1.3×10^{-18}
Curran[f]	4.3	6.7	
Asundi *et al.*[g] Relative	4.72	6.9	1.34×10^{-18}
Asundi *et al.*[g] Absolute	4.6	6.5	1.3×10^{-18}
Rapp and Briglia[h]	4.5	6.5	1.5×10^{-18}

[a]G. J. Schulz, Phys. Rev. 128, 178 (1962).

[b]J. D. Craggs, C. Thorburn, and B. A. Tozer, Proc. Roy. Soc. (London) A240, 473 (1957).

[c]P. L. Randolph and R. Geballe, thesis, University of Washington, 1958.

[d]W. W. Lozier, Phys. Rev. 46, 268 (1934).

[e]I. S. Buchel'nikova, Soviet Phys.—JETP 35 (8), 783 (1959).

[f]R. K. Curran as reported by G. J. Schulz, Phys. Rev. 128, 178 (1962).

[g]R. K. Asundi, J. D. Craggs, and M. V. Kurepa, Proc. Phys. Soc. (London) 82, 967 (1963).

[h]D. Rapp and D. D. Briglia, J. Chem. 43, 1480 (1965).

relative cross sections while in swarm experiments only the rate of capture $\alpha(E/P) \times w(E/P)$ can be calculated. However, in a few cases absolute cross sections have been calculated from total ionization measurements which did not include mass analysis. Table VII compares the value of 1.5×10^{-18} cm^2 obtained from the swarm-beam combination to those which are found in the literature. It is seen that most of these values are in agreement with the present work. The difference between 1.5×10^{-18} cm^2 obtained from this work and that of Buchel'nikova (see Table VII) is believed to be due to the different shapes of the O^- curves in the vicinity of the maximum where the cross section for O^- as reported by Buchel'nikova is considerably "flatter" than that shown in Figure 20. This statement is borne out by the fact that the integrated cross sections for the two different experiments are equivalent (3.0×10^{-18} cm^2 eV). The appearance potential of 4.9 eV found in the present work seems to be higher than the values listed in Table VII, however 4.9 eV is in exact agreement with the value reported by Thorburn (1954) and McDowell and Warren (1951). Notice also that the appearance potential as reported by Buchel'nikova would be 5.13 eV if the peak of the cross section is shifted to agree with 6.7 eV.

Finally, it should be pointed out that in the case of O^- from O_2 and Cl^- from C_7H_7Cl the delta function approximation is very poor. This is to be expected since the width of the electron capture resonances are quite broad. The delta function approximation will only be approximately correct

when the capture process is a narrow resonance. It will be found in the next section, however, that H^- from H_2O can be represented fairly well by this approximation.

CHAPTER IV

ELECTRON CAPTURE CROSS SECTIONS AS A FUNCTION OF ENERGY

I. INVESTIGATION OF H_2O

The electron swarm data used in the present swarm-beam investigation of water was taken from a previous publication by Hurst, O'Kelly, and Bortner (1961).

Schulz (1960a) and Buchel'nikova (1959) have performed total ionization experiments on the formation of negative ions in water. Their data combined with the mass spectrometric measurements of Cottin (1959) and Mann et al. (1958) have shown that the principle negative ion formed by electron impact in water is H^-. Negative atomic oxygen ions are about ten times less abundant and the main peak occurs at approximately 12 eV. In mass spectrometry studies, however, H^- is much less abundant than the O^- ion simply because of discrimination of ions with appreciable initial kinetic energy [see, for example, Berry (1950)]. Since H^- from H_2O possesses considerable kinetic energy, many of the H^- ions become lost to the walls of the ion source before they can be pulsed into the mass analysis section of the mass spectrometer. For this reason it was very important that the electron gate pulse be applied as soon as possible after application of the backing plate pulse.

The electron swarm-beam method was employed to obtain the electron capture cross section as a function of energy for H^- from H_2O. Owing to the small abundance of the O^- peak compared to the H^- peak and since the O^- peak occurs at electron energies which are well above the mean energy of the electron swarm, only the H^- ion curve was employed to determine the electron capture cross section. As a check to this approximation the total ionization ion curves of Schulz (1960a) were treated with the swarm-beam technique also. Figure 21 shows a comparison of the experimental αw's as a function of E/P with the rates calculated from the trial functions based on the two beam experiments. The data of Schulz required no energy shift (i.e., $T_j(\text{opt}) = 0 \rightarrow 0$) to obtain agreement with the swarm rates, whereas the beam data obtained in this work required a shift of + 0.2 eV. Figure 22 presents the electron capture cross section as a function of energy for H^- from H_2O. A summary of the results of this study compared with other values reported in the literature is presented in Table VIII. The cross section reported by Buchel'nikova (1959) is seen to be about 30 percent lower than the value reported herein. It is interesting to note that this is approximately the same difference observed in the comparison of the two cross sections obtained for O^- from O_2 (see previous section). Unlike the case of O^- from O_2 the integrated cross sections for the case of H^- from H_2O are considerably different as well. Therefore, the discrepancy in this case cannot be accounted for by different shapes of the ion current curves

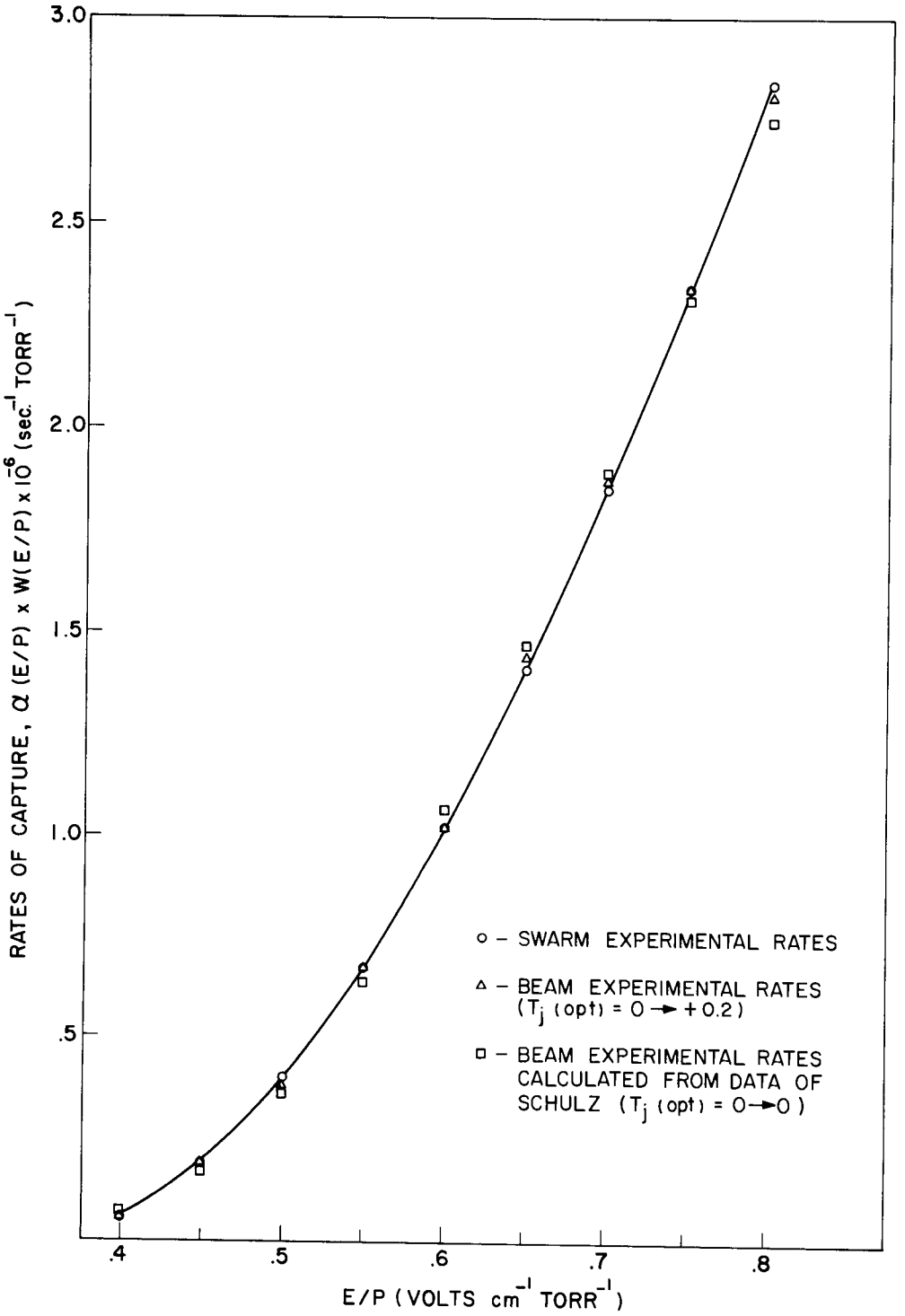

Figure 21. Experimental and calculated rates of capture vs E/P for water for trial functions based on beam experiments.

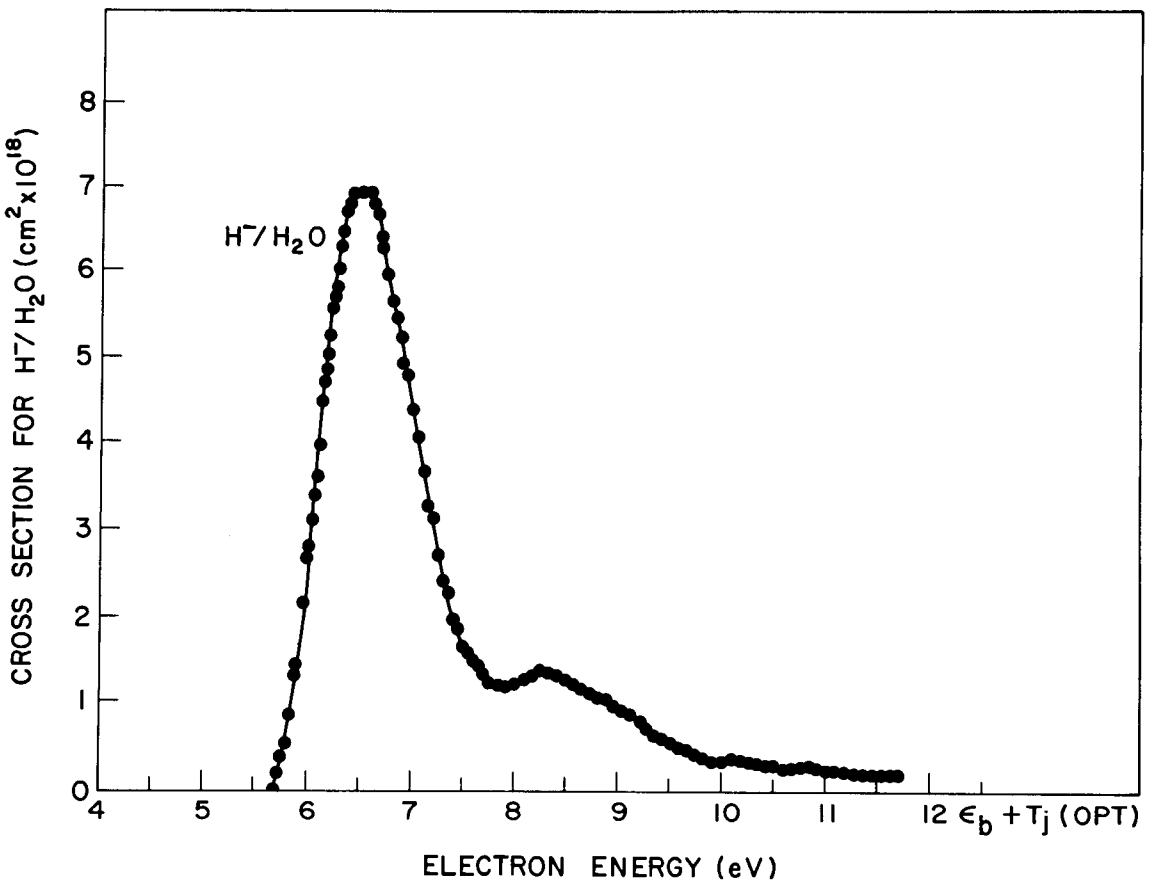

Figure 22. Electron capture cross section as a function of energy for atomic hydrogen negative ions from water.

TABLE VIII

DATA FOR THE PRODUCTION OF H^- AND O^- FROM H_2O

Reference	Probable Process	Onset	Position of Maximum	σ_b(max) (cm^2)
Cox[a]	$H^- + OH$	5.6 ± 0.5		
	$H^- + O + H$			
	$O^- + H_2$	7.5 ± 0.3		
Cottin[b]	$H^- + OH$	4.8 ± 0.2	6.0 ± 0.2	
	$H^- + O + H$		8.0 ± 0.2	
	$O^- + \ldots$	7.4 ± 0.3	9.15	
	$O^- + \ldots$		11.25	
Mann, Hustrulid, and Tate[c]	$H^- + OH$	5.6 ± 0.5	7.1	
	$H^- + O + H$		8.9	
	$O^- + \ldots$	7.5 ± 0.3	8.2	
	$O^- + \ldots$		11.1	
	$O^- + \ldots$		12.8	
Lozier[d]	$H^- + OH$		6.8	
	$H^- + O + H$		8.8	
Schulz[e]	$H^- + OH$	5.6 ± 0.1	6.5 ± 0.1	7.8×10^{-18}*
	$H^-(?) + OH$		8.5 ± 0.1	1.8×10^{-18}*
	$O^- + \ldots$		~ 12	
Buchel'nikova[f]	$H^- + OH$	5.45 ± 0.09	6.4 ± 0.1	$(4.8 \pm 1.5) \times 10^{-18}$
	$H^-(?) + OH$		8.6 ± 0.1	$(1.3 \pm 0.1) \times 10^{-18}$
Present Work	$H^- + OH$	5.7 ± 0.2	6.47	6.94×10^{-18}
	$H^- + OH$		8.6	1.33×10^{-18}
	$O^- + H_2$	4.5 ± 0.2	6.6	
	$O^- + \ldots$	7.5 ± 0.2	8.6	
	$O^- + \ldots$		11.1	

*As determined by the swarm beam technique (see text).

[a]B. C. Cox, Ph.D. thesis, University of Liverpool, 1953.

References to Table VIII (continued)

[b]M. Cottin, J. Chim. Phys. 56, 1024 (1959).

[c]M. M. Mann, A. Hustrulid, and J. T. Tate, Phys. Rev. 58, 340 (1940).

[d]W. W. Lozier, Phys. Rev. 36, 1417 (1930).

[e]G. J. Schulz, J. Chem. Phys. 33, 1661 (1960).

[f]I. S. Buchel'nikova, Soviet Phys.—JETP 35(8), 783 (1959).

in the two experiments.

The O^- ion current curve from H_2O is shown in Figure 23. The spectrum exhibits three peaks (see also Table VIII). The O^- peak at approximately 6.5 eV was not observed in the study of Cottin (1959), however it was observed by Mann et al. (1940), Cox (1953), and Melton (1963). It is quite possible that this peak is due to oxygen impurities in the water sample, however the ratio of this low-energy peak to the maximum is seen to be approximately the same in the four experiments in which it was observed. The chance that the same relative amount of oxygen was present in the three experiments seems unlikely.

Negative hydroxyl was not observed in mass spectrometry at low pressures ($\sim 10^{-6}$ mm Hg), however at higher pressures OH^- becomes the most abundant ion. The experiments of Muschlitz (1957) and Cottin (1959) showed that OH^- resulted from ion molecule reactions involving H^- and possibly O^- with H_2O. Figure 24 indicates that OH^- peaks correlate exactly with the appearance of H^- and O^-. In fact, the shape of the OH^- curve is identical to that of H^-. A plot of $\ell n(OH^-)$ vs $\ell nP(H_2O)$ yielded a slope between 1 and 2 as would be expected for the case of ion molecule reactions in which the primary ions (H^-) were being depleted by a secondary reaction. Furthermore, the OH^- ion current increased linearly with the time delay between the electron gate pulse and the ion pusher pulse which indicates that as the time in which H^- reacts with H_2O increases, the OH^- ion current

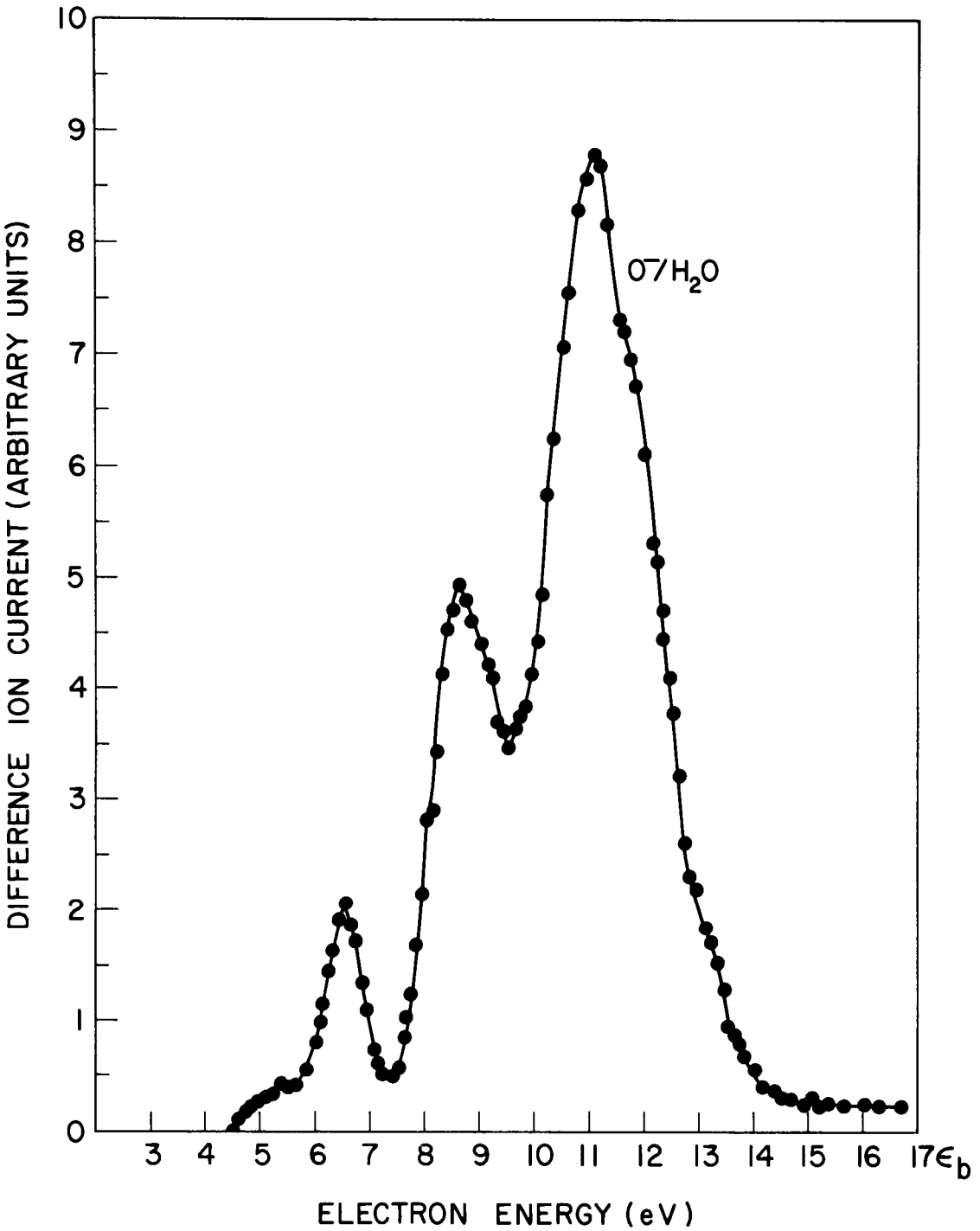

Figure 23. Atomic oxygen negative ions from water.

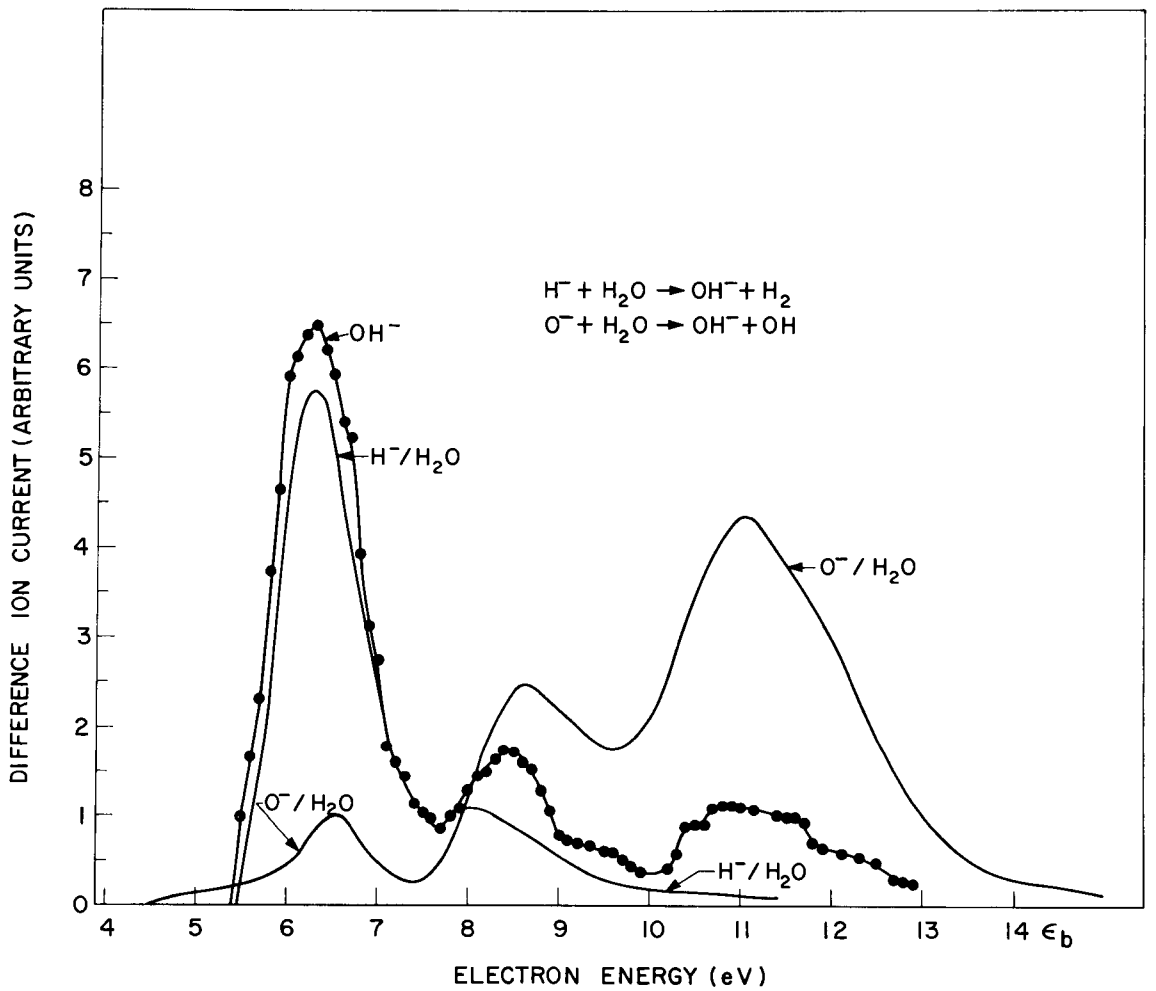

Figure 24. Hydroxyl negative ions produced by ion molecule reactions in water.

increases. Unfortunately, the effect of diffusion of H^- to the walls did not allow a measurement of the rate constant for the reaction to be made. From this work and that reported previously, there is little doubt that OH^- is produced in water vapor by the following mechanisms:

$$H^- + H_2O \rightarrow OH^- + H_2$$

$$O^- + H_2O \rightarrow OH^- + OH.$$

An explanation for the fact that OH^- does not appear at low pressure in electron impact experiments was first given by Ladier (1954). Ladier concluded that since OH^- ($^1\Sigma$) has such a stable electronic configuration, the approach of a hydrogen atom produces a very strong repulsion and, therefore, the negative ion state resulting from this configuration plays no role in electronic excitation. The negative ion states which result from direct electron impact would be less stable and most probably repulsive so that the negative ion states would dissociate into O^- rather than OH^-. For example, if H_2O^- (^2B) decomposes to form H ($^2S_{1/2}$) + OH^- ($^2\Pi$), then the OH^- ($^2\Pi$) would further decompose into O^- + H.

II. INVESTIGATION OF C_6H_5Cl, o-$C_6H_4Cl_2$, m-$C_6H_4Cl_2$, p-$C_6H_4Cl_2$, o-$C_6H_4CH_3Cl$; C_6H_5Br, C_6D_5Br, AND o-$C_6H_4CH_3Br$; C_6H_5I

The captioned molecules were studied by the swarm method in mixtures with N_2. Representative $\alpha(E/P)$ vs f_1P/f_2P curves in mixtures of halogenated benzene derivatives with N_2 are given in Figure 25 for o-$C_6H_4CH_3Br$. The electron swarm drift velocities in N_2 were almost identical with those obtained by Bortner, Hurst, and Stone (1957), and the effect of the impurity on w(E/P) was taken into account. From the representative data in Figure 25, it is clear that the values of $\alpha(E/P)$ fall on a straight line independently of the total pressure. The values of $\alpha(E/P)$ for $f_1P/f_2P \rightarrow 0$ are listed in Table IV, page 87, as $\alpha_o(E/P)$ for the N_2 mixtures. In Table IV the capture rates, $\alpha_o(E/P) \times w(E/P)$, are given also for a number of E/P for mixtures with N_2. The capture rates for mixtures with N_2 are independent of the total pressure for all of the sample gases studied. This indicates either (1) a dissociative process, (2) a non-dissociative process with complete stabilization occurring even at the lowest total pressure used in the swarm experiments, or (3) temporary non-dissociative capture with a lifetime greater than the $\sim$20 microseconds required by the swarm technique.

The difference ion currents for Cl^-, Br^-, or I^- were obtained from the beam experiments for the respective halogenated benzene derivatives. Typical curves for the chlorinated benzene derivatives are presented in

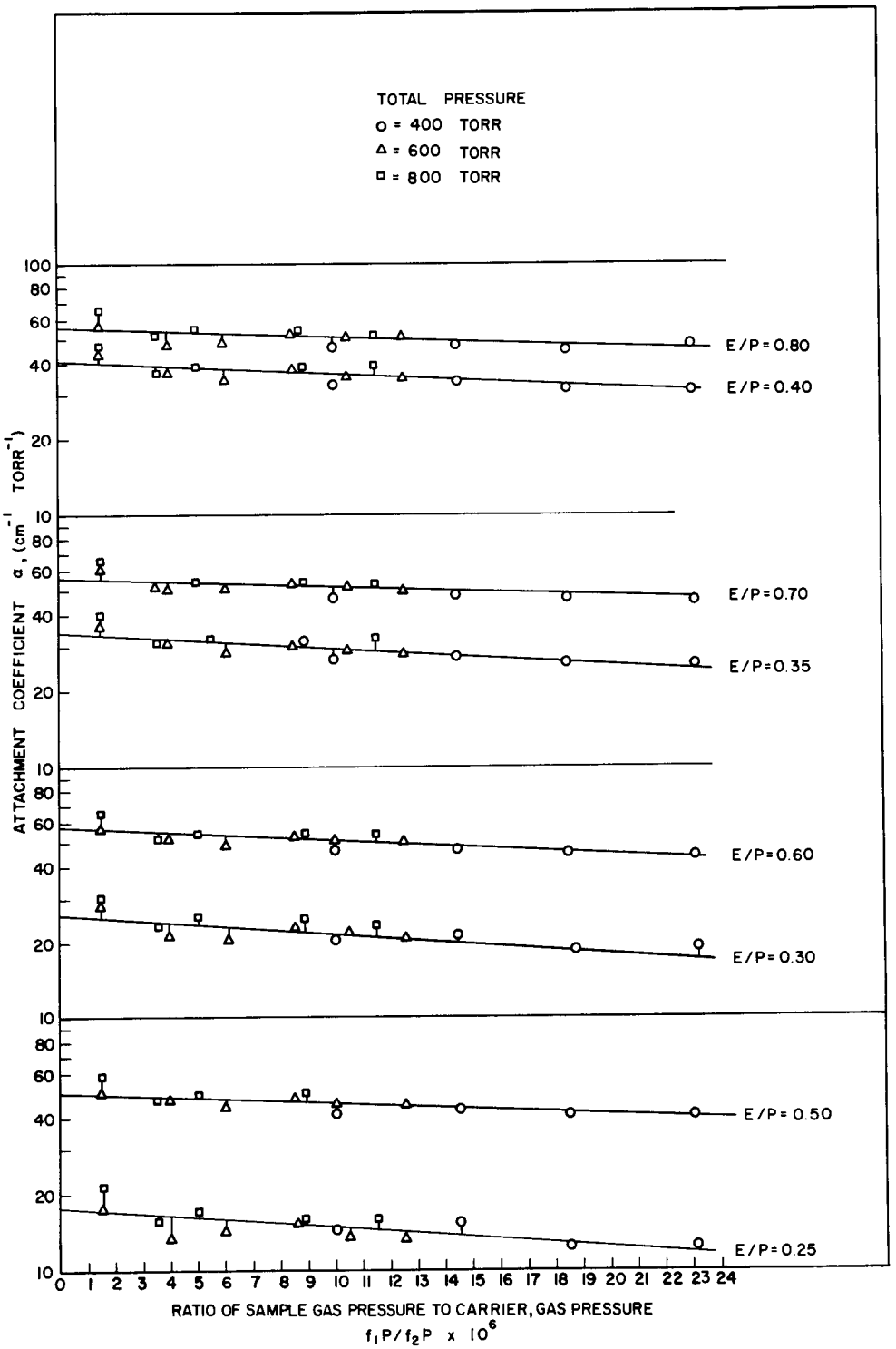

Figure 25. $\alpha(E/P)$ vs f_1P/f_2P for ortho-bromotoluene in nitrogen.

Figure 26. The SF_6 technique was employed to calibrate the electron energy scale. The Cl^- ion currents from o-, m-, and p-$C_6H_4Cl_2$ are observed to peak below 0.2 eV. Since the difference electron current is decreasing rapidly in this region, the energy at which the ion currents peak and the shape of the ion current curves as a function of electron energy are mainly instrumental. Therefore, it was not possible to treat m- and p-$C_6H_4Cl_2$ with the combined swarm-beam technique, and the treatment of o-$C_6H_4Cl_2$ is probably in error. It is clear, however, that the energy at which the capture process peaks decreased in the order o-$C_6H_4CH_3Cl$, C_6H_5Cl, o-, m-, and p-$C_6H_4Cl_2$ (see Table IX). The brominated benzene derivatives behave similarly to C_6H_5Cl.

Difficulties were encountered in establishing the electron energy scale for the case of I^- from C_6H_5I by use of SF_6. Since both processes, SF_5^- from SF_6 and I^- from C_6H_5I, occur at approximately zero energy and the two masses could not be sufficiently resolved (Δm = 0.07 amu) with the time-of-flight mass spectrometer, it was impossible to employ SF_6^- to calibrate the electron energy scale. Previous investigators [Frost and McDowell (1958)] overcame this difficulty in an investigation of I^- from HI by subtracting the predetermined SF_5^- current from the total $SF_5^- + I^-$ current measured with both gases present in the mass spectrometer. This procedure was unsatisfactory in the present experiment due to changes in electron current and electron energy distribution upon introduction of C_6H_5I

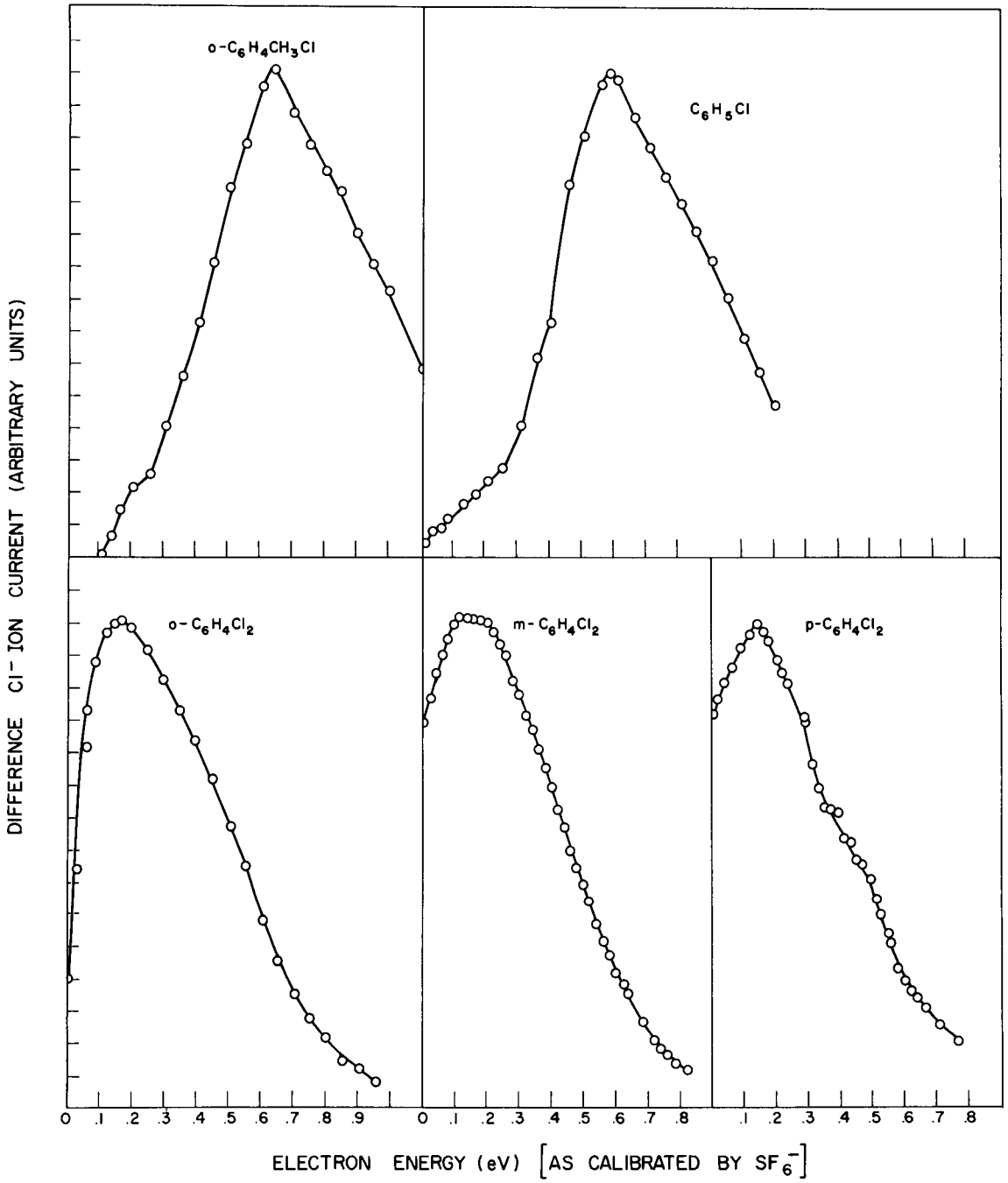

Figure 26. Cl^- ion current vs electron energy (as calibrated by SF_6^-) for chlorinated benzene derivatives.

TABLE IX

ELECTRON CAPTURE DATA OBTAINED BY THE SWARM-BEAM METHOD

Compound	Formula	Ion	ϵ_b(max) (eV)	ϵ_b(max) + T_j(opt) (eV)	σ_{bj}(max) $cm^2 \times 10^{17}$	D(A - X) (eV)	EA(X) (eV)
Chlorobenzene	C_6H_5Cl	Cl^-	0.60	0.86	1.4	3.73 ± 0.13[a, b, c]	
o-Dichlorobenzene	o-$C_6H_4Cl_2$	Cl^-	0.19	0.36(?)	43 (?)		3.613[d]
m-Dichlorobenzene	m-$C_6H_4Cl_2$	Cl^-	0.17(?)				3.76[e]
p-Dichlorobenzene	p-$C_6H_4Cl_2$	Cl^-	0.14(?)				3.71[f] 3.69[g]
o-Chlorotoluene	o-$C_6H_4CH_3Cl$	Cl^-	0.66	1.10	2.2		
Bromobenzene	C_6H_5Br	Br^-	0.51	0.84	9.6	3.04[a] 3.07[h]	
Deuterated Bromobenzene	C_6D_5Br	Br^-	0.51	0.80	10.4		3.363[d] 3.51[e] 3.45[g]
o-Bromotoluene	o-$C_6H_4CH_3Br$	Br^-	0.63	0.95	6.0		

TABLE IX (continued)

Compound	Formula	Ion	ϵ_b(max) (eV)	ϵ_b(max) + T_j(opt) (eV)	σ_{bj}(max) $cm^2 \times 10^{17}$	D(A - X) (eV)	EA(X) (eV)
Iodobenzene	C_6H_5I	I^-	0.00			2.47 ± 0.13[a, c, i]	3.063[d] 3.15[e] 3.23[f]
Chloroethane		Cl^-	0.40	0.80(?)	0.007(?)	3.47[j] 3.06[k] 3.51[l]	

[a] M. Szwarc and D. Williams, J. Chem. Phys. 20, 1171 (1952).

[b] W. N. Hubbard, J. W. Knowlton, and H. M. Huffman, J. Phys. Chem. 58, 396 (1954).

[c] A. A. Z. I'berman-Granovskaya and E. A. Shugam, Zhur. Fiz. Khim. 14, 1004 (1940).

[d] R. S. Berry and C. W. Reimann, J. Chem. Phys. 38, 1540 (1963).

[e] T. L. Bailey, J. Chem. Phys. 28, 792 (1958).

[f] I. N. Baculina and N. I. Ionov, Dokl. Acad. Nauk SSSR 105, 680 (1955).

[g] D. Cubiciotti, J. Chem. Phys. 31, 1646 (1959).

[h] T. L. Cottrell, The Strengths of Chemical Bands (Butterworths, London, 1958).

[i] A. S. Carson, E. M. Carson, and B. Wilmhurst, Nature 170, 320 (1952).

[j] M. Szwarc, Chem. Reviews 47, 75 (1950).

[k] A. P. Irsa, J. Chem. Phys. 26, 18 (1955).

[l] M. R. Lane, J. W. Linnett, and H. G. O. Oswin, Proc. Roy. Soc. (London) 216A, 361 (1953).

into the mass spectrometer. It was found, however, that $C_6H_5NO_2$ captures electrons through a very sharp (non-dissociative) resonance for which the $C_6H_5NO_2^-$ ion current curve is identical to that of the SF_6^- resonance (see later in this section). Therefore, the resonance capture process in $C_6H_5NO_2$ was used to give a first calibration of the electron energy scale and to estimate the electron beam energy distribution for the investigation of I^- from C_6H_5I.

In Figure 27 the I^- ion current (solid circles) and the $C_6H_5NO_2^-$ ion current (open circles) are shown as a function of the electron accelerating voltage. The two different ion currents were measured simultaneously. It was not possible to calculate $\sigma_c(\epsilon)$ for I^- from C_6H_5I because:

1. The swarm data were not accurate since the high capture cross sections at thermal energies required measurements at very low pressures, and this introduces a large error in the calculation of $\alpha(E/P) \times w(E/P)$.
2. The attachment process takes place at energies less than 0.1 eV so that the difference electron current is not constant and thus the shape of $\sigma_c(\epsilon)$ is not accurately determined.

I^- from C_6H_5I is observed to peak at the same electron energy as $C_6H_5NO_2^-$ and the width of the I^- resonance is approximately twice that of $C_6H_5NO_2^-$. The actual capture cross section consequently peaks below 0.03 eV. The I^- ion current peak is $\sim$ 12 times greater than the $C_6H_5NO_2^-$ peak. There also

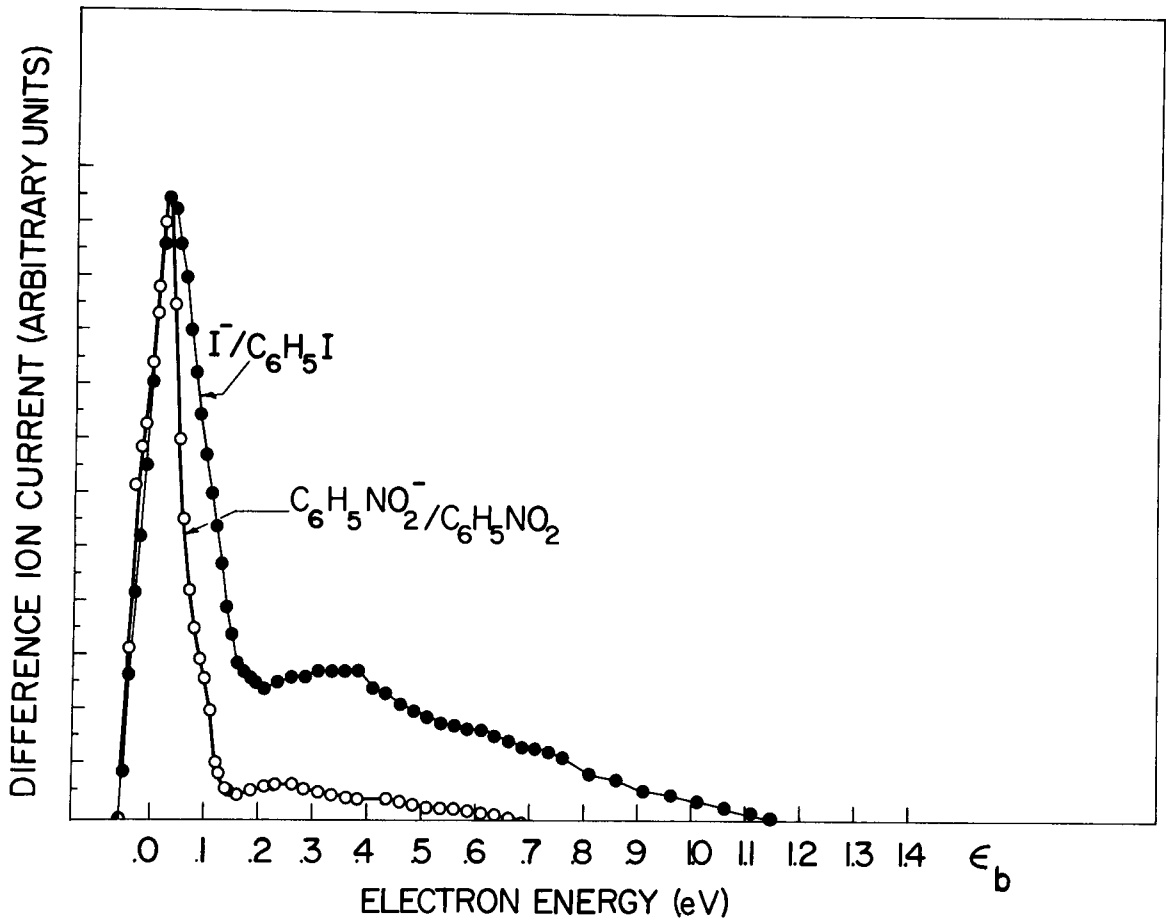

Figure 27. Iodine negative ions from iodobenzene as a function of electron energy.

appears to be a second maxima in the I^- ion current at 0.35 eV. However, the increased electron energy spread could be producing this second maxima. This is evidenced by a comparison of $C_6H_5NO_2^-$ ion current curves in Figures 27 and 33. This effect may be due to a change in surface conditions of the ion source in the presence of C_6H_5I, or secondary reactions in which an electron loses energy by collision with C_6H_5I and then is captured by $C_6H_5NO_2$. The electron swarm data, on the other hand, are indicative of a second electron capture process at energies > kT. A second process could be explained by dissociative electron capture in which $C_6H_5I^-$ is electronically excited or by dissociative electron capture by C_6H_5I molecules which were originally in the first vibrational level. At room temperature about eight percent population of the first excited vibrational state could explain the relative heights of the two I^- peaks in Figure 26, and the different crossing within the Franck-Condon region for these vibrationally excited molecules could explain the second maxima occurring at higher energy.

In Figures 28, 29, and 19, page 100, the capture cross section $\sigma_c(\epsilon)$ is given as a function of the electron energy for Cl^- from C_6H_5Cl, o-$C_6H_4Cl_2$, and o-$C_6H_4CH_3Cl$, respectively. The cross sections for Br^- from C_6H_5Br, C_6D_5Br, and o-$C_6H_4CH_3Br$ are given in Figures 30, 31, and 32, respectively. In these graphs ϵ_b is the electron beam energy scale as determined by SF_6^-, and $\epsilon_b + T_j(opt)$ is the electron beam energy scale corrected by the swarm-beam combination. The SF_6^- difference ion currents are included with the

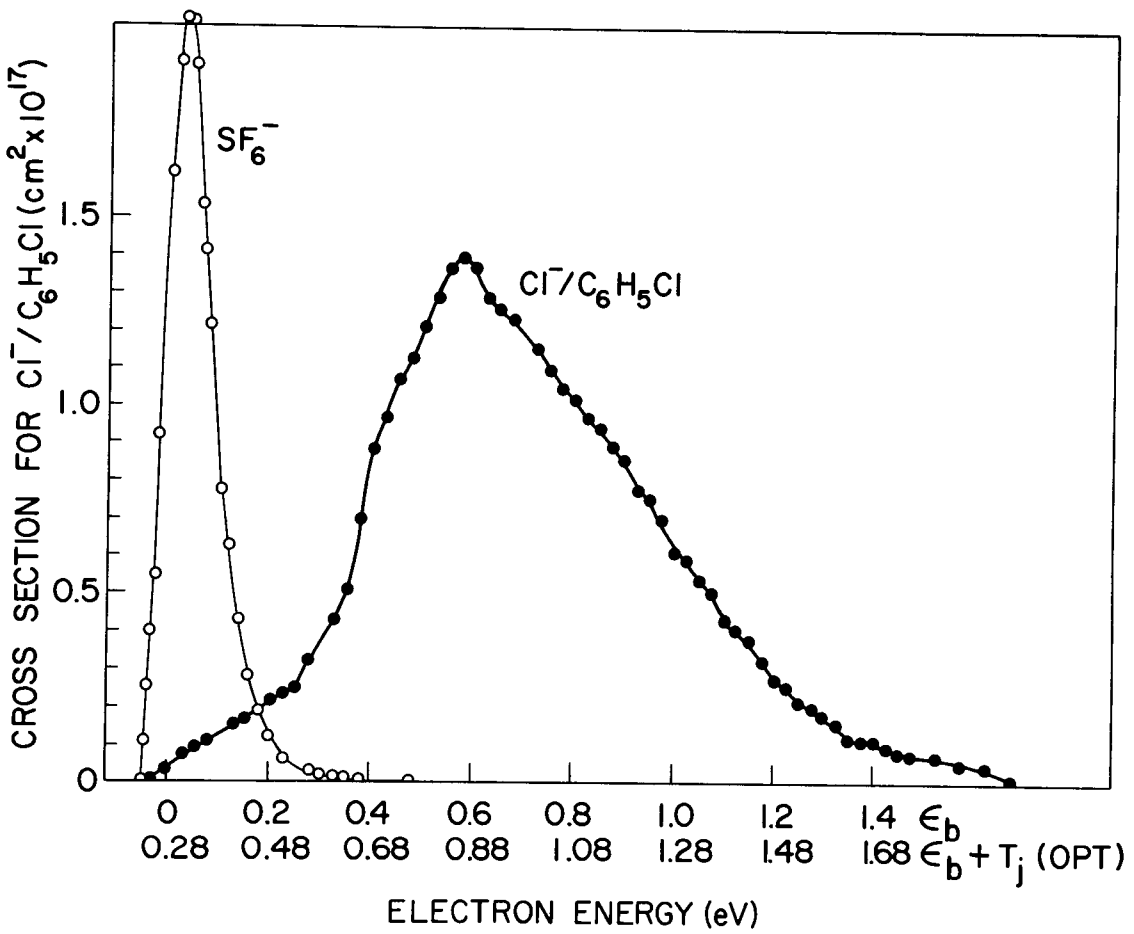

Figure 28. Electron capture cross section as a function of energy for chlorine negative ions from chlorobenzene.

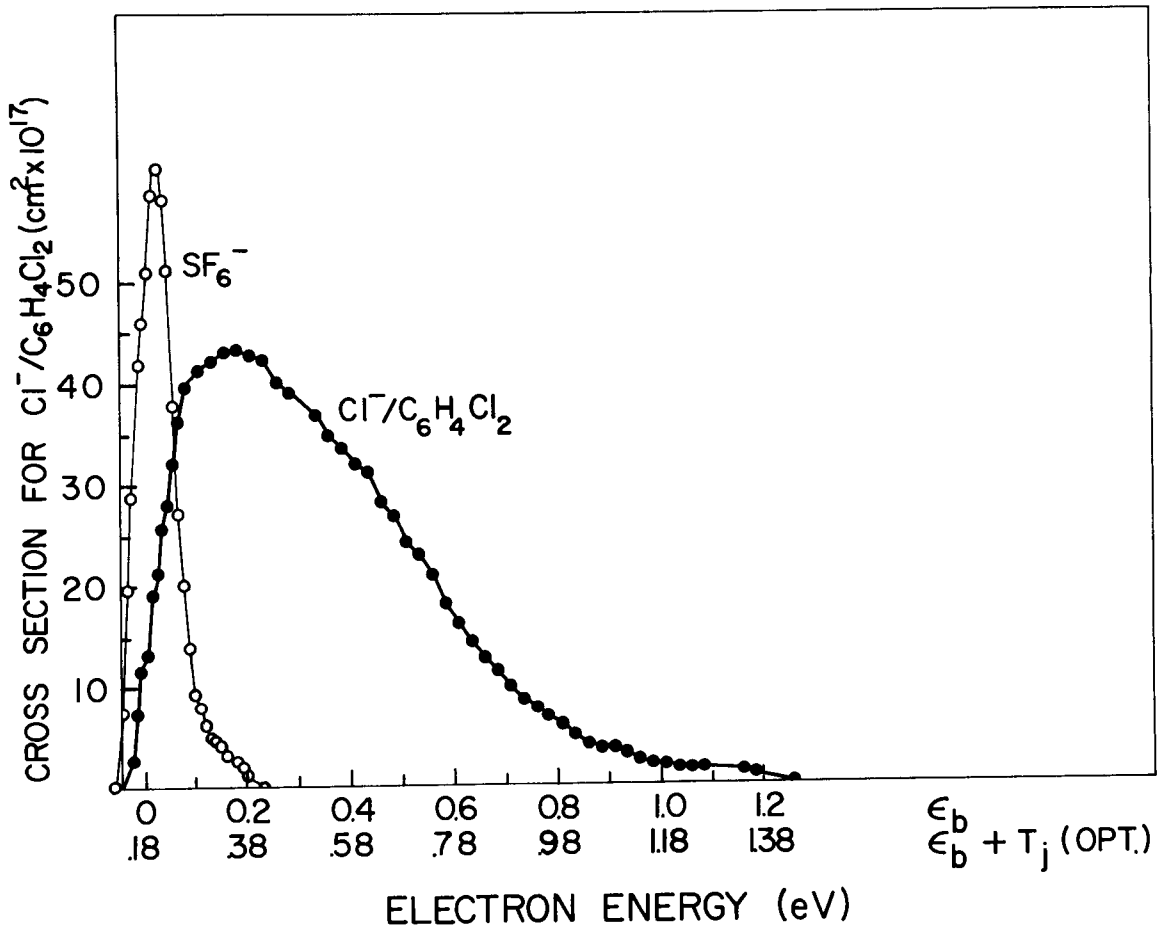

Figure 29. Electron capture cross section as a function of energy for chlorine negative ions from ortho-dichlorobenzene.

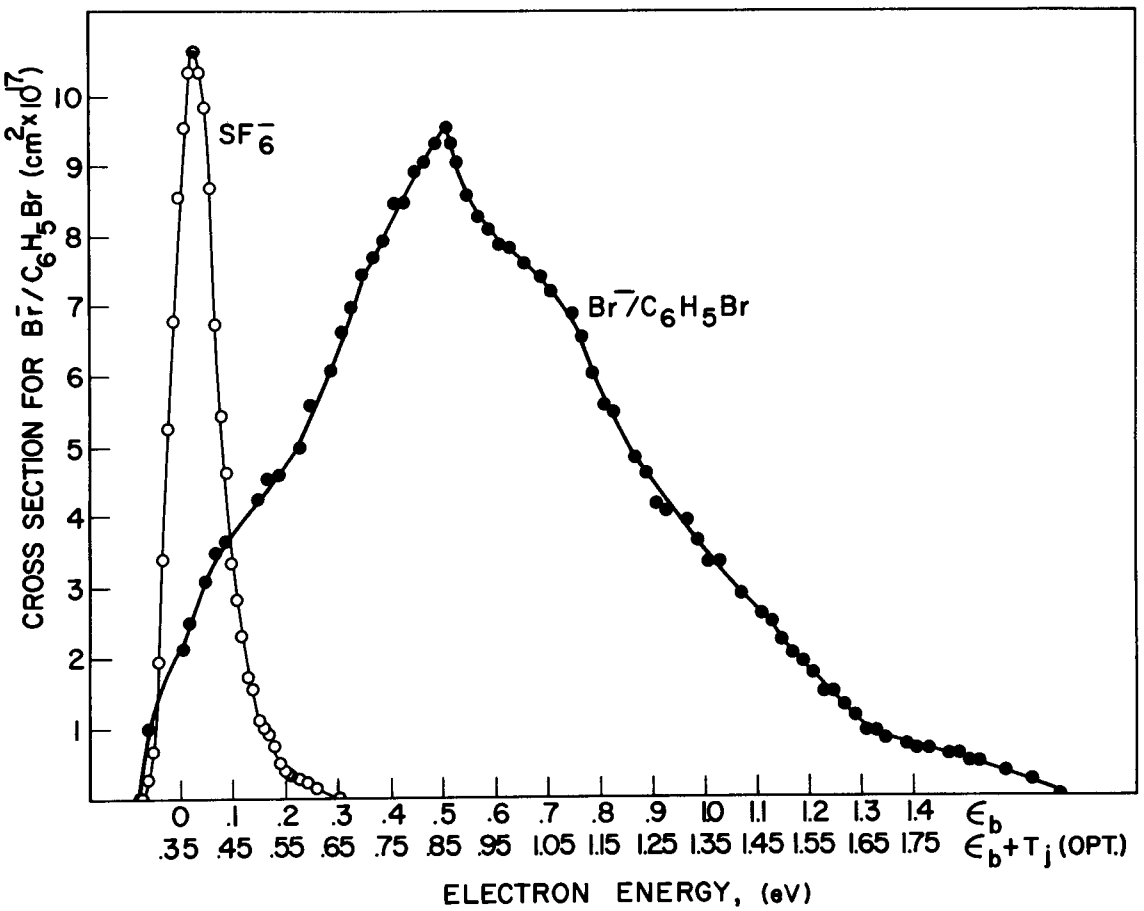

Figure 30. Electron capture cross section as a function of energy for bromine negative ions from bromobenzene.

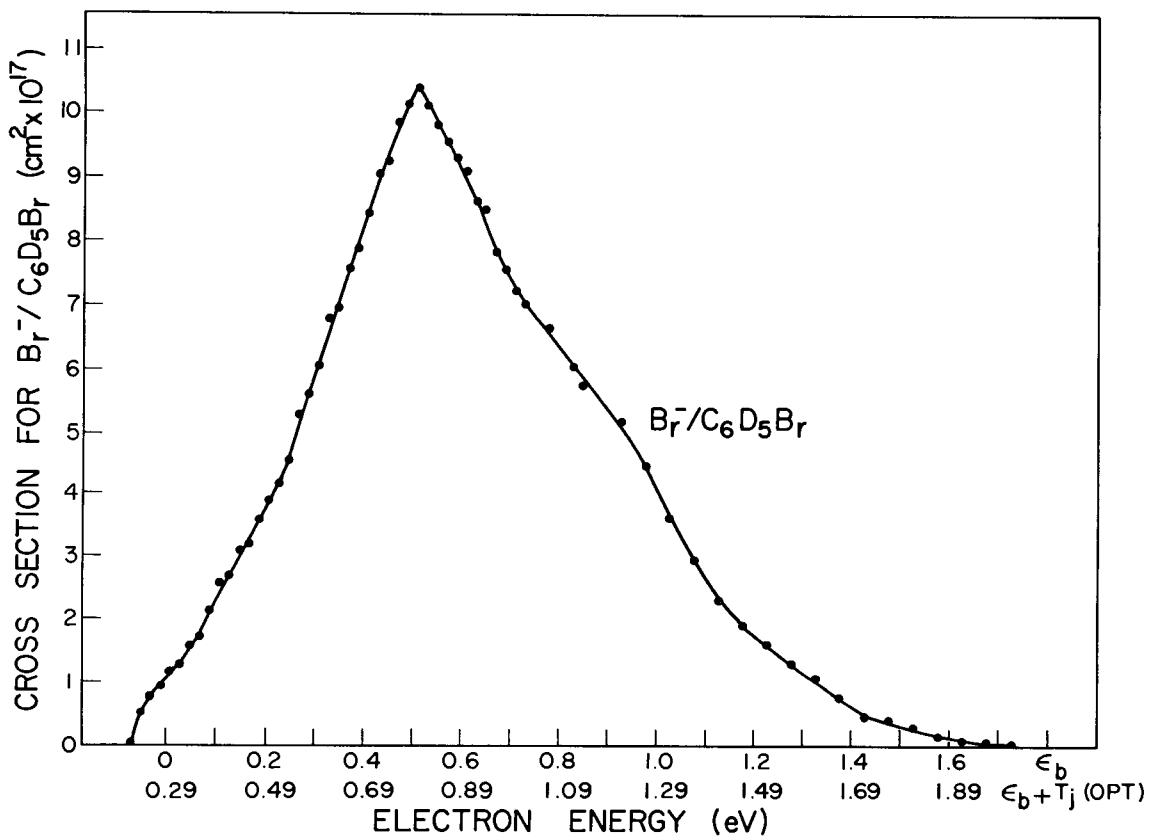

Figure 31. Electron capture cross section as a function of energy for bromine negative ions from deuterated bromobenzene.

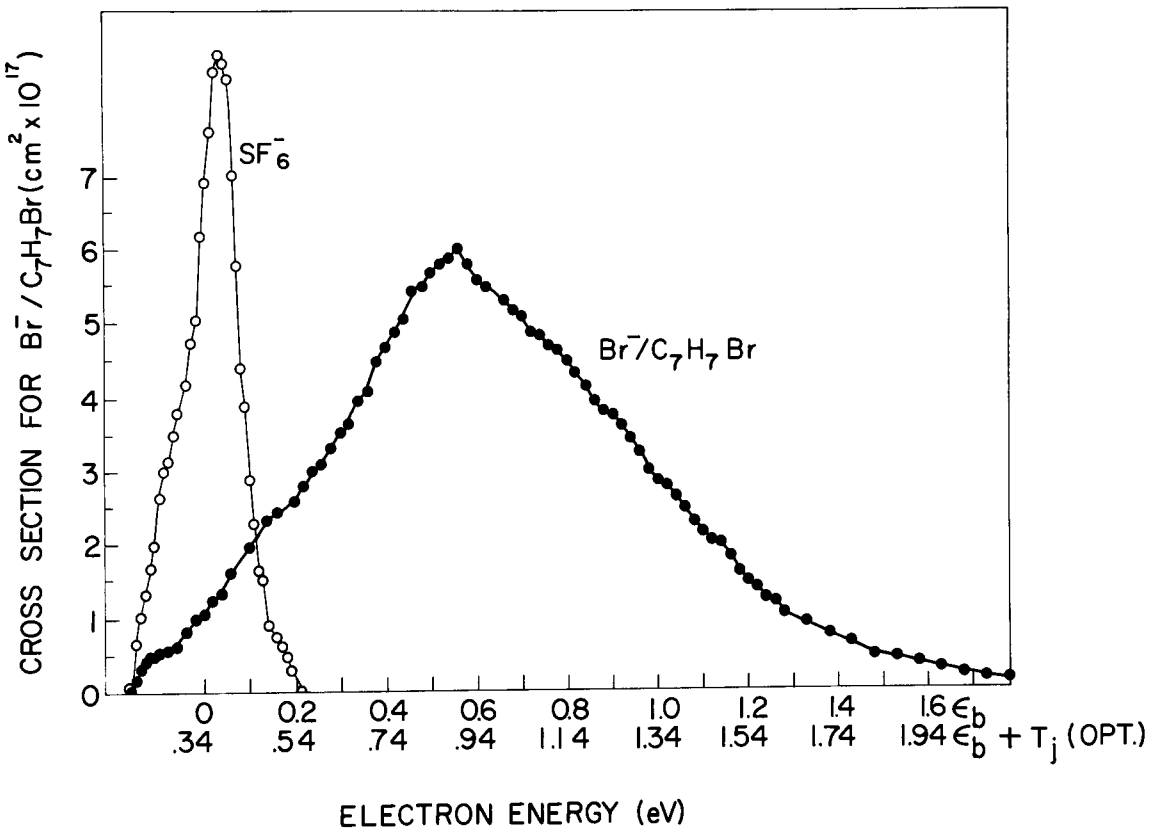

Figure 32. Electron capture cross section as a function of energy for bromine negative ions from bromotoluene.

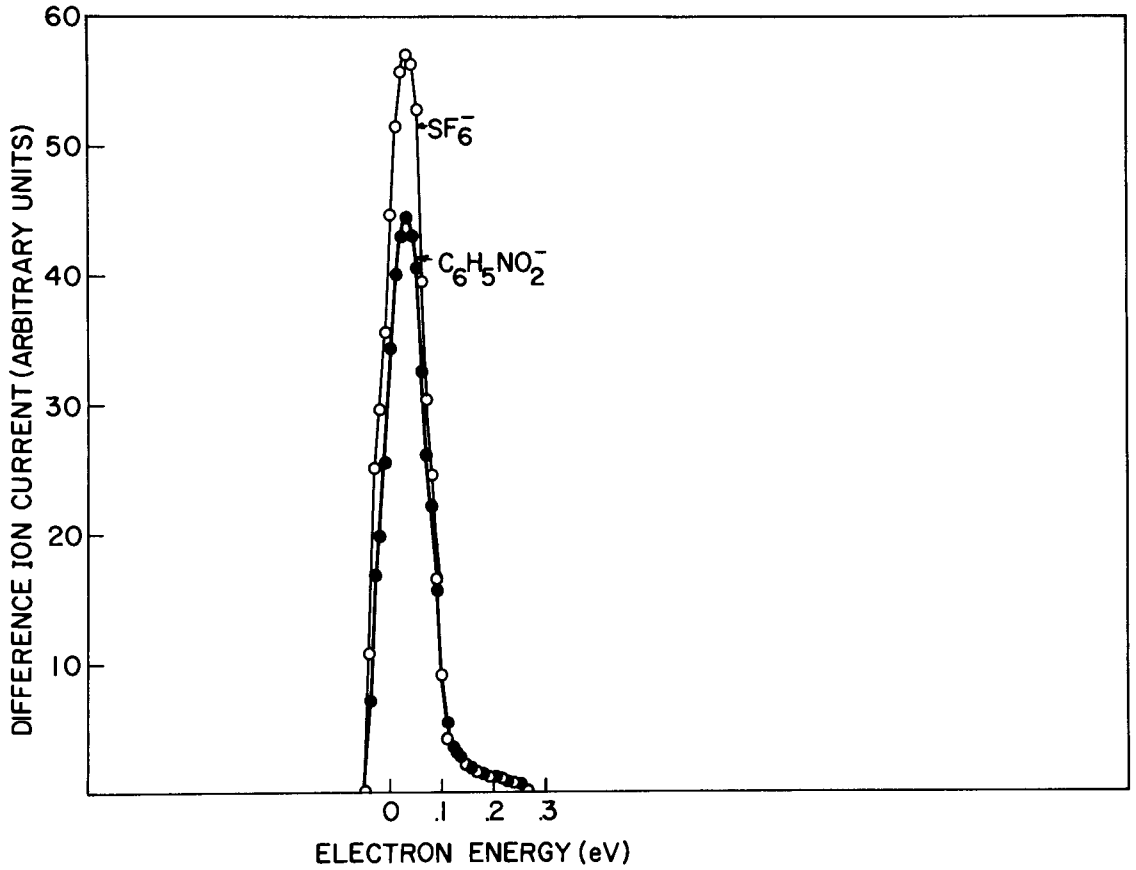

Figure 33. Comparison of $C_6H_5NO_2^-$ ion current with SF_6^- ion current as a function of electron energy.

cross section curves to indicate the approximate electron beam energy distribution. Since the electron beam energy distribution is relatively small compared to the width of the dissociative electron capture resonances, the shapes of the latter may be taken as a first approximation to the actual shape of $\sigma_c(\epsilon)$. In Table IX, page 120, the energy $\epsilon_b(\max) + T_j(\text{opt})$ at which $\sigma_c(\epsilon)$ peaks and the maximum value $\sigma_c(\epsilon)(\max)$ of $\sigma_c(\epsilon)$ are presented. No parent molecular negative ions were observed for any of these compounds. If a resonance non-dissociative process occurs, it should have a cross section less than 10^{-19} - 10^{-20} cm^2 for $\sim$ 0.05-eV electrons. The Cl^- (or Br^-) ion current curves (particularly the curves corresponding to Cl^- from o-, m-, and p-$C_6H_4Cl_2$) indicate that dissociative electron capture occurs down to 0.0 eV.

It is interesting to note that the cross section for electron attachment for C_6H_5Br and C_6D_5Br are essentially the same. The fact that the peak cross section occurs at the same energy for the two compounds rules out the possibility of vibrational excitation of the C-H or C-D stretching vibration prior to dissociation. The well known C-H stretching vibration in the benzene molecule requires $\sim$ 0.37 eV for excitation of the fundamental and $\sim$ 0.75 eV for excitation of the first overtone. Since $\epsilon_b(\max) + T_j(\text{opt})$ was found to be around 0.8 or 4.0 eV for most of the benzene derivatives studied, it was suggestive that the fundamental or the first overtone of the C-H stretching vibration is excited prior to dissociation. If this were the

case, $\epsilon_b(max) + T_j(opt)$ should be smaller for C_6D_5Br than for C_6H_5Br, since the excitation of the first overtone of the C-D stretching vibration requires $\sim$ 0.18 eV less energy than the excitation of the overtone of the C-H stretching vibration. It is found, however, that both compounds behave identically as far as the $\sim$ 1-eV process is concerned (see Table IX, page 120).

III. INVESTIGATION OF $C_6H_5NO_2$, o- AND m-$C_6H_4CH_3NO_2$

Electron beam data show that $C_6H_5NO_2$ captures electrons non-dissociatively at low electron energies and the normalized ion current as a function of electron energy coincides with that of SF_6^- (see Figure 33). The maximum of the cross section for the non-dissociative electron capture occurs below 0.03 eV and the width of the capture resonance as observed in Figure 33 is instrumental. Figure 34 shows that the $C_6H_5NO_2^-$ ion current varies linearly with pressure from 10^{-6} to 10^{-4} Torr. This indicates that the ions are not stabilized by collision. A complete detail of the non-dissociative electron capture process will be given in Chapter V.

Nitrobenzene also captures electrons dissociatively at $\sim$ 1 and $\sim$ 3.5 eV (Figure 35). The non-dissociative resonance in nitrobenzene was employed to calibrate the electron energy scale for the dissociative capture processes. In Figure 36 the appearance potential and the maximum of the $\sim$ 1-eV process occur at 0.43 and 1.07, respectively. Using $EA(NO_2) = 3.99$ eV, an upper limit of 4.42 eV is obtained for $D(C_6H_5\text{-}NO_2)$. A second dissociative process

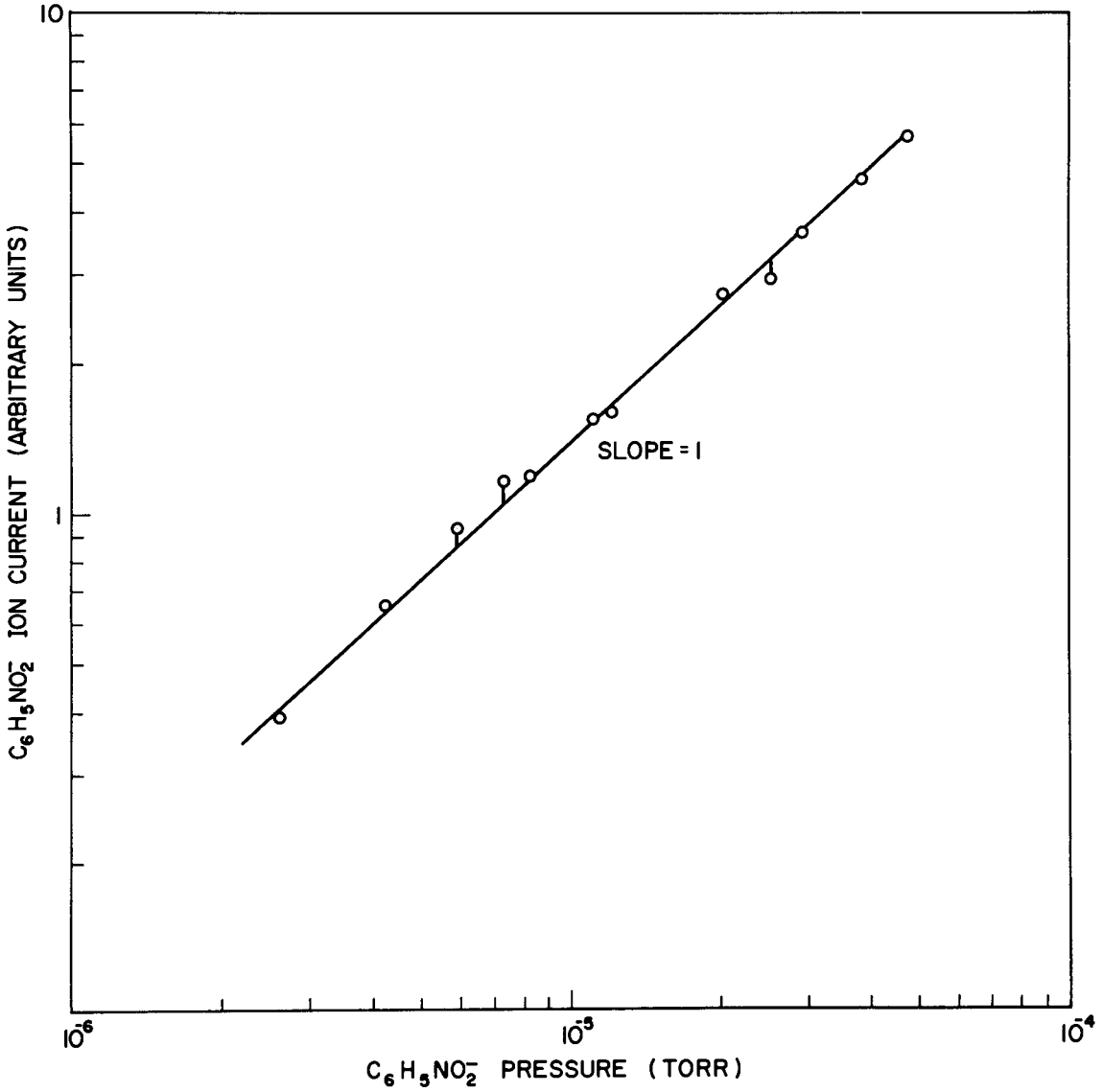

Figure 34. Pressure dependence of $C_6H_5NO_2^-$ ion current.

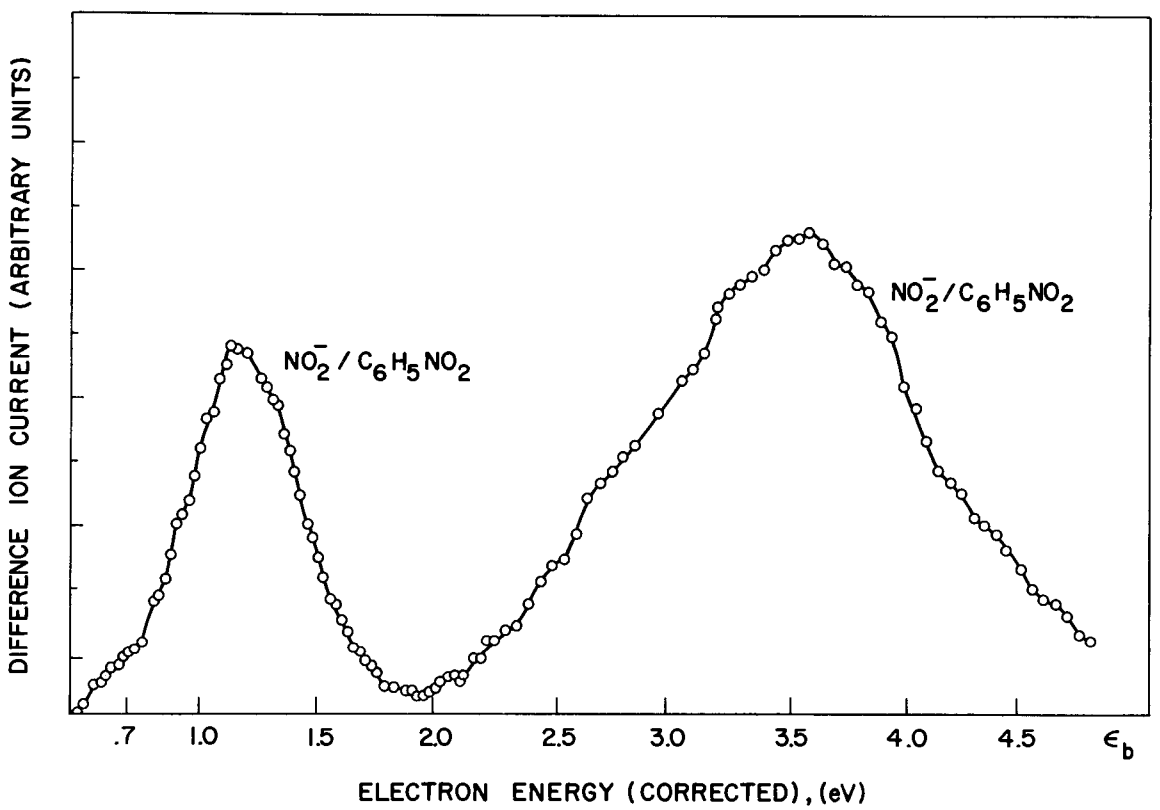

Figure 35. Dissociative electron capture in nitrobenzene.

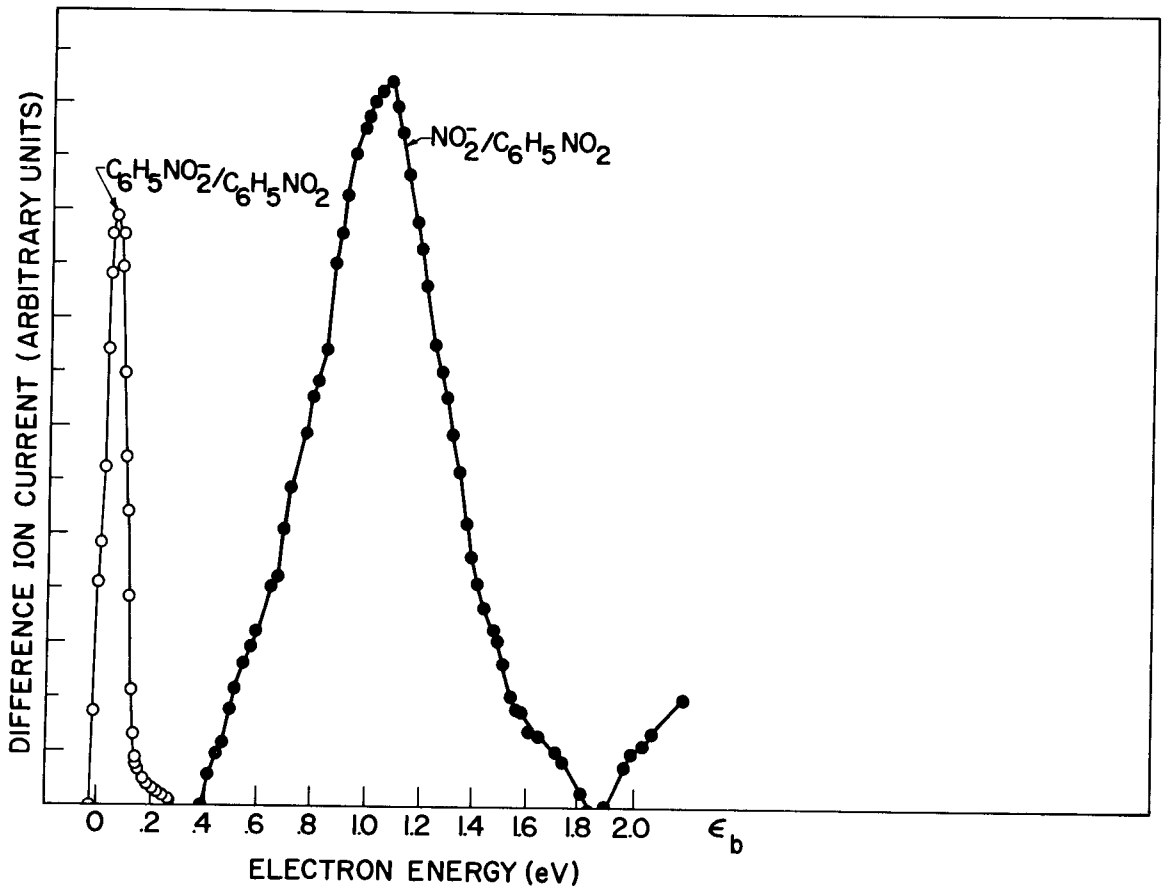

Figure 36. $C_6H_5NO_2^-$ and NO_2^- ion currents from nitrobenzene as a function of electron energy.

leading to NO_2^- appears at 1.92 eV and peaks at 3.5 eV.

Ortho- and meta-nitrotoluene were observed also to capture thermal electrons non-dissociatively. The shape of the o- and m-$C_6H_4CH_3NO_2^-$ ion currents as well as the energy at which the ion current maxima occur are equivalent to the SF_6^- ion current (see Figure 37). Thus, the actual cross section, as in the case of $C_6H_5NO_2^-$, peaks below 0.03 eV, and the widths of the ion current curves are instrumental.

In Figures 38 and 39 the NO_2^- difference ion currents are plotted for o- and m-$C_6H_4CH_3NO_2$. The non-dissociative electron capture resonances at 0.03 eV were employed to calibrate the corresponding electron energy scales for the NO_2^- ion currents. The appearance potentials and the peak energies for NO_2^- are given in Table X. From the data presented in Figure 39 and Table X it is seen that m-substitution of a CH_3 group for an H atom along the nitrobenzene ring decreases the ratio of the $\sim$1- and $\sim$4-eV dissociative processes, but does not affect the energy at which the two processes peak. Ortho substitution of a CH_3 group to nitrobenzene, however, decreases the energy of both dissociative peaks by about 0.3 eV. This lowering of energy can be accounted for by assuming a decrease in the dissociation energy due to the proximity of the CH_3 and NO_2 groups.

The appearance potential for NO_2^- from o-$C_6H_4CH_3NO_2$ gives an upper limit of 4.49 eV for D(o-$C_6H_4CH_3$-NO_2). Due to the small NO_2^- ion current from m-$C_6H_4CH_3NO_2$ at the threshold, it was not possible to determine

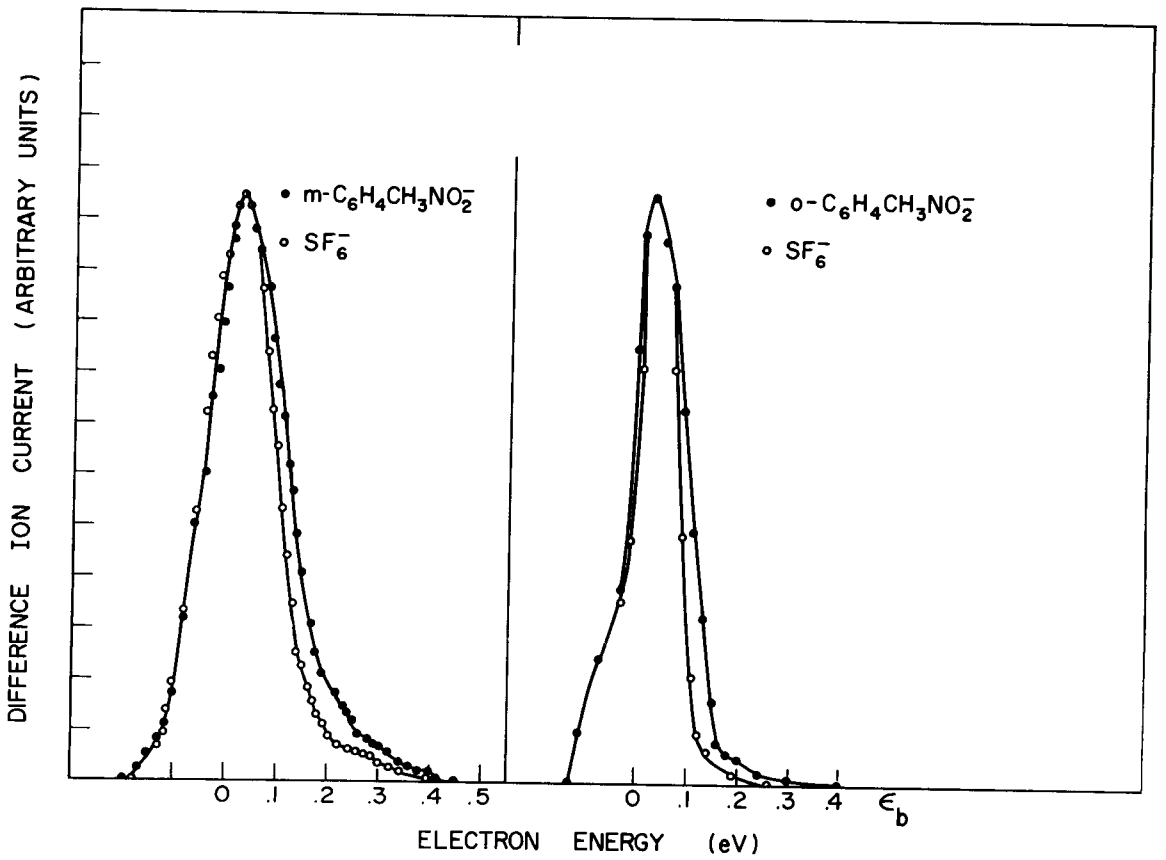

Figure 37. Comparison of o-$C_6H_4CH_3NO_2^-$ and m-$C_6H_4CH_3NO_2^-$ ion currents with SF_6^- ion currents as a function of electron energy.

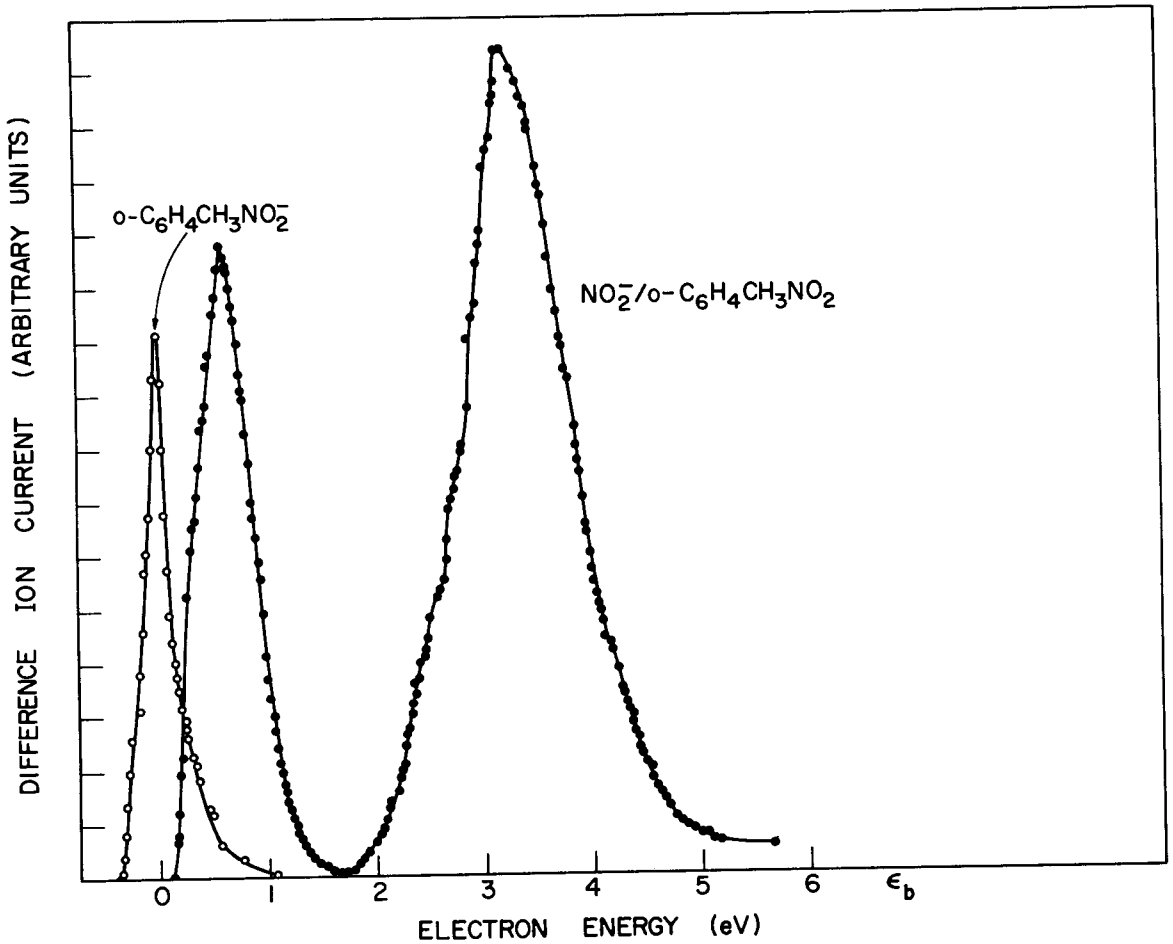

Figure 38. Dissociative electron capture in ortho-nitrotoluene.

TABLE X

ELECTRON CAPTURE DATA OBTAINED BY THE BEAM METHOD

Compound	Formula	Ion	ϵ(max) (eV)	Appearance Potential when SF_6^- was Used for Energy Calibration
Nitrobenzene	$C_6H_5NO_2$	$C_6H_5NO_2^-$	0.03	0.0
		NO_2^-	1.06	0.42
		NO_2^-	3.53	1.9
o-Nitrotoluene	o-$C_6H_4CH_3NO_2$	o-$C_6H_4CH_3NO_2^-$	0.03	0.0
		NO_2^-	0.62	0.5
		NO_2^-	3.22	2.1
m-Nitrotoluene	m-$C_6H_4CH_3NO_2$	m-$C_6H_4CH_3NO_2^-$	0.03	0.0
		NO_2^-	1.06	---
		NO_2^-	3.50	1.8

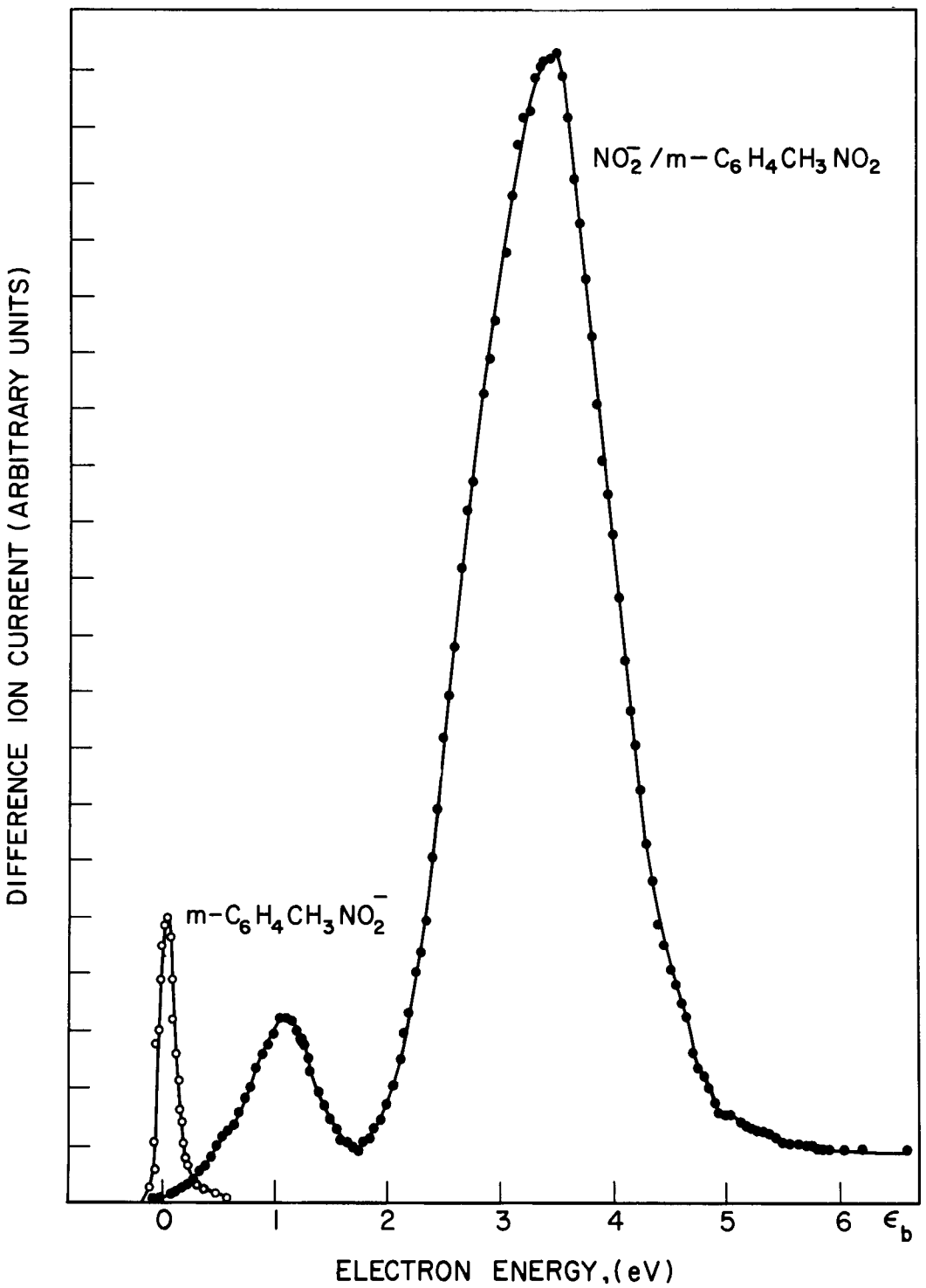

Figure 39. Dissociative electron capture in meta-nitrotoluene.

accurately the appearance potential for this process.

IV. INVESTIGATION OF C_2H_5Cl

Chloroethane is similar to the halogenated benzene derivatives studied in Section II of this chapter in that they are all hydrocarbons which satisfy the condition

$$EA(X) > D(A - X)$$

where D(A - X) is the dissociation energy for the halogen substituent and EA(X) is the electron affinity of the halogen X. Chloroethane differs from the molecules in Section II in that it is a non-aromatic. The capture rates for mixtures of C_2H_5Cl in N_2 are given in Table XI for various E/P. The observed rates of capture are much smaller than those observed for the halogenated benzene derivatives. The values of $\sigma_{bj}(max)$ and $\epsilon_b(max)$ are listed in Table IX, page 120. The ion current as a function of electron energy from 0 to 14 eV is given in Figure 40. The negative ion spectrum shows a narrow resonance at 0.40 eV which has a broad tail on the high-energy side. The negative ion spectrum shows also a smaller peak at 6.9 eV and a broad peak at approximately 9.2 eV.

The low-energy resonance was observed previously by Cox (1953), whereas Irsa (1955) has reported the two peaks occurring at higher electron energies. The shape of the low-energy resonance is extremely interesting. Within experimental error the appearance potential for Cl^-, as determined

TABLE XI

ATTACHMENT COEFFICIENTS AND RATES OF CAPTURE FOR CHLOROETHANE IN NITROGEN

E/P ($V\ cm^{-1}\ Torr^{-1}$)	$\alpha_o(E/P)$ ($cm^{-1}\ Torr^{-1}$)	$\alpha_o(E/P) \times w(E/P)$ ($sec^{-1}\ Torr^{-1}$)
0.3	0.025	11.2×10^3
0.4	0.028	13.6
0.6	0.044	24.7
0.8	0.050	33.4
1.0	0.060	45.8
1.2	0.068	58.3

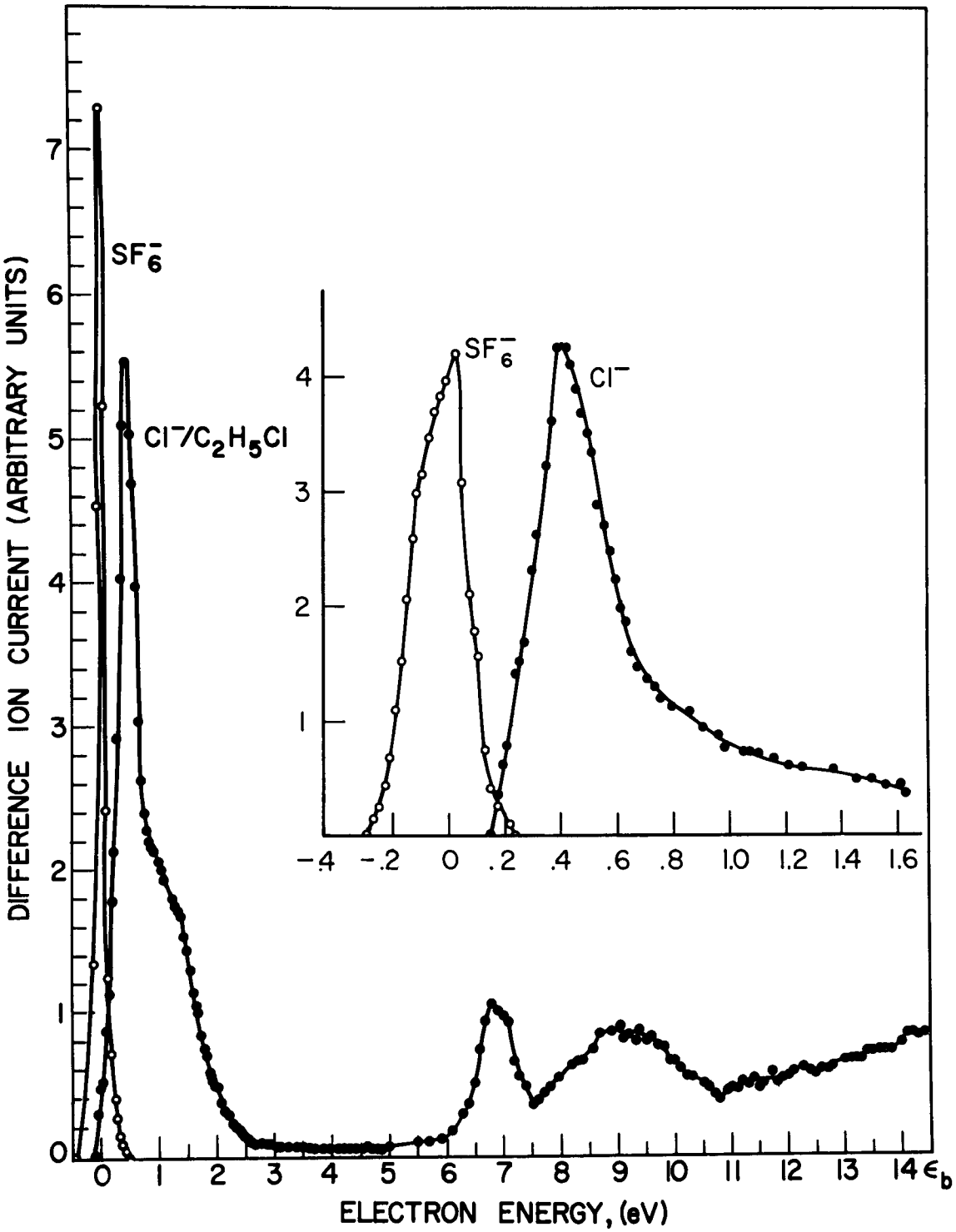

Figure 40. Chlorine negative ions from chloroethane.

from the energy difference between the onsets of SF_6^- and Cl^-, was the same as the energy for the maximum cross section. The shape of the SF_6^- and Cl^- peaks are also very similar except for a broad tailing off with energies above 0.6 eV (see Figure 40). Thus, for energies below the 0.4-eV peak the shape of the Cl^- resonance is due to the spread in the electron beam energy. [Fox (1957) first observed a situation such as this for Cl^- from HCl.] It was not possible to establish whether the broad tail at energies greater than 0.6 eV is due to the 0.4-eV resonance or due to a separate capture process. Because of the uncertainties in the shape of the resonance, $\sigma_{bj}(max)$ and $\epsilon_b(max) + T_j(opt)$ for C_2H_5Cl are subject to error.

The gradual increase in the Cl^- ion current beyond 11 eV is probably due to ion pair production leading to $C_2H_5^+ + Cl^-$.

V. DISCUSSION OF RESULTS FOR HALOGENATED COMPOUNDS

A summary of the results for the halogenated benzene derivatives and C_2H_5Cl has been presented in Table IX, page 120. The predominate electron capture process observed in the halogenated benzene derivatives leads to $A + X^-$ where X^- is the halogen negative ion and A the rest of the molecule AX. The dissociative electron capture resonances are quite broad ($\sim$ 1 eV), and the energies at which $\sigma_c(\epsilon)$ peak range from $\sim$ 1 eV for C_6H_5Cl, o-$C_6H_4CH_3Cl$, o-$C_6H_4CH_3Br$, C_6H_5Br, and C_6D_5Br to thermal energies for the dichlorinated benzene derivatives and C_6H_5I.

The energy at which the halogen negative ion peaks, $\epsilon_b + T_j(opt)$, is seen to decrease in going from C_6H_5Cl to C_6H_5Br to C_6H_5I. This decrease can be accounted for by an increase in the EA(X) - D(AX) energy difference. The increase in $\epsilon_b + T_j(opt)$ for the toluene derivatives over their corresponding benzene derivatives can also be attributed to changes in EA(X) - D(AX). The dissociation energies for the toluene derivatives would be expected to be larger than the corresponding benzene derivative since CH_3 donates electronic charge to the benzene ring. Similarly, since Cl attracts electronic charge from the benzene ring the dichlorinated benzene derivative should exhibit lower values of $\epsilon_b + T_j(opt)$ as does the monosubstituted benzene derivatives. Such a behavior is observed in Table IX, page 120.

The differences in the peak energies of the NO_2^- currents from $C_6H_5NO_2$, o-$C_6H_4CH_3NO_2$, and m-$C_6H_4CH_3NO_2$ can be attributed to interactions between the CH_3 and NO_2 groups. Table X, page 139, shows that $\epsilon_b(max)$ for NO_2^- from nitrobenzene was the same as meta-substituted CH_3 onto nitrobenzene. Ortho-substitution of CH_3 onto nitrobenzene lowered the NO_2^- peaks by about 0.3 eV.

The last two columns of Table IX give the dissociation energies, D(A - X), of the AX molecules studied and the electron affinities, EA(X), of the halogen atoms X. If E_{exc} is the energy which goes into excitation of A and/or X^- and E_{kin} is the kinetic energy of the dissociation products,

then

$$\epsilon_b(\max) + T_j(\text{opt}) = D(AX) - EA(X) + E_{exc} + E_{kin}. \qquad (48)$$

The products A and X^- will share considerable kinetic energy ($\sim$ 0.6 to 1.2 eV) when they are not left in an excited state.

The values of $\sigma_c(\epsilon)(\max)$ increase rapidly in going from Cl to Br (to I). This increase in attachment cross section is seen to correlate with several of the properties of these molecules. For example, $\sigma_c(\epsilon)(\max)$ increases with increasing resonance interaction between X and A, with increasing geometric cross section, or with decreasing energy (increasing de Broglie wavelength).

The effect of resonance interaction deserves some further comment. Resonance interaction is a result of overlap of the orbital containing the lone pair electrons of X with the Π-electrons of A. Classically, this is thought of as a migration of electric charge from the non-bonding $2P\Pi(P_z)$ orbitals of X into A. The resonance interaction increases in the order Cl < Br < I which correlates with increasing cross section. The fact that the attachment cross section for Cl^- from C_2H_5Cl is orders of magnitude smaller than the benzene derivatives further supports the notion that resonance interaction is playing an important role in the electron capture processes involving the benzene derivatives.

A search for parent molecular negative ions was carried out for all the halogenated benzene derivatives studied with the ion source adjusted to

give maximum SF_6^- ion current, but no parent molecular negative ions were observed. The upper limits put to the formation of parent molecular ions for the various benzene derivatives at electron energies $\sim$ 0.05 eV are 10^{-19} to 10^{-20} cm^2.

The non-dissociative electron capture by $C_6H_5NO_2$, o-$C_6H_4CH_3NO_2$, and m-$C_6H_4CH_3NO_2$ will be considered in some detail in the following chapter.

CHAPTER V

LIFETIMES OF NEGATIVE IONS

I. INTRODUCTION

The previous chapter was concerned with electron attachment in which stable negative ions are formed by dissociation into neutral fragments and atomic or molecular negative ions. When non-dissociative electron attachment occurs, metastable negative ions are formed and energy must be removed from the system in order for a stable negative ion to be formed. It is the purpose of this chapter to present data on molecules which capture electrons non-dissociatively and to set up a theoretical model which can account for the large attachment cross sections and long lifetimes.

There is considerable evidence for the existence of temporary negative ions. The classic example of temporary negative ion formation is the mechanism proposed by Bloch and Bradbury (1935) to explain the formation of negative ions of O_2 at low-electron energies. The Bloch-Bradbury mechanism is a two-step process involving an electron and two oxygen molecules. Temporary O_2^{-*} negative ions are formed which subsequently collide with other O_2 molecules, thereby transferring their excitation energy and becoming stabilized, i.e.,

$$e + O_2 \rightarrow O_2^{-*}$$

$$O_2^{-*} + O_2 \rightarrow O_2^{-} + O_2^{*} .$$

It is interesting to point out that the Bloch-Bradbury theory predicted temporary negative ions of O_2 in 1935. The first experimental evidence substantiating the theory, however, was presented by Hurst and Bortner (1956, 1957) 21 years later. This capture process has been verified by many other investigators and the lifetime of the excited negative ion is believed to be approximately 10^{-10} seconds.

Temporary negative ion intermediates have also been postulated to explain the large vibrational excitation cross sections exhibited by a number of molecules. For example, a large vibrational excitation process in nitrogen was observed by Haas (1957) in a swarm experiment. Because of the small mass ratio of the electron to a molecule, direct excitation of vibrational states is extremely improbable. Franck and Jordan (1926) proposed a mechanism for vibrational excitation by electron impact based on the idea that upon close approach of the electron to the molecule the internal field of the molecule is distorted, causing the atoms in the molecule to relax to a new equilibrium position. Therefore, when the electron is ejected, the molecule is left in an excited vibrational state.

Schulz (1959b) proposed the existence of temporary negative ions to explain his electron energy loss data on N_2 and CO. Later Schulz (1961) reported evidence for two temporary negative ion states of N_2O^- which lead to vibrationally excited N_2O and $N_2 + O^-$ at 0.7 eV and 2.2 eV, respectively. The lifetime of temporary negative ions such as these are believed to be

approximately 10^{-13} seconds.

Several theoretical studies have also been successful in treating the phenomena of vibrational excitation of molecules via temporary negative ion states. Chen and Magee (1962) showed that large vibrational excitation cross sections are to be expected when temporary negative ion states are possible. An expression for the vibrational excitation cross section was developed from second order perturbation theory in which the potential energy of the negative ion state was taken to be the perturbation. Applying this method to vibrational excitation in H_2 they obtained a cross section of the order of 1 $Å^2$. The magnitude of this cross section agreeded with experiment and is approximately one hundred times the cross sections previously calculated without assuming temporary negative ion intermediates.

Herzenberg and Mandl (1962) suggested that the narrow peaks in the energy loss spectrum of molecules such as nitrogen are due to resonances of the incident electron wave with the potential well of the molecule. The inverse width of the peak (in units of h) would then be the lifetime of the temporary negative ion state. They employed a modification of the Kapur-Peierls theory for resonance scattering in nuclear physics. Their calculations succeeded in predicting most of the intricate details of the energy loss spectra for electron collisions with nitrogen. The agreement between experiment [Schulz (1959b)] and this theory is indeed astounding.

J. C. Y. Chen (1964a, 1964b) has adopted the Feshbach definition of a resonance to examine subexcitation electron scattering by molecules through temporary negative ion states. His calculations of the vibrational excitation cross section for N_2 also agreed well with the experimental results of Schulz (1959b).

Helium is also known to form a temporary negative ion with a lifetime greater than 10^{-5} seconds [Sweetman (1960)]. The He^- ion was observed by Hilby (1939) in a gas discharge but was not generally recognized until Holøien and Midtal (1955) showed that the $^4P_{5/2}$ state of He^- is not liable to autoionization. They estimated the lifetime to be approximately equal to the radiative lifetime of He (^3S) ($\sim 10^{-3}$ seconds).

A number of molecules have been reported to attach electrons by unimolecular electron capture for times long enough to be observed in a mass spectrometer (e.g., $\tau > 10$ microseconds). A few such molecular ions are SF_6^-, $C_6F_6^-$, n-$C_7F_{16}^-$, $B_5H_9^-$, $C_7F_{14}^-$, $C_8F_{16}O^-$, $SO_2F_2^-$, $C_6N_2^-$, $C_4F_6^-$, and $C_4F_8^-$.

The fact that these molecules are large and symmetric suggests that the energy of the captured electron is shared with the many degrees of freedom of the molecule for a time long enough to be detected in a conventional mass spectrometer. There have been no theoretical treatments of this problem and, in fact, there are limited data on all of the above molecules except SF_6.

II. MEASUREMENT OF NEGATIVE ION LIFETIMES

It was observed early in the negative ion studies with the TOF mass spectrometer that particles traversing the flight tube which were produced by unimolecular electron capture consisted of a neutral component and a negative ion component. These two peaks could be separated in time by a retarding electrostatic field located at any point along the flight path. Edelson, Griffiths, and McAfee (1962) investigated autodetachment of electrons from SF_6^{-*} using a TOF mass spectrometer. They were able to determine the half life of SF_6^{-*} from the following consideration.

Assume that N_o metastable negative ions leave the ion source with velocity v at time t = 0. At a distance ℓ down the flight path a "flattop" potentital barrier is applied which decelerates the negative ions and leaves the neutral molecules unaffected. The potential barrier separates the negative ions from the neutral molecules after a time $t = \ell/v$ and, therefore, permits a measurement of the number of ions which have not delayed after a time t, $N^-(t)$, and the number of ions which have decayed into neutral molecules, $N^o(t)$. If we assume an exponential decay law for the autodetachment of electrons within this time t, the mean lifetime can be determined from

$$\tau = \frac{t}{\ln\left(\frac{N^- + N^o}{N^-}\right)} . \tag{49}$$

This technique has been applied to determine the lifetimes of SF_6^{-*}, $C_6H_5NO_2^{-*}$, and $C_4H_6O_2^{-*}$. The Bendix model 14-206 mass spectrometer was modified as shown in Figure 41 in order to carry out the measurements.

The following conditions must be fulfilled when lifetimes are determined with the technique described above:

1. Neutral molecules are counted with the same efficiency as charged molecules of the same kinetic energy.
2. Collisional detachment or charge transfer does not take place in the flight tube.
3. Detachment by the grids in the path of the ion beam is negligible.
4. Spontaneous dissociation or collision induced dissociation of the parent negative ion is negligible.

The Condition 1 is taken into account by employing single pulse counting techniques to detect both the negative ions and the neutral molecules. The discrimination level (see Figure 41) is set well below the pulse amplitude produced by the negative ions and neutral molecules.

The single particle counting also allows the pressure to be maintained quite low in the flight tube region ($\sim 10^{-7}$ Torr) and hence collision effects in the flight path are minimized. It was found that the ratio of neutral to total current was independent of the pressure in the range 10^{-4} to 10^{-6} Torr. If the neutral current were produced by collisional detachment or charge transfer, this ratio would increase with pressure. For these

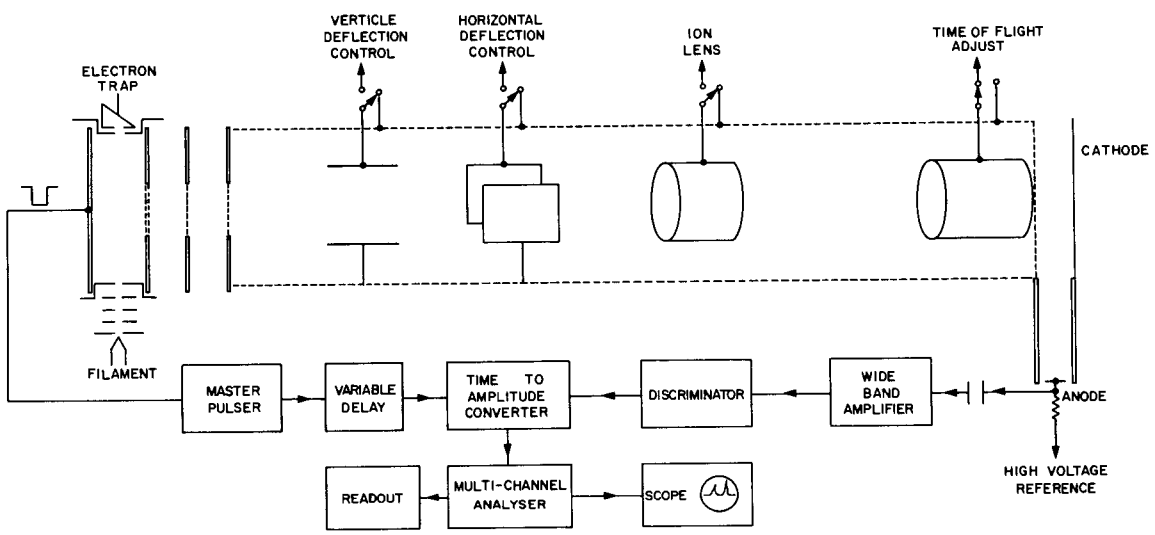

Figure 41. Schematic diagram of negative ion lifetime apparatus.

reasons Condition 2 is believed to be met.

Condition 3 was investigated by simultaneously separating the currents at two different positions along the flight path. The charged and neutral currents were first separated by the ion lens and, after an approximately equal time, the neutral component was further separated by the time-of-flight adjust. No appreciable change in the ratio of neutral to charge current was observed, and since there are no grids between the ion lens and the time-of-flight adjust, Condition 3 is satisfied.

If spontaneous dissociation or collisional dissociation of the parent negative ion occurs along the flight path before the ions reach the potential barrier, a negative ion current appears at longer flight times (than those for the parent negative ion), and neutral fragments appear at a flight time equal to that of the neutral parent molecule. Thus, nonfulfillment of Condition 4 will result in an erroneous measurement of the autodetachment lifetime. It is believed that in the investigation of SF_6^{-*} and $C_6H_5NO_2^{-*}$ Condition 4 is satisfied. A weak metastable mass peak from SF_6, resulting from the process $SF_6^{-*} \rightarrow SF_5^- + F$, was observed previously by Ahearn and Hannay (1953), which, however, is so weak that its contribution to our neutral peak is negligible.

It was necessary to connect all of the focusing electrodes to the potential of the flight tube in order to reduce discrimination for/or against either component. Separation of the neutral and charged currents was

carried out at the time-of-flight adjust which is approximately 170 cm from the ion source. A typical separation of neutral and charged currents for SF_6 is shown in Figure 42. The ratio of neutral current, N^o, to total current, N_o, was measured and the lifetime was calculated from

$$\tau = - \frac{t}{\ln(1 - N^o/N_o)} \quad . \tag{50}$$

This procedure was carried out for six different ion energies from 2000 to 4000 eV, and the results are given in Table XII. From these data an approximate lifetime for autodetachment was obtained, which is equal to $\sim$40 microseconds for $C_6H_5NO_2^{-*}$ and $\sim$25 microseconds for SF_6^{-*}. The lifetime can also be obtained from a plot of $-\ln(1 - N^o/N_o)$ vs t (see Figure 43). Each point on Figure 43 represents the average of approximately ten values of N^o/N_o. The spread in the points is due to the difficulty in obtaining optimum focusing conditions from one run to the next as well as for different ion accelerating voltages. The difference between this lifetime for SF_6^{-*} and the value of 10 microseconds by Edelson et al. (1962) is most probably due to different focusing properties of the neutral and charged particles or to different source conditions (temperature, electron energies, etc.). The important information which results from the present study aside from the measurement of lifetimes is that the negative ions produced by unimolecular electron capture are metastable and are not stabilized by collision or radiation.

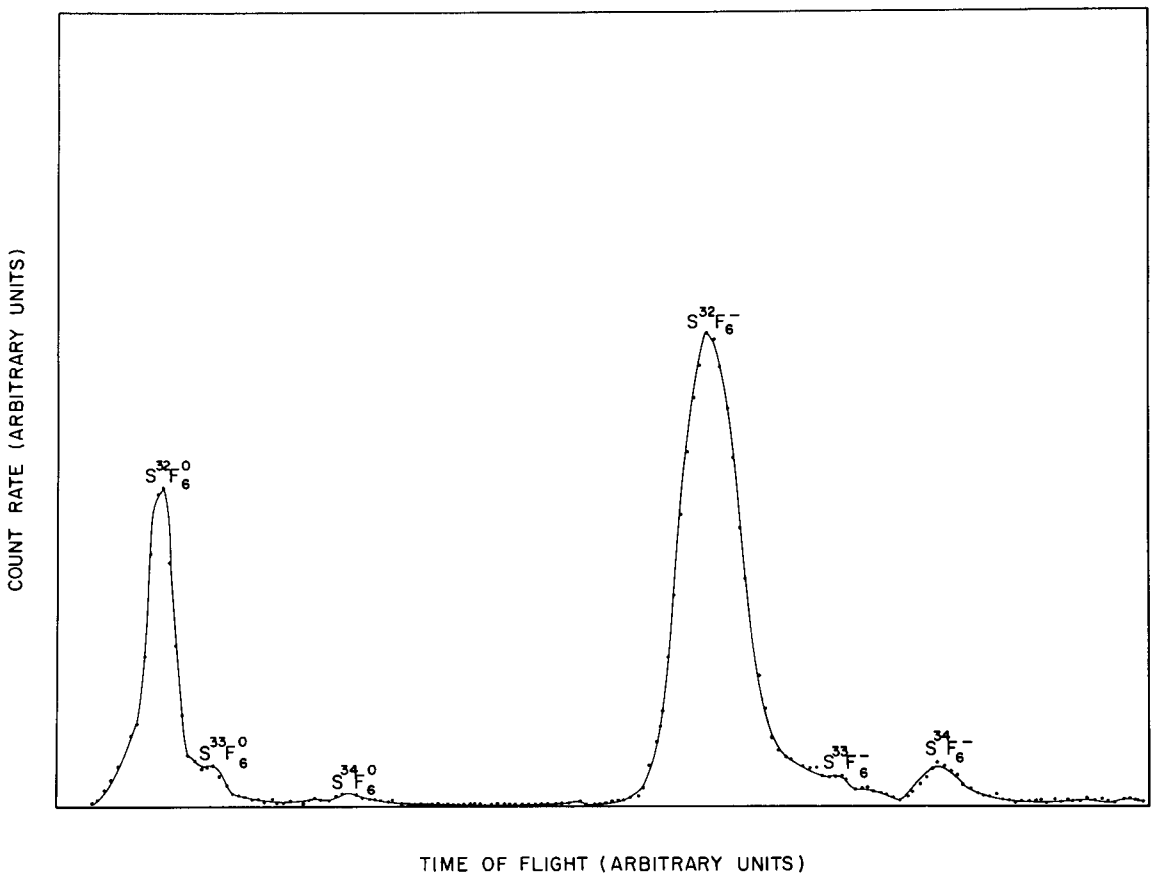

Figure 42. Separation of neutral and negative currents of sulphur-hexafluoride.

TABLE XII

LIFETIMES OF TEMPORARY NEGATIVE IONS
FOR VARIOUS ION ENERGIES

Ion Energy (eV)	Lifetime (μsec)	
	$C_6H_5NO_2^{-*}$	SF_6^{-*}
2000	31	24
2500	38	28
2750	38	26
3000	38	27
3500	43	24
4000	42	24

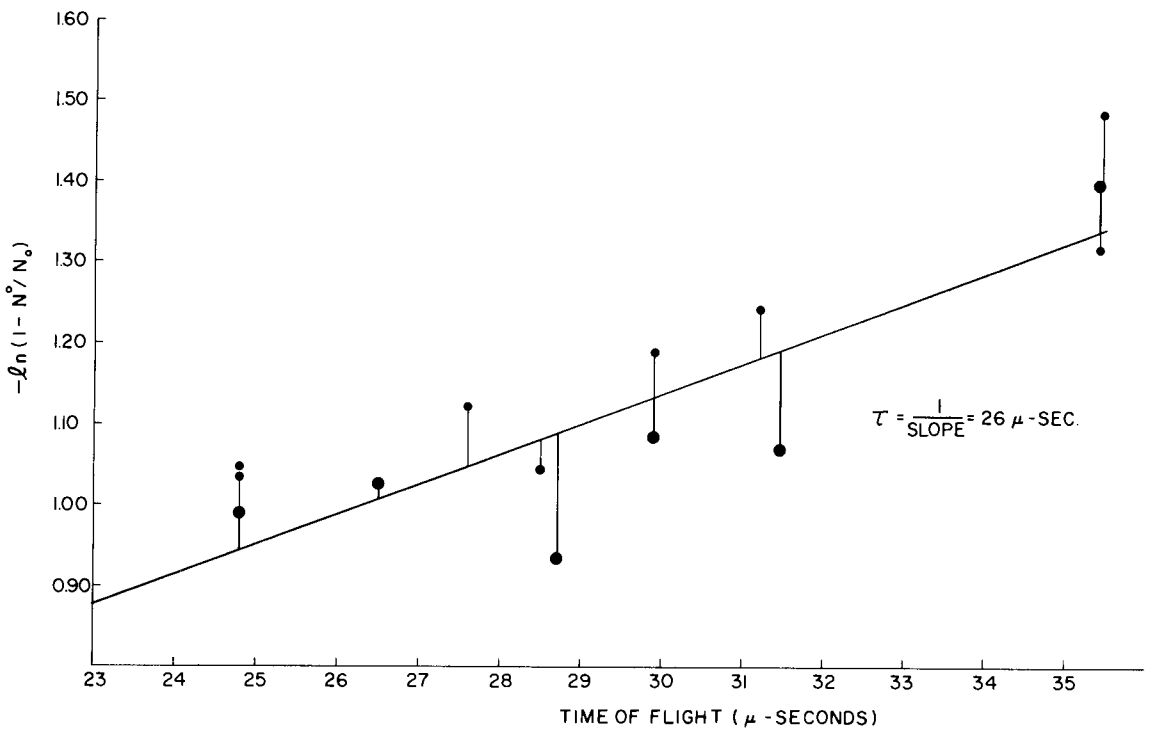

Figure 43. Determination of SF_6^{-*} autodetachment lifetime.

Biacetyl, $(CH_3CO)_2$, was also observed to attach electrons non-dissociatively at very low electron energies and the energy dependence of the $(CH_3CO)_2^{-*}$ ion current was equivalent to that of SF_6^- (i.e., instrumental). Measurements of the lifetime were carried out at two different ion acceleration voltages with the result $\tau \approx 12$ microseconds. This was the shortest lifetime observed in these experiments.

III. THEORY OF LONG-LIVED NEGATIVE IONS

A theoretical model will now be discussed in order to interpret the experimental data on SF_6, $C_6H_5NO_2$ and $(CH_3CO)_2$.

When a low-energy electron interacts with a polyatomic molecule, the electron may transfer some of its kinetic energy to the molecule in the form of vibration or rotation. When capture takes place, the excess energy of formation is distributed among the various degrees of freedom of the molecule. The electron subsequently becomes bound into a metastable state of the negative ion, the system being in the continuum and is subject to autoionization, until it reaches a configuration from which decay is possible.

Consider a metastable negative ion originally in state 2 decaying to give an electron and molecule in state 1, i.e.,

$$\underset{2}{(AB \cdot\cdot CD)^{-*}} \rightleftharpoons \underset{1}{AB \cdot\cdot CD} + e \cdot$$

From first-order, time-dependent perturbation theory, the lifetime of the negative ion state 2 is given by

$$\tau \equiv \frac{1}{T_{21}} = \frac{h}{4\Pi^2 \left|\mathcal{H}'_{21}\right|^2 \rho_1} \tag{51}$$

where T_{21} is the transition probability for decay, $\mathcal{H}'_{21}$ is the matrix element of the kinetic energy operator of the perturbed nuclei evaluated over the states 2 and 1, ρ_1 is the density of final states for the electron plus molecule. Although ρ_1 can be easily evaluated for any electron energy, lifetime calculations are usually prevented by lack of knowledge of the wave functions needed to calculate $\mathcal{H}'_{21}$.

The lifetime of the negative ion can be related to the electron capture cross section in the following. The transition probability per unit time from a free state to a negative ion state is

$$T_{12} = \frac{4\Pi^2}{h} \left|\mathcal{H}'_{12}\right|^2 \rho_2 \tag{52}$$

where ρ_2 is the density of states of the negative ion. The transition probability per unit time for attachment, T_{12}, is related to the lifetime of the negative ion through the principle of microscopic reversability (detailed balancing), i.e.,

$$\tau \equiv \frac{1}{T_{21}} = \frac{\rho_2}{\rho_1} \frac{1}{T_{12}} \quad . \tag{53}$$

If the incoming electrons are normalized to one electron in a unit volume, the electron capture cross section, σ_c, is given by T_{12}/v. The expression relating the autodetachment lifetime and attachment cross section then becomes

$$\tau = \frac{\rho_2}{\rho_1} \frac{1}{v\sigma_{(v)}} . \tag{54}$$

When the molecule is left in its ground state, the density of final states would be that of a free electron traveling with velocity v, i.e.,

$$\rho_1 = 1 \times \rho_e = 2 \times \frac{4\Pi}{8\Pi^3 \hbar^3} P^2 \frac{dP}{dE} = \frac{m^2 v}{\Pi^2 h^3} , \tag{55}$$

where the spin degeneracy has been included in the calculation of the density of states of the electron, ρ_e.

Determination of density of states of molecules (or ions) possessing excess energy is a difficult problem in itself. However, classical and semiclassical expressions are available which will afford a fairly good approximation to this quantity. Marcus and Rice (1951) proposed the following semiclassical energy density expression for a molecule (or ion) having N degrees of freedom and vibrational frequencies ν_i:

$$\rho(\epsilon) = \frac{(\epsilon + \epsilon_z)^{N-1}}{\Gamma_{(N)} \prod^{N} h\nu_i} \tag{56}$$

where ϵ_z is the zero point energy, ϵ is the energy in excess of ϵ_z, and $\Gamma_{(N)}$ is the gamma function. The zero point energy, ϵ_z, is taken to be

one-half the sum of the first vibrational state energies. This expression is good only for very large values of the ratio ϵ/ϵ_z. Rabinovitch and Diesen (1959) have modified Equation (56) to allow for a more accurate calculation of ρ_2 at lower values of ϵ/ϵ_z by including an empirical correction factor, a, which is to be evaluated for each particular value of ϵ/ϵ_z,

$$\rho(\epsilon) = \frac{(\epsilon + a\epsilon_z)^{N-1}}{\Gamma_{(N)} \prod^{N} h\nu_i} . \tag{57}$$

The parameter a is evaluated to make the sum over all states in Equation (57) best fit the accurate quantum mechanical sum, i.e.,

$$\sum_{\epsilon_\nu = 0}^{\epsilon} P_{(\epsilon)} = \frac{(\epsilon + a\epsilon_z)^{N}}{\Gamma_{(N+1)} \prod^{N} h\nu_i} . \tag{58}$$

Substituting Equations (55) and (57) into Equation (54) (the spin degeneracy of the negative ion is assumed to be 2), the lifetime becomes

$$\tau = \frac{2\Pi^2 \hbar^3}{m^2 v} \frac{(\epsilon + a\epsilon_z)^{N-1}}{\Gamma_{(N)} \prod^{N} h\nu_i} \frac{1}{v\sigma_{(v)}} . \tag{59}$$

The quantity ϵ is defined as a summation of the kinetic energy of the incident electron, electron affinity, and the vibrational energy of the molecule prior to attachment. Notice that in cases where attachment takes place only to

molecules in the ground state, a measurement of τ and $\sigma_{(v)}$ affords a very accurate determination of the electron affinity.

In order to calculate the lifetime from Equation (59), the electron capture cross section as a function of energy must be known. It has been pointed out in Chapter IV that the true energy dependence of the attachment cross section for non-dissociative electron attachment is unknown; therefore, an effort must be made to obtain an expression for $\sigma_c(v)$ in order to establish a basis for comparing Equation (59) with experiment.

The simplest approximation for $\sigma_c(v)$ is

$$\sigma_c(v) = (2\ell + 1)\,\Pi\lambda\!\!\!^{-2} = (2\ell + 1)\,\Pi\frac{\hbar^2}{m^2 v^2} \tag{60}$$

where ℓ is the angular momentum quantum number, and $\lambda\!\!\!^{-}$ is the de Broglie wavelength of the incident electron. Equation (60) gives the maximum possible attachment cross section as a function of the electron energy [see Blatt and Weisskopf (1962)]. The justification for assuming such a cross section should be commented upon. The attachment cross sections for non-dissociative electron attachment for SF_6 and C_7F_{14}, for example, are extremely large ($> 10^{-16}$ cm^2) and the cross section peaks at zero electron energy. Another possible justification for the use of Equation (60) can be inferred from the following consideration. Substitution of Equation (60) into the theoretical expression for the rate of removal of electrons from a

thermal electron swarm [see Equation (40) in Chapter III] gives the maximum rate,

$$(\alpha W)_{max} = (2\ell + 1)\, N_o \frac{2\pi\hbar^2}{m^2} \left(\frac{m}{2\pi kT}\right)^{1/2} . \tag{61}$$

Since attachment takes place at very low energies, only S-wave electrons can be assumed to be captured. Under this assumption $(\alpha W)_{max}$ becomes 1.78×10^{10} second^{-1} Torr^{-1}. Unfortunately, only two values of αW have been measured for non-dissociative attachment [Bouby, Fiquet-Fayard, and Abgrall (1964)] so that a comparison with experiment will be meager. The measured rates of attachment of 1.1×10^9 second^{-1} Torr^{-1} for $(CH_3CO)_2$ and 3×10^9 second^{-1} Torr^{-1} for $CH_3CO\text{-}COC_2H_5$ are reasonably close to the value predicted by Equation (61). Also, the ion current for SF_6^- from the mass spectrometric experiments was observed to be larger than that for $(CH_3CO)_2^-$, indicating that the αW for SF_6^- would be of the order of magnitude of 10^{10} second^{-1} Torr^{-1}.

Employing $\pi\lambda\!\!\!^{-2}$ as the capture cross section, the negative ion lifetime becomes

$$\tau = \frac{h}{\Gamma_{(N)}} \frac{(\epsilon + a\epsilon_z)^{N-1}}{\prod^{N} h\nu_i} . \tag{62}$$

It should be emphasized that this relation is valid only if the molecule is left in an unexcited state after autodetachment takes place. By inspection of Equation (62), the uncertainty principle predicts that the width of the

negative ion resonance will be

$$\Gamma_{width} = \frac{\Gamma_{(N)} \prod^{N} h\nu_i}{(\epsilon + a\epsilon_z)^{N-1}} . \tag{63}$$

This width is identically equal to the average spacing of the negative ion energy levels (i.e., $\Gamma_{width} = 1/\rho_2$). This interesting fact is a result of using a smooth electron attachment cross section, i.e., $\sigma_{(v)} = \Pi\lambda\!\!\!^{-2}$.

It is possible to calculate the lifetime of SF_6^{-*} from Equation (62) by assuming that its vibrational frequencies are the same as those of SF_6 and by using the $a(\epsilon)$ parameters evaluated by Whitten and Rabinovitch (1963). The vibrational frequencies and degeneracies of SF_6 have been summarized by Pistorius (1958). Kay and Page (1964) have measured the electron affinity of SF_6 to be 1.49 ± 0.2 eV. The energy expression $\epsilon + a\epsilon_z$ in Equation (62) will be defined as E. When capture takes place to molecules in the ground vibrational state, E is given by

$$E = \epsilon_e + \epsilon_A + a\left(\frac{\epsilon_e + \epsilon_A}{\epsilon_z}\right)\epsilon_z \tag{64}$$

where ϵ_e is the electron kinetic energy and ϵ_A is the electron affinity. The quantity E is to be distinguished from the internal energy of the ion ($E_{internal} = \epsilon_e + \epsilon_A + \epsilon_z$). The dotted curves in Figures 44, 45, and 46 show the lifetime of SF_6^{-*} as a function of E for three values of the electron affinity. The lifetime calculations are seen to be very sensitive to the electron affinity of the molecule.

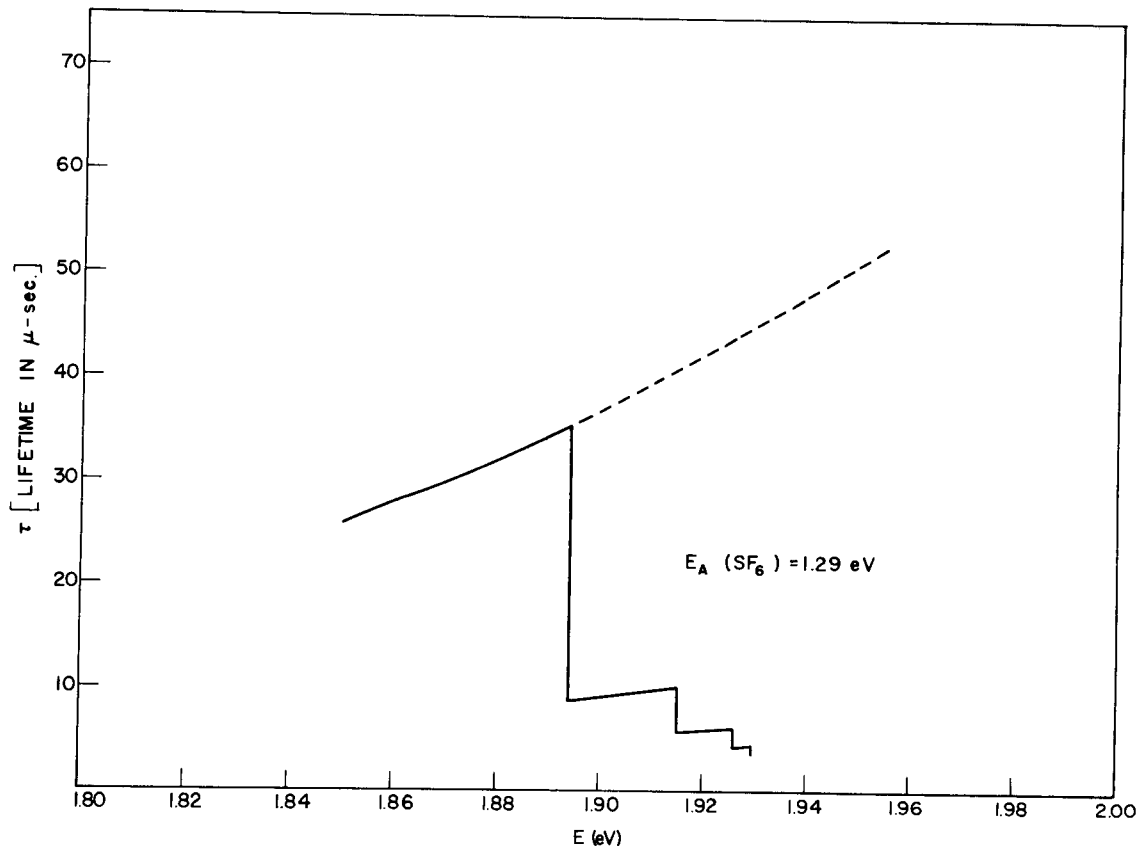

Figure 44. Lifetime of SF_6^{-*} as a function of E. [$E_A(SF_6)$ = 1.29 eV].

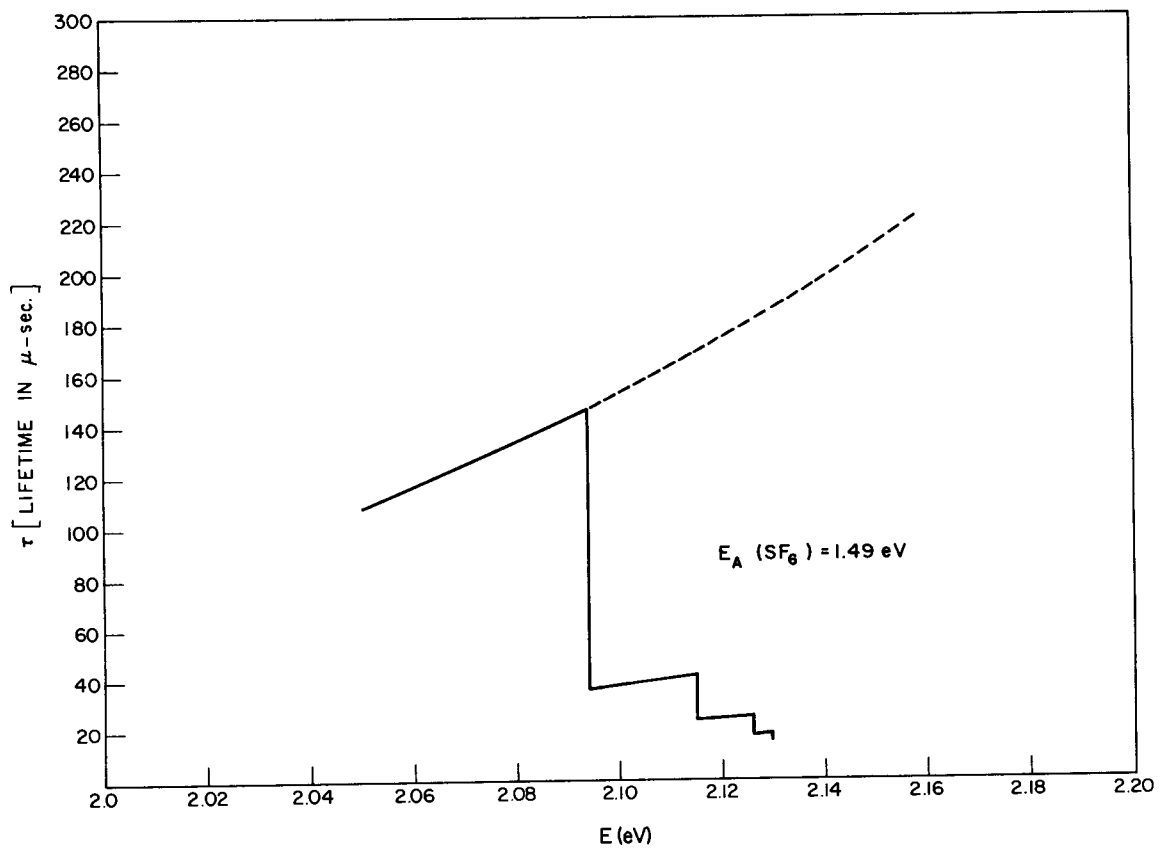

Figure 45. Lifetime of SF_6^{-*} as a function of E. [$E_A(SF_6) = 1.49$ eV].

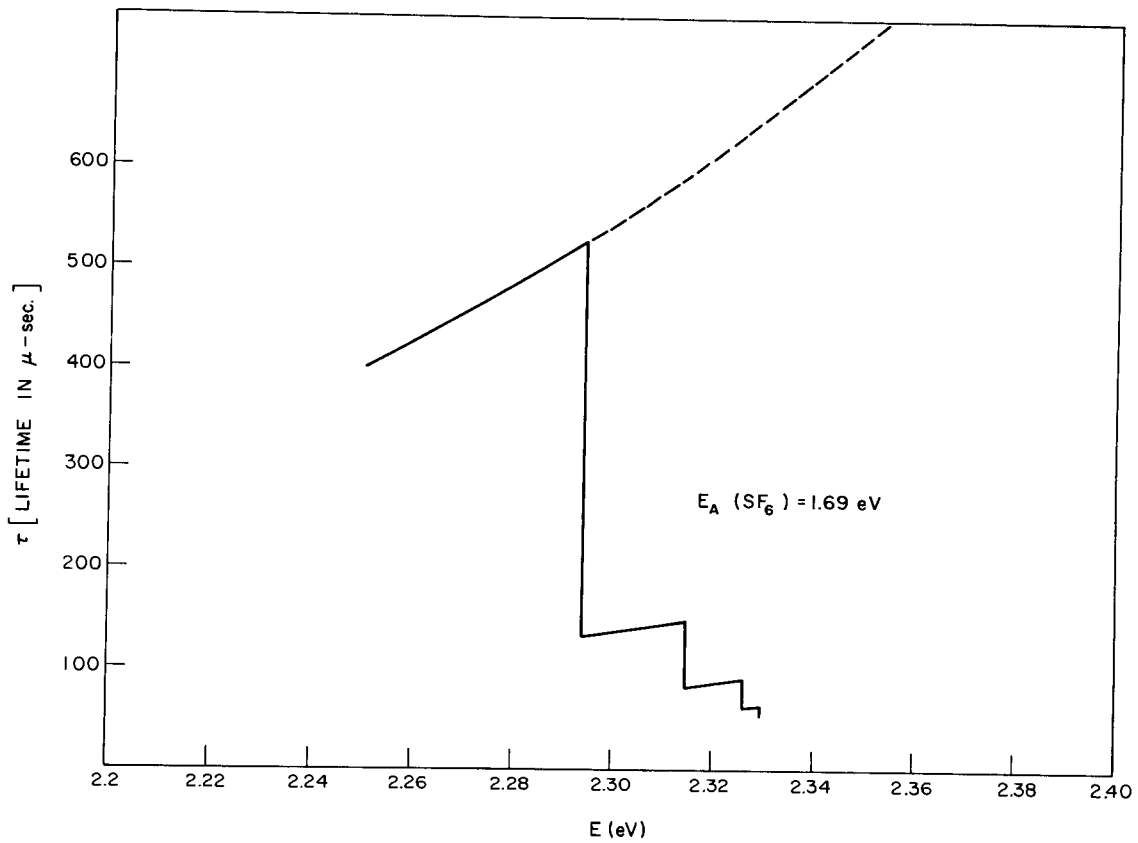

Figure 46. Lifetime of SF_6^{-*} as a function of E. [$E_A(SF_6) = 1.69$ eV].

When the internal energy of the negative ion minus the sum of the electron affinity and zero point vibrational energy is greater than the first vibrational state energy, $h\nu_1$, but less than the second, $h\nu_2$, the total rate of decay of the negative ion will be the rate for the process $SF_6^{-*} \rightleftarrows SF_6 + e$ plus the rate for $SF_6^{-*} \rightleftarrows SF_6^{*}(h\nu_1) + e$. Since the first excited vibrational state of SF_6 is triply degenerate, the lifetime of the negative ion for $h\nu_2 > E_{internal} - \epsilon_A - \epsilon_z > h\nu_1$ would be

$$\tau = \frac{1}{4} \frac{h}{\Gamma_{(N)}} \frac{(\epsilon + a\epsilon_z)^{N-1}}{\prod^{N} h\nu_i} . \tag{65}$$

Similarly, when $E_{internal} - \epsilon_A - \epsilon_z$ is greater than $h\nu_2$, the lifetime will be further reduced. This is illustrated by the solid line in Figures 44, 45, and 46. It is seen that the lifetime of the negative ion is dependent on the internal energy of the negative ion and consequently dependent on the energy of the incident electron. Assuming that the ion current peaks at 0.03 eV in the electron beam experiments and that most of the ions are in the ground vibrational state before electron capture takes place, E would be approximately $0.03 + \epsilon_A + a\epsilon_z$. Figures 44 and 45 show that the calculated lifetimes using $\epsilon_A = 1.29$ and $\epsilon_A = 1.49$ are consistent with the measured value of $\sim$25 microseconds. However, the calculated lifetime using $\epsilon_A = 1.69$ is not consistent with experiment. The theoretical calculations also show that the lifetime of the ions will be very sensitive to the ion source conditions such

as temperature and electron energy.

For purposes of comparison with experiment, an expression can be developed which relates the lifetime of temporary negative ions to the rate of removal of electrons, αW, from an electron swarm. Since αW is a velocity integrated quantity, the lifetime calculation will contain similar expressions. The transition probability for any particular velocity, v, is given by $T_{12} = v\sigma_{(v)}$; therefore, the average transition probability which is observed in electron swarm experiments is defined by

$$\overline{T}_{12} = \int_{o}^{\infty} v\sigma_{(v)} f_{(v)} dv. \tag{66}$$

Employing the density of states of the ejected electron to be the same as that of an electron traveling with the average energy in the electron swarm, substituting Equation (66) into Equation (53), and replacing $\overline{T}_{12}$ by $\alpha W/N_o$ yields

$$\overline{\tau} = \frac{(\epsilon + a\epsilon_z)^{N-1}}{\Gamma_{(N)} \prod^{N} h\nu_i} \frac{2\Pi^2 \hbar^3 N_o}{m^2 \overline{v}\, \alpha W}. \tag{67}$$

Equation (67) represents the average lifetime of the ions formed in a thermal electron swarm experiment.

Equation (67) can be applied to biacetyl, $(CH_3CO)_2$, in an attempt to determine the electron affinity. All of the vibrational frequencies for biacetyl have been tabulated by Sidman and McClure (1955) with the exception

of the CH_3 torsional frequencies, which can be approximated by those of acetone, $(CH_3)_2CO$ [Fateley and Miller (1962)]. Employing the αW measurements of Bouby, Fiquet-Fayard, and Abgrall (1965) and the measured lifetime of 12 microseconds, E of the negative ion is calculated from Equation (67) to be 3.27 eV. This value for E can be used to obtain the electron affinity of $(CH_3CO)_2$ from Equation (64). Substitution of the calculated values for E and ϵ_z into Equation (64) gives

$$3.27 = \epsilon_e + \epsilon_A + 2.5\, a\left(\frac{\epsilon_e + \epsilon_A}{2.5}\right). \tag{68}$$

Since $a\left(\frac{\epsilon_e + \epsilon_A}{\epsilon_z}\right)$ is an empirical function of $\frac{\epsilon_e + \epsilon_A}{\epsilon_z}$ [see Whitten and Rabinovitch (1963)], Equation (68) can best be solved graphically. Equation (68) is satisfied for $\epsilon_e + \epsilon_A = 1.15$ eV. Using $\epsilon_e \approx 0.05$ eV, the electron affinity is found to be ~ 1.1 eV. This is a reasonable electron affinity to be expected for biacetyl, and the result is taken to add further support to the model describing non-dissociative electron capture presented in this chapter.

If $(\alpha W)_{max}$ is assumed for SF_6, Equation (67) gives a lifetime of 80 microseconds (using $\epsilon = 1.49$ eV). In view of the crudeness of this calculation, the experimental measurement of 25 microseconds is compatible with this calculation.

CHAPTER VI

SUMMARY

A method was developed which combined the electron swarm and electron beam techniques to obtain electron capture cross sections as a function of the electron energy. As examples of the method, electron capture cross sections were explicitly determined for chlorotoluene (peaking at ~ 1 eV) and oxygen (peaking at ~ 7 eV). The procedure proved to be a powerful method in determining both the magnitude of the attachment cross section and the electron energy scale. In the case of oxygen good agreement with the data of total ionization experiments was found with respect to the magnitude and energy dependence of the cross section.

The dissociative electron attachment cross section for H^- from water was determined. In addition, ion molecule reactions leading to OH^- were definitely attributed to the following processes:

$$H^- + H_2O \rightarrow OH^- + H_2$$

$$O^- + H_2O \rightarrow OH^- + OH \ .$$

The swarm-beam method was also employed to study electron attachment in a series of halogenated hydrocarbons. Certain correlations were observed to exist between the magnitude and position of the cross section and the type of halogen substituent. Dissociative attachment in iodobenzene

leading to iodine negative ions was observed to peak at electron energies below kT.

Non-dissociative electron attachment to complex molecules was investigated both experimentally and theoretically. Unimolecular electron attachment was observed in the following molecules: SF_6, $C_6H_5NO_2$, o-$C_6H_4CH_3NO_2$, m-$C_6H_4CH_3NO_2$, and $(CH_3CO)_2$. It was demonstrated that the parent negative ions thus formed are metastable, and the half lives against autodetachment for SF_6^{-*}, $C_6H_5NO_2^{-*}$, and $(CH_3CO)_2^{-*}$ were determined to be 25, 40, and 12 microseconds, respectively.

A theoretical study of long-lived negative ions was presented which treated the molecule as a system of harmonic oscillators. Specifically, the negative ion lifetime was related to the electron capture cross section by the principle of detail balance. The attachment cross section was assumed to be the maximum possible (i.e., $\Pi\lambda\!\!\!^{-2}$). The theory successfully accounted for the measured lifetime of the SF_6^{-*} ion.

The possibility of combining electron capture cross sections and negative ion lifetime measurements to determine electron affinities was pointed out. As an example, the electron affinity of $(CH_3CO)_2$ was calculated to be ~ 1.1 eV.

BIBLIOGRAPHY

BIBLIOGRAPHY

Ahearn, A. J., and N. B. Hannay, J. Chem. Phys. 21, 119 (1953).

von Ardenne, M., K. Steinfelder, and R. Trümmer, Angew. Chem. 73, 136 (1961).

Bardsley, J. N., A. Herzenberg, and F. Mandle, "The Dissociation of Hydrogen Molecules by Resonant Electron Scattering," In Atomic Collision Processes. ed. M. R. C. McDowell (North Holland Publishing Co., Amsterdam, 1964), p. 415.

Bardsley, J. N., A. Herzenberg, and F. Mandl, "Vibrational Excitation and Dissociative Attachment in the Collisions of Electrons with Hydrogen Molecules," In Proc. IVth International Conference on the Physics of Electronic and Atomic Collisions (Science Bookcrafters, Inc., New York, 1965), p. 359.

Bates, D. R., Atomic and Molecular Processes (Academic Press, New York, 1962).

Berry, C. E., Phys. Rev. 78, 597 (1950).

Biondi, M. A., and S. C. Brown, Phys. Rev. 75, 1700 (1949).

Biondi, M. A., Phys. Rev. 109, 2005 (1958).

Biondi, M. A., and R. E. Fox, Phys. Rev. 109, 2012 (1958).

Blatt, J. M., and V. F. Weisskopf, Theoretical Nuclear Physics (John Wiley and Sons, New York, 1963), p. 318.

Bloch, F., and N. E. Bradbury, Phys. Rev. 48, 689 (1935).

Born, M., and J. R. Oppenheimer, Ann. Physik 84, 457 (1927).

Bortner, T. E., and G. S. Hurst, Health Phys. 1, 39 (1958).

Bouby, L., F. Fiquet-Fayard, and H. Abgrall, Compt. Rend. 261, 4059 (1965).

Branscomb, L. M., "Negative Ions," in Advances in Electronics and Electron Physics (Academic Press, New York, 1957), Vol. IX, pp. 43-94.

Branscomb, L. M., J. Chem. Phys. 29, 452 (1958).

Buchel'nikova, I. S., Soviet Phys.—JETP 35, 783 (1959).

Chen, J. C. Y., and J. L. Magee, J. Chem. Phys. 36, 1407 (1962).

Chen, J. C. Y., Phys. Rev. 129, 202 (1963).

Chen, J. C. Y., J. Chem. Phys. 40, 3507 (1964a).

Chen, J. C. Y., J. Chem. Phys. 40, 3513 (1964b).

Christophorou, L. G., R. N. Compton, G. S. Hurst, and P. W. Reinhardt, J. Chem. Phys. 43, 4273 (1965).

Cottin, M., J. Chem. Phys. 56, 1024 (1959).

Cox, B. C., Ph.D. thesis, University of Liverpool, 1953 (unpublished).

Craggs, J. D., R. Thorburn, and B. A. Tozer, Proc. Roy. Soc. (London) A240, 473 (1957).

Demkov, Yu. N., Phys. Letters 15, 235 (1965).

Dibeler, V. H., and J. A. Walker, J. Chem. Phys. 43, 1842 (1965).

Dunn, G. H., Phys. Rev. Letters 8, 62 (1962).

Edelson, D., J. E. Griffiths, and K. B. McAfee, Jr., J. Chem. Phys. 37, 917 (1962).

Fateley, W. G., and F. A. Miller, Spectrochimica Acta 18, 977 (1962).

Feshbach, H., Ann. Phys. 19, 287 (1962).

Fiquet-Fayard, F., "Attachment e'electronique en phase Gaseuse," in Actions Chimiques et Biologiques des Radiations. ed. H. Haissinsky (Masson, Paris, 1965), p. 31.

Fite, W. L., and R. T. Brackman, "Electron Collisions with Atomic and Molecular Oxygen," in Proc. VII Conference Ionized Gases, Paris, 1963. eds. P. H. P. Hubert and E. Cremieu-Alcan, p. 21.

Fite, W. L., R. T. Brackman, and W. R. Henderson, "Dissociative Attachment of Electrons to Hot O_2," in Proc. IVth International Conference on the Physics of Electronic and Atomic Collisions (Science Bookcrafters, Inc., New York, 1965), p. 100.

Fox, R. E., W. M. Hickam, D. J. Grove, and T. Kjeldaas, Jr., Rev. Sci. Instr. 26, 1101 (1955).

Fox, R. E., J. Chem. Phys. 26, 1281 (1957).

Fox, R. E., Phys. Rev. 109, 2008 (1958).

Fox, R. E., and R. K. Curran, J. Chem. Phys. 34, 1595 (1961).

Franck, J., and P. Jordan, Anregung von Quanten-sprüngen durch Stösse (Springer-Verlag, Berlin, 926).

Frost, D. C., and C. A. McDowell, J. Chem. Phys. 29, 964 (1958).

Goodrich, G. W., and W. C. Wiley, Rev. Sci. Instr. 32, 846 (1961).

Haas, R., Z. Physik 148, 177 (1957).

Harrison, M. A., and R. Geballe, Phys. Rev. 91 (1953).

Hasted, J. B., Physics of Atomic Collisions (Butterworths, London, 1964).

Herzenberg, A., "The Quasi-Stationary-State Approach to Resonances in the Scattering of Electrons from Atoms and Molecules," in Proc. IVth International Conference on the Physics of Electronic and Atomic Collisions (Science Bookcrafters, Inc., New York, 1965), p. 1.

Herzenberg, A., and F. Mandl, Proc. Roy. Soc. (London) A270, 48 (1962).

Hickam, W. M., and R. E. Fox, J. Chem. Phys. 25, 642 (1956).

Hiby, J. W., Ann. Phys. 34, 473 (1939).

Holøen, E., and J. Midtdal, Proc. Phys. Soc. (London) A68, 815 (1955).

Holstein, T., Phys. Rev. 84, 1073 (1951).

Hurst, G. S., and T. E. Bortner, "Electron Attachment in Gas Mixtures Containing O_2," in Oak Ridge National Laboratory Report ORNL-2151 (October 18, 1956), p. 43.

Hurst, G. S., and T. E. Bortner, "Electron Attachment in Mixtures Containing Oxygen," in Oak Ridge National Laboratory Report ORNL-2384 (November 11, 1957), p. 97.

Hurst, G. S., and T. E. Bortner, Rad. Res. Suppl. 1, 547 (1959).

Hurst, G. S., L. B. O'Kelly, and T. E. Bortner, Phys. Rev. 123, 1715 (1961).

Irsa, A. P., J. Chem. Phys. 26, 18 (1955).

Kapur, P. L., and R. E. Peierls, Proc. Roy. Soc. (London) A166, 277 (1938).

Kay, J., and F. M. Page, Trans. Faraday Soc. 60, 1042 (1964).

Kronig, R., Z. Physik 50, 347 (1928).

Ladier, K. J., J. Chem. Phys. 22, 1740 (1954).

Mann, M. M., A. Hustrulid, and J. T. Tate, Phys. Rev. 58, 340 (1940).

Marcus, R. A., and O. K. Rice, J. Phys. Colloid. Chem. 55, 894 (1951).

Massey, H. S. W., Negative Ions (Cambridge Press, Cambridge, 1950), 2nd Edition.

Massey, H. S. W., and E. H. S. Burhop, Electronic and Ionic Impact Phenomena (University Press, Oxford, 1952), p. 34.

McDaniel, E. W., Collision Phenomena in Ionized Gases (John Wiley and Sons, New York, 1964).

McDowell, C. A., and J. W. Warren, Discussions Faraday Soc. 10, 53 (1951).

McDowell, M. R. C., Observatory 81, 240 (1961).

Melton, C. E., "Negative Ions," in Mass Spectrometry of Organic Ions. ed. F. W. McLafferty (Academic Press, New York, 1963), p. 163.

Muschlitz, E. E., J. Appl. Phys. 28, 1414 (1957).

O'Malley, T. F., "Resonant Dissociative Attachment," in Proc. IVth International Conference on the Physics of Electronic and Atomic Collisions (Science Bookcrafters, Inc., New York, 1965), p. 97.

Pauly, H., H. Petmecky, and C. Schmidt, Z. Angew. Phys. XIX, 20 (1965).

Pistorius, G.W.F.T., J. Chem. Phys. 29, 1328 (1958).

Rabinovitch, B. S., and R. W. Diesen, J. Chem. Phys. 30, 735 (1959).

Rapp, D., T. E. Sharp, and D. D. Briglia, Phys. Rev. Letters 14, 533 (1965).

Schulz, G. J., Phys. Rev. 113, 816 (1959a).

Schulz, G. J., Phys. Rev. 116, 1141 (1959b).

Schulz, G. J., J. Chem. Phys. 33, 1661 (1960a).

Schulz, G. J., J. Appl. Phys. 31, 1134 (1960b).

Schulz, G. J., J. Chem. Phys. 34, 1778 (1961).

Schulz, G. J., and R. K. Asundi, Phys. Rev. Letters 15, 946 (1965).

Sidman, J. W., and D. S. McClure, J. Am. Chem. Soc. 77, 6471 (1955).

Stanton, R. E., J. Chem. Phys. 32, 1348 (1960).

Stockdale, J. A., and G. S. Hurst, J. Chem. Phys. 41, 255 (1964).

Sweetman, D. R., Proc. Phys. Soc. (London) 76, 998 (1960).

Thorburn, R., "Atomic Ions Produced in Oxygen by Electron Bombardment," in Applied Mass Spectroscopy (The Institute of Petroleum, London, 1954), p. 185.

Tozer, B. A., J. Electronics and Control 4, 149 (1958).

Van Vleck, J., Phys. Rev. 33, 467 (1929).

Whitten, G. Z., and B. S. Rabinovitch, J. Chem. Phys. 38, 2466 (1963).

Wildt, R., Astrophys. J. 89, 295 (1935).

INTERNAL DISTRIBUTION

1. Biology Library
2-4. Central Research Library
5. Reactor Division Library
6-7. ORNL Y-12 Technical Library Document Reference Section
8-57. Laboratory Records Department
58. Laboratory Records, ORNL R. C.
59. E. T. Arakawa
60. R. D. Birkhoff
61. R. E. Boughner
62. J. F. Burns
63-87. R. N. Compton
88. A. M. Craig, Jr.
89. F. J. Davis
90-114. G. S. Hurst
115. C. E. Klots
116. W. H. Jordan
117. C. E. Larson
118. H. G. MacPherson
119. K. Z. Morgan
120. C. E. Melton
121. D. R. Nelson
122-146. P. W. Reinhardt
147. R. H. Ritchie
148. H. C. Schweinler
149. M. J. Skinner
150. W. S. Snyder
151. E. B. Wagner
152. A. M. Weinberg
153. T. E. Bortner (consultant)
154-178. L. G. Christophorou (consultant)
179. G. M. Fair (consultant)
180. K. Fox (consultant)
181. J. C. Frye (consultant)
182. L. W. Cochran (consultant)
183. J. B. Hursh (consultant)
184. R. J. Lovell (consultant)
185. E. P. Odum (consultant)
186. R. L. Platzman (consultant)
187. H. O. Wyckoff (consultant)

EXTERNAL DISTRIBUTION

188. M. H. Abgrall, Laboratoire de Chimie Physique, Faculte des Sciences, Orsay (Seine-et-Oise), France
189. T. L. Bailey, Department of Physics, University of Florida, Gainesville
190. N. F. Barr, Division of Biology and Medicine, USAEC, Washington, D. C.
191. M. L. Bouby, Laboratoire de Chimie Physique, Faculte des Sciences, Orsay (Seine-et-Oise), France
192. Berea College Library, Berea, Kentucky
193. J. C. Y. Chen, J. I. L. A., University of Colorado, Boulder
194. D. C. Conway, Department of Chemistry, Purdue University, West Lafayette, Indiana
195. R. W. Crompton, Research School of Physical Sciences, The Australian National University, Ion Diffusion Unit, Box 4, G. P. O., Canberra A. C. T., Australia
196. C. L. Dunham, Division of Biology and Medicine, USAEC, Washington, D. C.
197. D. Edelson, Bell Telephone Laboratories, Inc., Murray Hill, New Jersey
198. U. Fano, National Bureau of Standards, Washington, D. C.
199. Florence Fiquet-Fayard, Laboratoire de Chimie Physique, Faculte des Sciences, Orsay (Seine-et-Oise), France
200. Wade L. Fite, Department of Physics, University of Pittsburgh, Pittsburgh, Pennsylvania

201. J. H. Green, Department of Nuclear Chemistry and Radiation, University of New South Wales, Kensington, Sydney, Australia
202. W. T. Ham, Medical College of Virginia, Richmond
203. G. W. Hoffman, Department of Electrical Engineering, University of Tennessee, Knoxville
204. W. P. Jesse, St. Procopius College, Physical Sciences Laboratory, Lisle, Illinois
205. S. Allen Lough, Division of Biology and Medicine, USAEC, Washington, D. C.
206. J. L. Magee, Radiation Laboratory, University of Notre Dame, Notre Dame, Indiana
207. H. S. W. Massey, University College, London, England
208. K. B. McAfee, Jr., Bell Telphone Laboratories, Inc., Murray Hill, New Jersey
209. Earl W. McDaniel, School of Physics, Georgia Institute of Technology, Atlanta, Georgia
210. E. E. Muschlitz, Department of Physics, University of Florida, Gainesville
211. A. H. Nielsen, Department of Physics, The University of Tennessee, Knoxville
212. F. H. W. Noll, Berea, Kentucky
213. T. F. O'Malley, Defense Research Corporation, P. O. Box 3587, Santa Barbara, California
214. A. V. Phelps, Westinghouse Research Laboratories, Churchill Borough, Pittsburgh 35, Pennsylvania
215. R. D. Present, Department of Physics, The University of Tennessee, Knoxville
216. G. J. Schulz, Westinghouse Research Laboratories, Churchill Borough, Pittsburgh 35, Pennsylvania
217. J. A. Stockdale, A.A.E.C. Research Establishment, Private Mail Bag, Sutherland, N.S.W., Australia
218. T. D. Strickler, Department of Physics, Berea College, Berea, Kentucky
219. G. L. Weissler, Department of Physics, University of Southern California, Los Angeles
220. Research and Development Division, AEC, ORO
221-235. Division of Technical Information Extension